RNA BINDING PROTEIN SYNCRIP IS REQUIRED FOR MAINTAINING NORMAL HEMATOPOIETIC AND LEUKEMIA STEM CELL SELF-RENEWAL

A Dissertation

Presented to the Faculty of the Louis V. Gerstner, Jr.

Graduate School of Biomedical Sciences,

Memorial Sloan Kettering Cancer Center

in Partial Fulfillment of the Requirements for the Degree of

Doctor of Philosophy

by

Florisela Herrejon Chavez

March 2023

ABSTRACT

The hematopoietic system is reliant on hematopoietic stem cell's (HSC) ability to self-renew and to differentiate. The mechanisms for how HSCs make cell fate decisions remain to be fully elucidated. In recent years, RNA binding proteins (RBPs) have emerged as being important players in maintaining normal hematopoiesis. One such RBP is MSI2, which has been shown to promote HSC self-renewal and regulates cell fate decisions. An shRNA screen investigating MSI2's interactome identified the RBP SYNCRIP as a novel regulator of myeloid leukemia. However, it remains unclear if and how SYNCRIP regulates both normal and malignant blood. Our laboratory developed a new conditional knockout mouse model to investigate SYNCRIP biology. We found SYNCRIP to be modestly required for steady state hematopoiesis but essential for maintaining long-term HSC self-renewal capacities under conditions of regenerative stress, especially during serial transplantation. Mechanistically we found SYNCRIP to be involved in maintaining proteostasis in HSCs. Upon SYNCRIP depletion, scRNA-seq revealed gene signatures indicating activation of the chaperone and unfolded protein response. Upon further investigation, we confirmed SYNCRIP loss in HSCs results in an increase in global translation, increased endoplasmic reticulum stress, higher amounts of unfolded protein, and an altered epichaperome. This effect was found to be unique to HSCs and not observed in multipotent progenitors. Additionally, using a multi-omic strategy, consisting of RNA-seq, mass spectrometry, and HyperTRIBE, we've been able to uncover SYNCRIP's direct binding targets that are translationally regulated in HSCs. Among the list of targets are several other RBPs, as well as many RHO-GTPase associated targets. Out of these hits, we focused on the RHO-GTPase CDC42, which was found to be translationally regulated by SYNCRIP and is already known to be important for HSCs, cytoskeletal organization, and cell polarity. Further examination revealed that SYNCRIP loss, also results in HSC defects in tubulin polarity. We also observed defects in HSC

asymmetric division upon SYNCRIP depletion. Using NUMB as a marker of cell fate, we observed an increase in symmetric renewing cells, and a loss of asymmetric and symmetric commitment cells. We also observed decreased LAMP1 and unfolded protein asymmetric division in KO HSCs, leading to reduced clearance of misfolded proteins in HSCs. Forced expression of CDC42 partially rescued SYNCRIP's KO HSC self-renewal serial plating defect *in vitro*. Altogether, SYNCRIP was found to be important in maintaining HSC's self-renewal, by maintaining proteostasis and through direct translational regulation of the RHO-GTPase CDC42.

In addition to their role in normal hematopoiesis, RBPs have also been found to be important in maintaining malignant hematopoiesis, such as acute myeloid leukemia (AML). AML is characterized by an accumulation of immature precursor cells and a block in myeloid differentiation. Leukemia stem cells (LSCs) are the growth initiating stem cells that drive the disease. Although it has been previously shown that SYNCRIP co-regulates the leukemia stem cell program, SYNCRIP's functional role in regulating LSCs and leukemia stem cell fate remained unclear. Using the same SYNCRIP conditional knockout mouse we've found SYNCRIP depletion delays leukemia progression and is important for leukemia initiation and maintenance. However, transcriptomic profiling of these transplants demonstrates a powerful transcriptional compensation mechanism that promotes stemness, and western blot and qPCR analysis confirms upregulation of *Hoxa9* transcripts. Separately, we've performed iCLIP and HyperTRIBE to identify novel SYNCRIP mRNA targets in the RN2 cell line as well as LSCs. We've been able to verify known transcripts, like *Hoxa9*, and identified novel targets which consist of other RBPs including those involved in translation and splicing. Altogether we've been able to establish that SYNCRIP functionally regulates leukemia stem cell function and identified novel resistance mechanisms for SYNCRIP loss. Our studies demonstrate that SYNCRIP represents a potential therapeutic target in AML.

ACKNOWLEDGMENTS

I would like to thank everyone who was involved in my scientific training and has helped contribute to the presented work. I'd especially like to thank my advisor, Dr. Michael Kharas, for his continued guidance and support throughout my entire time in the lab. I'd also like acknowledge and thank Dr. Ly Vu, who initiated this project, for her expert advice and for helping tremendously in generating and interpreting data. I'm grateful to the members of Dr. Christina Leslie's lab, Karen Chu and Alli Pine, and Illyes Baali from Quaid Morris' lab, who helped with the bioinformatics analysis. I'd also like to thank our collaborators, Dr. Yuning Hong, Dr. Gabriela Chiosis, and Dr. Alex Kentsis for providing critical reagents and expertise. Additionally, I'd like to thank everyone else who helped perform experiments for this study: Hanzhi Luo, Paolo Cifani, Ersilia Barin, Alex Schurer, Mandy Chan, Kathryn Chang, Grace Han, Aspen Pierson, Michael Xiao, Lindsey Kuehm, Xuejing Yang, Diu Nguyen, Tom Rohwetter, and Chiara Evans. I am very thankful to all the members of the Kharas lab for their friendship and for all their advice throughout the last five years.

I would like to acknowledge all the funding sources that have supported me and this work which include the ASH Minority Hematology Graduate Award, an NIH diversity supplement from R01CA186702, and the MSKCC Olayan Fellowship for Graduate Students.

Importantly, I'm very appreciative of the GSK administrative office (past and present members), for their tremendous support and for taking great care of GSK students. Finally, I want to thank my thesis committee members, Minkui Luo and Andrea Ventura, for providing so much scientific advice and feedback, which has been essential to my scientific education.

TABLE OF CONTENTS

LIST OF TABLES

LIST OF FIGURES

LIST OF ABREVIATIONS

HSC	Hematopoietic Stem Cell
LT-HSC	Long Term Hematopoietic Stem Cell
ST-HSC	Short Term Hematopoietic Stem Cell
MPP	Multipotent Progenitor
CMP	Common Myeloid Progenitor
LMPP	Lymphoid Primed Multipotent Progenitors
MEP	Megakaryocyte Erythroid Progenitors
GMP	Granulocyte Macrophage Progenitors
CLP	Common Lymphoid Progenitor
EP	Erythroid Progenitor
HSPC	Hematopoietic Stem and Progenitor Cell
CKI	Cyclin Dependent Kinase Inhibitor
MPP	Mitochondrial Membrane Potential
ECM	Extracellular Matrix
RBP	RNA Binding Protein
RBD	RNA Binding Domain
RRM	RNA Recognition Motif
KH	K-homology
ZF	Zinc Finger
dsRBD	Double Stranded RNA-Binding Domain
CSD	Cold Shock Domain
m^6A	N^6-methyladenosine
YTH	YT521-B Homology
hCB HSCs	Human Cord Blood HSCs

snRNPs	Small Nuclear Ribonucleoproteins
snRNA	Small Nuclear RNA
WBC	White Blood Cell
RBC	Red Blood Cell
HGB	Hemoglobin
MDS	Myelodysplastic Syndrome
ESE	Exonic Splicing Enhancer
ADAR	Adenosine Deaminases on RNA
OPP	OP-Puro
4E-BPs	eIF4E Binding Proteins
MSI1	MUSASHI-1
MSI2	MUSASHI-2
PABP	Poly(A) Binding Protein
LSC	Leukemia Stem Cells
AML	Acute Myeloid Leukemia
NCI	National Cancer Institute
HSCT	Hematopoietic Stem Cell Transplantation
SCID	Severe Combined Immune-Deficient Mice
WT	Wildtype
KO	Knockout
PDX	Patient Derived Xenograft
MDS-RS	MDS Ringed Sideroblasts
SSA	Spliceostatin A
NES	Nuclear Export Signal
SINE	Selective Inhibitors of Nuclear Transport

BC-CML	Blast Crisis Chronic Myeloid Leukemia
8-aza	8-Azadenosine
MNK	MAP Kinase-Interacting Kinases
RHT	Rohinitib
B-ALL	B cell Acute Lymphoblastic Leukemia
Ro	Ro 08-2750
CLIP	Crosslinking Immunoprecipitation
SYNCRIP	Synaptotagmin Binding Cytoplasmic RNA Interacting Protein
RGG	Arginine–Glycine–Glycine Repeat
NLS	Nuclear Localization Signal
SMN2	Survival Motor Neuron 2
T-ALL	T-cell acute lymphoblastic leukemia
cKO	Conditional Knockout
pIpC	Polyinosinic: polycytidylic acid
BM	Bone Marrow
PB	Peripheral Blood
PY	Pyronin Y
CB-CD34+	Human Cord Blood CD34+
scRNA-seq	Single Cell RNA Sequencing
UMAP	Uniform Manifold Approximation and Projection
t-SNE	t-Distributed Stochastic Neighbor Embedding
GSEA	Gene Set Enrichment Analysis
UPR	Unfolded Protein Response
TMI	Tetraphenylethene Malemide

LSK	Lineage -, Sca1+, cKit+
PU-FITC	PU-H71 conjugated to FITC
TEM	Transmission Electron Microscopy
ER	Endoplasmic Reticulum
NE	Nuclear Envelope
S-ADAR	SYNCRIP-ADAR
EV	Control Empty Vector
CDC42 OV	CDC42 Overexpression
4-OHT	4-Hydroxytamoxifen
CDS	Coding Sequence
3'UTR	3'Untranslated Region

Chapter I: Role of RNA Binding Proteins in Maintaining Hematopoietic Stem Cell and Leukemia Self-Renewal

Introduction

Hematopoiesis, or the process of blood formation, is a highly organized system with hematopoietic stem cells (HSCs) at the top of the hierarchy. They lead to the formation of intermediate progenitors and ultimately differentiated blood cells [1-3]. HSCs are responsible for generating an organism's lifelong blood compartment. This enormous demand is accomplished by HSC's careful balance between self-renewal and differentiation [4]. Abnormal hematopoiesis can occur if HSCs experience changes in their self-renewal capacity or have acquired genetic alterations that lead to malignant transformation [5-7]. The consequences of abnormal HSC activity are severe, and can lead to bone marrow failure [8, 9], blood malignancies [10, 11], and ultimately death.

Within the hematopoietic hierarchy, HSCs are divided into two subpopulations LT-HSC (long term HSCs) and ST-HSC (short term HSCs also referred to as MPP1), where LT-HSCs have more reconstitution potential. ST-HSCs differentiate to multipotent progenitor (MPPs) populations. The combination of the HSC and MPP populations is often referred to as the hematopoietic stem and progenitor cell (HSPC) compartment. Subsequen MPPs differentiate into myeloid and lymphoid lineage restricted downstream progenitors. This continuous differentiation process proceeds until ultimately mature myeloid and lymphoid cells are formed (Figure 1.1) [3].

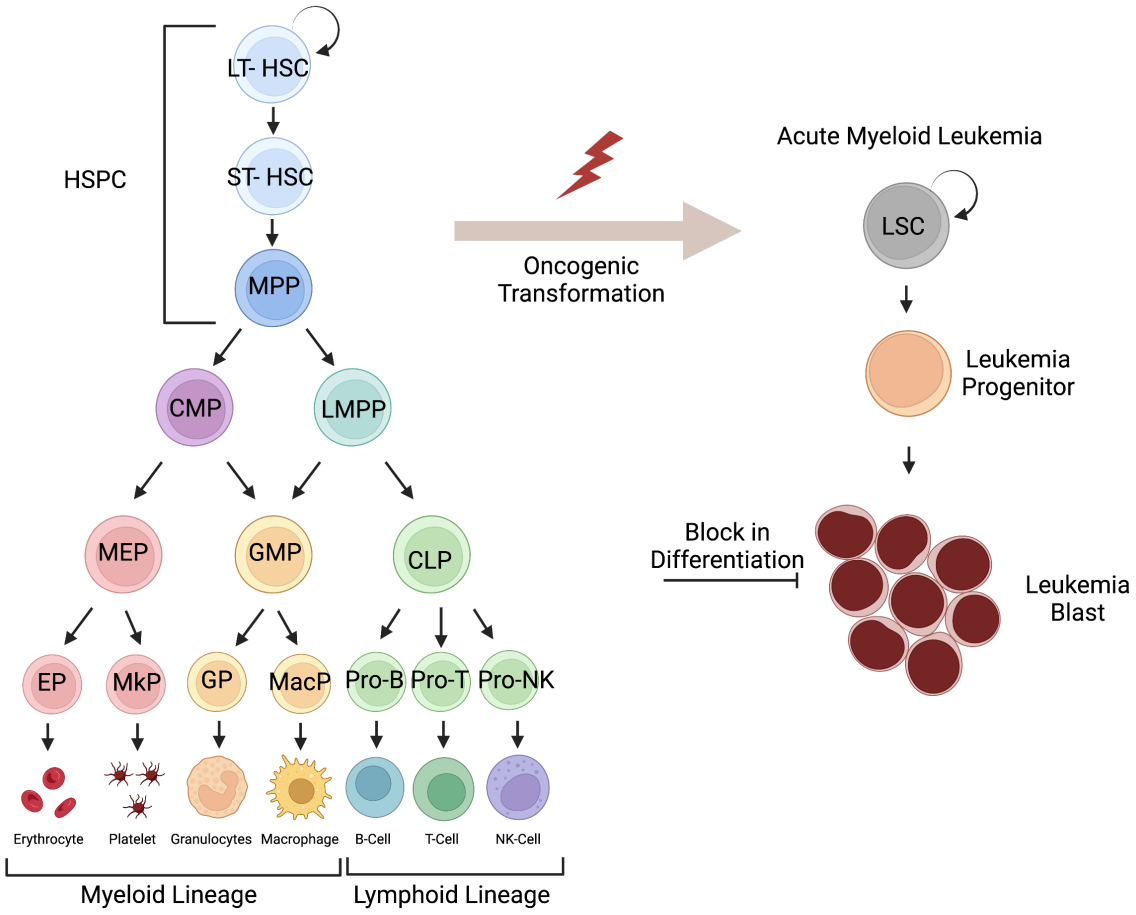

Figure 1.1 Normal hematopoiesis transformation into malignant hematopoiesis
Left schematic depicts the hematopoietic hierarchy where hematopoietic stem cells (HSC) can self-renew or undergo differentiation into multipotent progenitors (MPP). The combination of HSCs and MPPs is referred to as hematopoietic stem and progenitor cells (HSPC). MPPs further differentiate into common myeloid progenitors (CMP) or lymphoid primed multipotent progenitors (LMPP). These progenitors give rise to more downstream progenitors: megakaryocyte erythroid progenitors (MEP), granulocyte macrophage progenitors (GMP) and common lymphoid progenitor (CLP). Further differentiation gives rise to more restricted progenitors like erythrocyte progenitors (EP), megakaryocyte progenitors, granulocyte progenitors, macrophage progenitors, as well as all the lymphoid progenitors (Pro-B, Pro-T, Pro-NK). Ultimately this leads to fully differentiated myeloid and lymphoid lineages. Right schematic depicts formation of acute myeloid leukemia (AML). Upon oncogenic transformation, which can include genetic mutations or alterations in HSCs, MPPs or more committed progenitors, can cause AML leukemia stem cells (LSC) to arise. LSCs poses self-renewal capacities, as well as the ability to differentiate into leukemia blasts with blocks in differentiation. Figure adapted from *Long et al. Stem Cell Rev and Rep 2022* [12].

HSCs are highly regulated and held in a quiescent state to preserve their long-term maintenance and self-renewal capacities. The mechanisms that regulate HSC quiescence have been extensively studied and include both intrinsic and extrinsic factors [13]. Intrinsic factors include cell cycle regulators, transcription factors, epigenetic factors, mitochondrial activity, and autophagy/lysosomal metabolism. For example, to maintain quiescence, LT-HSCs contain low abundance of cyclin-dependent kinase 6 (CDK6) and forced CDK expression promotes an exit from quiescence without impacting normal HSC function [14]. Expression of cyclin dependent kinase inhibitors (CKI) like p57 [15] and p21 [16] promotes quiescence in HSCs. Several transcription factors, like p53 and c-Myc, are also involved in maintenance of HSC cell proliferation, where expression of p53 [17] and homeostatic balance of Myc expression preserves proper HSC functions [18, 19]. Additionally, mitochondrial activity or mitochondrial membrane potential (MMP) has also been implicated in regulating quiescence, where low MMP HSCs are described as more quiescent than high MMP HSCs [20]. Autophagy activity is also involved in regulating quiescence, loss of autophagy by deletion of autophagy factors like Atg5 [21] and Atg7 [22] results in HSPC activation and exhaustion. Lysosome activity has recently been implicated to play a role in HSC quiescence, where inhibition of lysosome activity has been shown to enhance HSCs repopulation potential and large lysosomes are key in maintaining HSC quiescence [20].

Extrinsic factors that regulate HSC quiescence include interactions with the extracellular matrix (ECM), bone marrow niche secretions, and cell to cell interactions. Physical properties in the bone marrow's ECM, like stiffness and elasticity, play a role in HSCs cell fate. Where there is an increase in proliferation of *in vitro* cultured HSPC's on collagen matrix vs laminin coated substrate. Additionally, stiffer fibronectin substrate promotes HSPC primitive myeloid progenitor maintenance, where softer laminin

promotes differentiation [23]. Adhesion to fibronectin has also been seen to play a role in *ex vivo* culture of human HSCs, and shown to be important in maintenance of HSC's reconstitution potential [24]. ECM adhesion receptor proteins (like integrins and cadherins) also play an important role in maintaining HSC quiescence. It's been seen that depletion of Integrin-αv causes HSCs to proliferate faster *in vitro* [25]. Forced expression of N-cadherin has been seen to promote HSC quiescence [26] and N-cadherin+ niche cells residing in the bone marrow endosteum have been shown to play a role in maintaining chemotherapy resistant reserve HSCs [27]. Bone marrow microenvironment secretions (or secretions from distal tissues) are also implicated in maintaining HSCs, such as CXCL4 [28, 29], TGF-β [30] and THPO [31] which are involved in promoting HSC quiescence. Direct interactions with other bone marrow niche cells, like macrophages have also been shown to provide a quality check on HSCs [32].

HSCs proliferate rarely, but under conditions of hematopoietic insult (transplantation, chemotherapy, inflammation, etc.) HSCs are activated to reconstitute the blood compartments that are damaged [33]. During activation, HSCs make cell fate decisions that determine whether they self-renew or differentiate. When an HSC divides, it produces a daughter cell, where they can both self-renew (symmetric self-renewal), both commit to differentiate (symmetric commitment), or they can undergo asymmetric division where one cell self-renews and the other commits to differentiate [34].

The mechanisms that determine how an HSC makes cell fate decisions is not fully understood, however several factors and organelles have been identified to be implicated in asymmetric cell division and cell fate determination. Among some of these asymmetrically segregated factors are NUMB [35-37], CD71[35, 38], CDC42 [39, 40], and organelles like lysosomes and mitochondria [35, 41, 42]. NUMB, an inhibitor of

NOTCH, has been used as a marker of cell differentiation in HSCs and in non-blood related stem cells [35-37]. CD71 is another protein seen to be asymmetrically divided and expressed more in maturing cells [35, 38]. CDC42 is a key regulator of cell polarity and cytoskeletal organization in HSCs [43]. For cells to asymmetrically segregate cellular components, a polar axis must be established, and the cytoskeletal network reorganized. CDC42 is involved in producing the polar axis and cytoskeletal organization conditions necessary for asymmetric cell division [44, 45]. However, how CDC42 influences the fate and differentiation activity of HSCs remains unclear.

In addition to individual proteins, recent work using quantitative live cell imaging, has linked asymmetric lysosomal inheritance to HSC cell fate. Where HSC daughter cells that inherit less lysosomes express differentiation markers like CD71 [35]. Interestingly it has also been shown that quiescent HSCs are associated with larger lysosome quantities and lower lysosomal activity [20]. Besides lysosomes, mitochondria have also been shown to be asymmetrically inherited in HSCs and its been seen that HSCs retain dysfunctional mitochondria after asymmetric division [42]. How exactly mitochondrial inheritance influences HSC fate remains to be fully investigated.

Although many aspects of HSC biology have been explored, a class of proteins that have only recently emerged as important in HSC activity are RNA binding proteins (RBP) [46]. RBPs are key players in regulating post transcriptional processes like mRNA editing, stability, splicing, transport, and translation. RBPs utilize structural RNA binding domains (RBD) to bind RNA, some canonical structures include RNA recognition motifs (RRM), K-homology (KH), zinc finger (ZF), double stranded RNA-binding domain (dsRBD) and cold-shock domain (CSD) [47]. Large scale studies have identified over 1500 known RBPs in mice and humans and there may be several more with non-

canonical RBDs according to the eukaryotic RBP database [48]. However, the role for most RBPs in blood cells has not been fully explored. In recent years, several RBPs have emerged as key regulators in normal and malignant hematopoiesis, and some have even resulted in advancements towards novel therapeutic treatments. This chapter will cover how RBPs influence stem cell properties within the hematopoietic system, in particular HSCs and leukemia, with a focus on those that are being explored for their therapeutic potential.

RNA Binding Proteins in Normal Hematopoiesis

RBPs Involved in RNA Methylation

After transcription, RNAs can undergo post-transcriptional modification, adding an extra layer of regulation for proper gene expression. Over 150 RNA modifications have been identified [49], but the most common is N^6-methyladenosine (m^6A) [50]. This form of RNA methylation is dynamic, reversable and regulated by a family of RBPs known as m^6A "writers", "readers" and "erasers". As of now, the only known eraser proteins are FTO and ALKBH5, and ALKBH5 has been shown to not have a significant effect on the normal hematopoietic system [51]. However various reader and writer proteins have been found to play important roles in normal HSPC function.

Writers: METTL3, METTL14 and RBM15

The m^6A writer complex is composed of various proteins including METTL3, METTL14, RBM15, KIAA1429, ZC3H13 and WTAP [50]. Several of these writer RBPs have been found to play a role in HSC function. For example, METTL3, which is key for m^6A writer complex methyltransferase catalytic activity, has been shown to be essential for HSPCs

during definitive hematopoiesis. In zebrafish, *mettl3* impacts cell fate during the endothelial-to-hematopoietic transition (EHT), where *mettl3* depletion leads to a blockage in HSPC generation. m^6A profiling identified *notch1a* as a target for m^6A modification, which led to its repression by YTHDF2 mediated RNA decay [52]. Since it's been previously shown that activation of Notch1 signaling impairs HSPC emergence [53], regulation of the mettl3/ m^6A - notch1a – YTHDF2 axis maintains proper HSPC formation during EHT in zebrafish. This was also found to be the case during mouse embryogenesis, where *Mettl3* depletion in endothelial cells resulted in impaired HSPC formation and an increase of *Notch1* mRNA expression. Bioinformatic analysis of m^6A profiling found a m^6A peak near the stop codon of *Notch1* mRNA that could be recognized by *Ythdf2* [54], suggesting a conserved mechanism in mouse and zebrafish. In contrast, the role of METTL3 in adult hematopoiesis is not fully characterized, however several studies have been conducted to elucidate some of its function. One study found that *Mettl3* depletion in mice during adult hematopoiesis led to an accumulation of HSCs with reduced reconstitution potential *in vivo* and a blockage in their ability to differentiate [55]. In a separate study conducted by our group, *Mettl3* depletion resulted in an accumulation of dysfunctional HSCs that were less quiescent and functionally defective in their reconstitution potential [56]. This study also demonstrated, through single cell profiling, the emergence of a new population of HSCs in the *Mettl3* knockout (KO) condition, which resembled MPPs functionally and molecularly. It was also found that *Mettl3* influences cell fate, where *Mettl3* KO HSCs experienced a loss of symmetric commitment and an increase in symmetric renewal [52]. Both studies also identified *Myc* mRNA as a target of m^6A, and showed m^6A regulated *Myc's* expression through translation [55] and mRNA stability [56] mechanisms. Interestingly, c-MYC was also found to have a segregation pattern similar to NUMB, where it could be inherited asymmetrically, symmetrically low or symmetrically

high in dividing HSCs [56]. In addition to having a pattern similar to NUMB, MYC inheritance also correlates with CD71 expression [35], altogether suggesting MYC abundance can act as another marker for HSC commitment.

METTL14, acts as an adaptor to METTL3, and together they forma a stable dimer [57]. Depletion of *Mettl14* in mice did not show expansion of HSCs or exit from quiescence like *Mettl3* depletion does. However, simultaneous depletion of *Mettl3* and *Mettl14* shows a similar HSC defect as *Mettl3* loss alone [58] suggesting *Mettl3* has unique catalytic properties in the methyltransferase complex. Despite not influencing HSCs in the same manner as *Mettl3*, *Mettl14* depletion has been seen to cause a mild reduction in HSC self-renewal capacity, as shown by reduction in transplantation potential [59]. Additionally, *Mettl14* is more highly expressed in HSCs and HSPCs when compared to downstream progenitor cells [58, 59]. In human CD34+ HSPCs METTL14 depletion resulted in accelerated monocytic differentiation, suggesting that METTL14 plays a role in myeloid differentiation [59].

RBM15 and its paralog RBM15B have also been implicated in influencing the m^6A methylation complex, by promoting its recruitment to specific binding sites on transcripts like the lncRNA *XIST* [60]. Depletion of RBM15 results in impaired XIST mediated gene silencing, and simultaneous knockdown of RBM15 and RBM15B reduced m^6A levels [60], further suggesting RBM15's role in the m^6A methyltransferase complex. Depletion of RBM15 in adult hematopoiesis results in an expansion of HSPCs and myeloid cells, with a decrease in B cell differentiation [61]. It's been separately shown that RBM15 depletion expands LT-HSCs, through a mechanism that blocks LT-HSC differentiation into ST-HSC [62]. These RBM15 depleted LT-HSCs also have defects in long term serial transplantation capacities, and they display upregulation of adhesion molecules N-

Cadherin and β1-integrin creating abnormal niche interactions [62]. These RBM15 depleted HSCs also have abnormal megakaryocyte development. Overexpression of RBM15 in wildtype (WT) HSCs results in increased c-MYC levels and forced expression of c-MYC in RBM15 KO HSCs partially rescues the megakaryocyte developmental defects [62]. Despite the similar phenotype as METTL3 loss, the exact role m^6A plays between RBM15 and the RNA methylation program in the blood is unclear.

Readers: YTHDF2, YTHDF3

The m^6A readers are a class of RBPs involved in exerting a variety of effects that determine the fate of the RNA, such as mRNA stability [63], transport [64], and translation [65]. A major class of these proteins are the YTH (YT521-B homology) domain proteins which include: YTHDF1, YTHDF2, YTHDF3, YTHDC1 and YTHDC2. Some of these readers have been found to play a role in normal hematopoiesis, for example YTHDF2, which is described above as being involved in embryonic hematopoiesis through its regulation of mRNA decay on transcripts, is also involved in adult hematopoiesis. Depletion of *Ythdf2* leads to expansion of mouse HSCs and improved reconstitution potential as shown by transplantation studies [66]. Knockdown of YTHDF2 in human cord blood HSCs (hCB HSCs) also led to an expansion of HSCs, including an increase in colony forming units, and an increased frequency of functional human cord blood HSCs [66]. This is different from the phenotype observed with *Mettl3* loss and suggests YTHDF2 selectively targets specific transcripts to enhance stemness, unlike METTL3 which is responsible for the deposition of all m^6A modifications and may have a broader role. m^6A profiling in YTHDF2 depleted HSPCs found that m^6A marks were enriched in genes associated with HSC self-renewal and maintenance such as *Gata2*, *Etv6*, and *Tal1.* iCLIP-seq showed YTHDF2 bound to these transcription factor's

mRNAs [66]. Further investigation found that YTHDF2 depletion also led to an increase in these self-renewal associated transcripts, and that YTHDF2 mediates these transcripts decay by localizing them to mRNA decay sites [66]. Surprisingly, HSC long term repopulation capacities are impaired by YTHDF2 depletion, as demonstrated in a secondary transplantation [67]. Altogether, this highlights the importance of YTHDF2 for HSC function and the variability a reader protein may have depending on the cellular state of an HSC.

Another m^6A reader that's been seen to be involved in normal hematopoiesis is YTHDF3. It has been found that *Ytfdf3* depletion in mice impairs HSC reconstitution capacities. Bone marrow transplantations with YTFDF3 deficient HSCs creates a defect in engraftment similar to *Mettl3* depleted HSCs, however not as severe [68]. Upon further investigation, it was found that *Ythdf3* depletion in LSK cells also depleted CCND1 protein as determined by western blot. However, *Ccnd1* mRNA expression remained unchanged, suggesting a translational effect from *Ythdf3*. Rescue experiments demonstrated that forced expression of CCND1, could rescue the transplantation defects from *Ythdf3* depleted HSPCs *in vivo* [68]. *Ccnd1* was also found to be a target of METTL3, and forced CCND1 expression could partially rescue the reconstitution capacity of hairpin knockdown *Mettl3* HSPCs [68]. Further work will be necessary to fully characterize how readers influence other mRNA transcripts that are regulated by m^6A modifications.

RBPs involved in Splicing: SF3B1, U2AF1, SRSF2, ZRSR2

After pre-RNA is transcribed, it undergoes additional processing to ensure proper gene expression. One of the integral steps pre-RNA must undergo is splicing. Splicing is the

process of removing introns and ligating flanking exons to create mature RNA (mRNA). A gene's pre-RNA can also undergo alternative splicing expanding the genetic diversity of transcripts. Splicing is carried out by the spliceosome. For the major spliceosome machinery (U2 spliceosome) this consists of five small nuclear ribonucleoproteins (snRNPs) as well as small nuclear RNAs (snRNA) and numerous proteins [69]. Several splicing factors have been identified to play roles in normal hematopoiesis, such as SF3B1, U2AF1, SRSF2, and ZRSR2.

SF3B1 is a component of the U2 snRNP machinery, which is involved in recognizing the 3' splice site at intron-exon junctions [70]. Previous work has identified homozygous *Sf3b1* knockout mice as embryonically lethal with mice dying around the 16-32 cell stage, however heterozygous mice only exhibit mild skeletal transformations [71]. To study *Sf3b1*'s role in normal hematopoiesis, studies have utilized a heterozygous mice, *Sf3b1*$^{-/+}$. During steady state hematopoiesis, heterozygous loss of *Sf3b1* only has mild effects like an increase in HSPC apoptosis [72]. A separate study also found *Sf3b1*$^{-/+}$ mice had a reduction in the frequency and absolute numbers of HSPCs under steady state hematopoiesis [73]. It was also identified that *Sf3b1*$^{-/+}$ HSPCs had compromised reconstitution potential during *in vitro* colony formation assays [73] as well during *in vivo* competitive mouse transplants with WT cells [72, 73]. There was further loss of HSC function upon a secondary transplantation with *Sf3b1*$^{-/+}$ cells [73]. Upon hairpin knockdown of *Sf3b1* in *Sf3b1*$^{-/+}$ HSPCs, the defect in reconstitution potential was even more pronounced *in vivo*, and these cells also showed decreased proliferation capacities *in vitro* [72]. All this suggests *Sf3b1* plays an important role in regulating HSC number and activity.

U2AF1 is another component of the spicing machinery, it's a part of the U2 auxiliary factor complex. U2AF1 promotes the binding of the U2 snRNP to the 3' branch splice site by recognizing and binding the AG-dinucleotides [70]. U2AF1 has been shown to be essential for normal hematopoiesis. Conditional ablation of *U2af1* in homozygous *U2af1*$^{+/+}$ Mx1-Cre mice resulted in fatal bone marrow failure, where mice died between 10-14 days after their initial pIpC injection [74]. Analysis done between day 8-10 found that these mice had significant loss of white blood cells (WBC), neutrophils, red blood cells (RBC), hemoglobin (Hb) and platelet counts. Blood smears also demonstrated pancytopenia and severe aplasia upon *U2af1* loss [74]. There were also severe hematopoietic development defects observed, as *U2af1* loss resulted in reduction of the entire HSPC compartment, as well as a reduction of downstream progenitors and myeloid cells. This defect was found to be cell autonomous, and it was shown that *U2af1* deficiency reduced HSPC function *in vivo* through competitive transplants [74]. The defect in HSPC function was so severe that it was not possible to test long term self-renewal capacity through secondary transplants. Mechanistically, it was found that depletion of *U2af1* caused apoptosis in blood cells and led to an increase in phosphorylated ser139 **γ**-H2AX, indicative of DNA damage [74]. Transcriptomic profiling of *U2af1* depleted HSPCs showed a loss of the HSC specific program and enrichment in DNA damage response genes. *U2af1* depleted HSPCs also experienced aberrant splicing, with exon skipping/inclusion (cassette exons) being the most frequent event [74]. Differential gene expression and altered splicing were observed in *Nfya* and *Pbx1* transcripts and forced expression of NFYA and PBX1 could partially rescue the colony formation defects in *U2af1* depleted HSPCs [74]. U2AF1 is also a commonly mutated target in myelodysplastic syndrome (MDS), with mutations in ~11% of MDS patients [75]. The most common U2AF1 mutation in human cancers is U2AF1(S34F) [76]. In normal hematopoiesis conditional *U2af1 S34F* knock-in causes defects in blood cells and

abnormal splicing patterns [77]. Upon conditional induction of *U2af1 S34F* expression through an Mx1-Cre system, mice develop multilineage cytopenia, experiencing reduction in RBCs, WBCs, as well as reduction in the frequency of HSPCs [75, 77]. These mutant expressing HSPCs also have a loss of function, as they lose their reconstitution capacity during competitive transplantation [75, 77].

SRSF2, a member of the serine arginine rich protein family, is another important factor in the splicing machinery. SRSF2 is involved in exon recognition by binding pre-mRNA through its RRM domain and promoting spliceosome assembly at the splice sites [70, 78]. Several studies have investigated SRSF2's role in hematopoiesis and have identified it's essential role in normal blood development. Homozygous depletion of *Srsf2* during embryonic development results in defective fetal liver hematopoiesis as shown by reduced fetal liver HSPCs, and increased apoptosis and quiescence [79]. *Srsf2* depleted embryos also died between embryonic days 16.5 – 18.5, with severe anemia and edema [79]. Fetal liver cells also had reduced *in vitro* clonogenicity abilities [79]. During adult hematopoiesis, loss of *Srsf2* resulted in similar phenotypes in mice, with reduced HSPC number and a loss of reconstitution capacities during competitive transplants [79]. A separate study found *Srsf2* depletion reduced WBCs and caused BM aplasia [80]. Investigating a common MDS SRSF2 mutation, using heterozygous mice with *Srsf2 P95H* mutation, it was found that this mutation causes defects in adult hematopoiesis distinct from loss of *Srsf2*. This *Srsf2 P95H* mutation caused myeloid and erythroid dysplasia, not seen in the knockout mice [80]. These mutant mice also showed an expanded HSPCs compartment with an increase of HSPCs undergoing cell cycling, and an increase in apoptosis [80]. Competitive transplant experiments with mutant mice showed a loss of HSPC function in the *Srsf2* depleted mice, as seen by a dramatic loss of chimerism. The *Srsf2 P95H* mutant mice also showed a loss of chimerism, but not as

dramatic as the loss of *Srsf2* [80]. Very interestingly, at 18 weeks post-transplant, the knockout mice showed low chimerism and HSPC numbers, but the *Srsf2 P95H* instead showed an expansion of the HSPC compartment. Suggesting that mutant *Srsf2's* role in regulating hematopoiesis is distinct from loss of *Srsf2* [80]. Transcriptomic profiling demonstrated that *Srsf2 P95H* mutations alter its normal preference to exonic splicing enhancer (ESE) sequences [80].

Besides the major splicing machinery, there is a second class of intron processing that is spliced by a separate spliceosome complex, referred to as the minor spliceosome (or U12) [81]. ZRSR2 is a component of the minor spliceosome and is involved in recognition of 3' intron splice sites. ZRSR2 has also been found to play a role in normal hematopoiesis. Conditional ablation of *Zrsr2* resulted in enhanced proliferation and colony formation capacity *in vitro*, as well as enhanced *in vivo* HSC self-renewal capacity as shown by competitive transplant assays [82]. It was also observed that there were increased number of LT-HSCs and HSPCs following primary and secondary transplantations [82]. Additionally, there was more cell cycling (as measured by BrdU incorporation) and apoptosis in the LT-HSCs with depleted *Zrsr2* [82]. RNA-sequencing demonstrated that *Zrsr2* loss led to increased U12 type intron retention, creating an altered gene profile. Furthermore, it was identified that intron exclusion of LZTR1 conferred competitive advantage in *Zrsr2*-null HSPCs [82].

RBPs involved in RNA Editing: ADAR1

Adenosine deaminases on RNA (ADAR) are a family of proteins involved in adenosine to inosine (A to I) conversion during post-transcriptional RNA editing [83]. This level of post transcriptional regulation adds additional genetic variation that may not be directly

encoded in the genome. Several studies have shown that loss of ADAR1 during embryogenesis results in embryonic lethality during embryonic day 11-12 [84, 85]. It has been seen that ADAR1 is dispensable for the emergence of HSCs during embryogenesis [86]. However, loss of ADAR1 in embryos also results in widespread apoptosis across numerous tissues [84]. During adult hematopoiesis ADAR1 depletion results in a dramatic reduction in reconstitution potential during non-competitive transplantation [87]. There is also preferential dependency in progenitors instead of on HSCs, with an increase in apoptosis in progenitors upon ADAR1 depletion [87]. A separate study also identified changes in adult hematopoiesis upon ADAR1 depletion, in which ADAR1 deficient mice experienced an expansion of HSPCs and induction of apoptosis in HSPCs [86]. Mechanistically it was found that ADAR1 depletion upregulates interferon pathways in HSPCs [86]. Suggesting ADAR1 is essential in HSPC maintenance and provides a protective role in suppressing interferon activation.

RBPs involved in Translation/Translational machinery

Proteins are synthesized from mRNA through the process of translation, which utilizes the ribosome as well as multiple associated factors. It has been demonstrated that there is a careful balance of protein synthesis in HSCs, and increased or decreased protein synthesis impairs proper HSC function [88]. For example, decreased protein synthesis through ribosomal mutation *Rpl24*$^{Bst/+}$ results in a reduction in reconstitution potential during competitive transplants [88]. Alternatively, increased protein synthesis through *Pten* depletion ultimately results in hematopoietic malignancies like leukemias [88]. Interestingly, OP-Puro (OPP) incorporation has shown that HSC's synthesize less protein per hour than other hematopoietic cells [88]. Thus, proteostasis (protein homeostasis) is essential for proper HSC function, where maintaining low synthesis

rates is imperative. In addition to this, HSCs must also maintain high protein quality. Recent work has shown increased protein synthesis led to reduced protein quality (increased misfolded proteins), and that even a modest decline in protein quality results in impaired HSC self-renewal [89]. In addition to protein synthesis and quality, several factors in the translation machinery, as well as other RBPs known to regulate translation have been identified to have an impact on HSC function.

Translation Factors: 4E-BP1, 4E-BP2

Translation is divided into multiple stages: initiation, elongation, and termination. The initiation step is the binding of the ribosome to the mRNA, elongation is the process of creating the peptide chain, and termination is when the stop codon is encountered, and the ribosome dissociates from the mRNA [90]. Each of these processes require various translation factors, some of which have been seen to be involved in regulating HSC protein synthesis and HSC function. For example, several eIF4E binding proteins (4E-BPs) have been shown to regulate HSC function [91]. 4E-BPs act as translation initiation inhibitors by binding the cap-binding protein eIF4E and preventing the eIF4F complex assembly. mTORC1 phosphorylation of 4E-PBs releases the 4E-BPs from eIF4E and allows cap-dependent translation initiation to commence [90]. Total levels of 4E-BP1 and 4E-BP2 are higher in HSCs compared to downstream progenitors like Gr1+, Pro-B, Pre-B and IgM+ B cells. There are also higher amounts of phosphorylated 4E-BP1 and 4E-BP2 in HSCs, compared to downstream progenitors [91]. Depletion of either 4E-BP1 or 4E-BP2 doesn't alter global protein synthesis, but simultaneous depletion of both 4E-BP1 and 4E-BP2 increases protein synthesis in HSCs and not in the other hematopoietic progenitors [91]. Steady state hematopoiesis remains largely unchanged during 4E-BP1/2 loss, however upon competitive serial transplantation with combined 4E-BP1 and

4E-BP2 depleted it was seen that there is a loss of HSC reconstitution potential during secondary transplantation [91].

MUSASHI Family of RBPs: MSI1 and MSI2

The MUSASHI family, which consists of MUSASHI-1 (MSI1) and MUSASHI-2 (MSI2), are a pair of RBPs that both contain two RRM domains to bind RNA. Both MSI1 and MSI2 have been implicated in stem cell function in various tissue types [92]. For example MSI1 has been seen to promote neural stem cell maintenance by binding to the 3'UTR of *m-Numb* transcripts and repressing their translation [93]. Additional work has also shown that MSI1 has translation repression activity, through a mechanism that involves MSI1 binding to poly(A) binding protein (PABP) and completing with eIF4G for PABP binding sites. This prevents the formation of the 80S ribosome complex [94].

In the hematopoietic system, the predominant MUSASHI protein expressed is MSI2 and it has been shown to be highly expressed in HSCs with its expression decreasing as cells differentiate [95]. Several studies have found MSI2 to be essential for HSC function, with shRNA mediated knockdown of MSI2 leading to impaired self-renewal and reconstitution potential [95, 96]. This has also been demonstrated in mouse models with a conditional Mx1-Cre MSI2 and gene-trap MSI2 model, where MSI2 depletion resulted in impaired transplantation potency [36, 97]. Additionally, MSI2 depletion also results in a reduced number of HSPCs and HSCs, as well as increased cell cycling [36, 97]. Alternatively, overexpression of MSI2 increased the frequency of HSPCs and activates HSPCs into cell cycling [95]. Additionally MSI2 has been seen to impact cell fate decisions in HSPCs, where overexpression of MSI2 increases asymmetric division of NUMB [95] and MSI2 depletion causes an increase in symmetric commitment [36].

Mechanistic investigation has revealed a transcriptional program that downregulates the proliferative program in MSI2 depleted mice (gene trap model) [97]. Transcriptomic profiling of the Mx1-Cre Msi2 mouse model found *Msi2* depleted HSPCs had a loss of the self-renewal program and an increase in differentiation [36]. Through HITS-CLIP in K562 cells it was demonstrated that MSI2 directly targets RNA regulation/metabolism and the self-renewal signaling program [36]. Follow-up on the TGF-β signaling pathway demonstrated that there was an increase in TGFBR1 protein expression upon MSI2 depletion but a decrease in the downstream targets of the pathway, as shown by decreased phosphorylated SMAD2/3 in HSCs and reduced p57 expression indicating MSI2 depletion reduces TGF-β signaling [36].

Recent work has uncovered MSI2's transcriptional binding profile within the HSPC compartment. Utilizing the HyperTRIBE technique, MSI2 has been shown to bind predominantly to transcripts in the 3'UTR region in all HSPC populations [98]. It was also seen that HSCs have more MSI2 edit sites and more gene targets compared to MPP populations, suggesting higher MSI2 binding activity in HSCs [98]. ENRICHR pathway analysis demonstrated that MSI2 targets in HSCs are associated with stem cell programs, where MSI2 targets in MPPs are enriched for lineage programs [98]. This indicates that MSI2 activity is cell context dependent. Most interestingly, it was also found that MSI2 binding activity in HSPCs differed from its activity in leukemia stem cells (LSCs) where there was more MSI2 binding activity in LSCs. It was also seen that MSI2 is more required in LSCs in order to maintain expression of certain MLL associated targets, such as HOXA9. Depletion of MSI2 in HSPCs doesn't reduce HOXA9 proteins or transcripts but depletion of MSI2 in LSC cells resulted in a dramatic reduction of HOXA9 protein [98].

RBP Therapeutic Strategies in Leukemia

Leukemia is a hematological disorder characterized by rapid accumulation of immature myeloid or lymphoid progenitor cells that have a block in their ability to differentiate [99]. Among one of the classes of leukemia is acute myeloid leukemia (AML), which is most prevalent in older adults and has a 30.5% survival rate after diagnosis according to the National Cancer Institute (NCI) SEER dataset. AML is a heterogeneous disease that can present itself with various molecular and cytogenetic abnormalities, among these can include mutations in TP53, RUNX1, NPM1, ASXL1 as well as translocations involving MLL1 and AML1 rearrangements [100]. The standard of care since the 1970's has been the 3 + 7 (3 days of daunorubicin + 7 days of cytarabine) chemotherapy regimen [100]. Additionally, some patients can also undergo hematopoietic stem cell transplantation (HSCT), but this option is not possible for those who are elderly or have a comorbidity that would put them at risk. Although some patients see effective results with these styles of therapy, many often relapse after chemotherapy or HSCT [101].

LSCs were first identified as a rare population of CD34+CD38- stem cells capable of initiating leukemia in severe combined immune-deficient mice (SCID) [102]. LSCs are believed to arise from HSCs and progenitor cells [103] but the exact root of their initiation varies in patients. Through stepwise acquisition of multiple genetic mutations or alterations, LSCs are formed from stem or progenitor cells [104, 105] (Figure 1.1). LSCs develop proliferative or survival advantages and result in suppression of normal hematopoiesis [12]. Since LSCs are believed to drive the disease, it's imperative to target them during therapy. Unfortunately, because they maintain cell cycle quiescence, they're often chemotherapy resistant and the cause of relapse for some patients [106]. Therefore, it is important for the development of new therapeutic targets for LSCs. In

recent years, RBPs have emerged as important regulators of leukemia and LSCs and represent a novel therapeutic approach. The remainder of this chapter describes various RBPs involved in leukemia and LSC function, including several that have resulted in potential therapeutic approaches or are in development for treatment of AML.

RNA Methylation RBPs in AML: METTL3/METTL14, FTO

METTL3, a member of the m^6A methyltransferase complex, has been implicated to be necessary for the maintenance of the leukemic state and a therapeutic target in AML as shown in various studies. In two independent CRISPR screens, one with mouse MLL-AF9 driven leukemia, and the other including Flt3-ITD driven leukemia, *Mettl3* was identified as a hit and shown to be essential for leukemia maintenance [107]. *Mettl3* depletion in AML was found to reduce colony formation after serial re-plating, and cells also experienced increased differentiation and a loss of cell proliferation capacity *in vitro* [107]. *In vivo*, *Mettl3* depletion in mice results in a significant increase in survival [107]. A separate study found that human AML cell lines and patient samples had higher levels of METTL3 than CD34+ cord blood HSPCs [108]. Additionally, it was shown that METTL3 hairpin mediated depletion in human AML reduced m^6A levels and proliferation, while also increasing apoptosis and differentiation [108]. *In vivo* xenograft mouse models with human AML showed METTL3 depletion delayed leukemia progression [108]. Overexpression of METTL3 also increased cell growth, however overexpression of catalytic dead METTL3 did not impact on growth, suggesting this effect is mediated through METTL3's m^6A deposition activity [108]. Mechanistically it was found that METTL3 depletion led to decrease in c-MYC, BCL2, and PTEN protein levels through translational control [108]. Another key component of the m^6A complex, METTL14 has also been implicated in regulating AML function. Similar to its effects on normal HSPCs,

METTL14 is more highly expressed in AML patient samples and human cell lines compared to bone marrow mononuclear cells from healthy donors. This overexpression is observed in mice with various AML oncogenic backgrounds [59]. Treatment with differentiation inducing agents caused a reduction in METTL14 transcripts and total m^6A levels [59]. Using a conditional mouse model, it was also shown that *in vivo Mettl14* depletion prolonged survival and demonstrated that *Mettl14* is essential for MLL-AF9 leukemia maintenance. This effect continued in a secondary leukemia transplant, implicating *Mettl14* in regulating LSC function [59]. *In vitro* colony formation assays also demonstrated a reduction in colony number and size after serial plating. Additionally, assessment of LSC frequency through an *in vivo* limiting dilution assay demonstrated a reduction of LSC frequency upon *Mettl14* KO, with the WT group having 1/433 LSCs, and the *Mettl14* KO having 1/3218 LSCs [59].

The m^6A demethylase FTO has also been shown to be important in AML function. For example, FTO is seen to be overexpressed in AMLs with various oncogenic backgrounds such as those with MLL rearrangement, FLT3-ITD and NPM1 mutations [109]. Forced expression of FTO in human AML cell lines promoted cell growth, while hairpin based knockdown reduced cell growth. *In vivo* forced expression of FTO also caused accelerated MLL-AF9 leukemogenesis, and depletion of *Fto* caused a delay in leukemia [109]. It was found that FTO targets AML functional transcripts like *Asb2* and *Rara,* by regulating their expression. The effects of FTO depletion can be largely rescued by overexpression of ASB2 or RARA [109].

Chemical modulation and inhibition of these RNA modifying proteins is still in its infancy, but multiple companies have begun developing therapeutics against various RBPs with RNA modification activity [110]. Among these potential chemical inhibitors is STM2457,

a therapeutic developed by STORM Therapeutics, which has recently been described to be an inhibitor of METTL3. Via crystal structure STM2457 has been shown to be in complex with METTL3-METTL14 [111]. Treatment of AML human cell lines with STM2457 resulted in reduced proliferation [111]. There is also an increase in differentiation, and apoptosis in mouse and human AML, all without impacting normal HSPCs under the same dosage [111]. *In vivo* efficacy investigation using AML patient derived xenograft (PDX) models found that mice treated with STM2457 had prolonged survival with multiple oncogenic backgrounds (MLL-AF6, NPM1c). The mice also didn't experience any overt toxicity [111]. To determine METTL3's inhibition on LSC activity, levels of CD93+ and L-GMP populations were assessed, and it was found that both CD93+ and L-GMP populations were reduced. Upon secondary transplantation, the delay in leukemia was increased in the STM2457 re-transplanted samples, compared to the control re-transplanted group [111]. All this indicates that METTL3 inhibition by STM2457 treatment leads to loss of LSC functional activity *in vivo*. Most recently, in 2022, STORM Therapeutics has taken a METTL3 inhibitor, STC-15, to humans with a clinical trial in a phase one study (NCT05584111).

Multiple FTO inhibitors have also been in development to target LSCs in AML. Based on rational design, two FTO inhibitors FB23 and FB23-2 were identified to have selective inhibition in FTO demethylase activity. Treatment with these inhibitors led to reduced cell proliferation, and treatment with FB23-2 also led to increased differentiation, apoptosis and an arrest in cell cycle [112]. Moreover, treatment with FB23-2 demonstrated an increase in survival *in vivo* using PDX and human cell line xenograft mouse models [112]. More recently, a series of compound screens identified more small molecule FTO inhibitors, among the most promising were CS1 and CS2 [113]. Modeling suggests that both these small molecules block FTO's catalytic activity. Treatment with these

molecules showed a reduction in cell viability selective to AML patient samples, and no significant effect in healthy controls [113]. FTO inhibition with CS1 and CS2 also demonstrated an increase in apoptosis and reduction in cell cycling. Multiple *in vivo* limiting dilution assays also showed that CS1 and CS2 reduced the frequency of LSCs [113]. Altogether these results highlight the promising future for FTO targeting therapeutics in treating AML.

Splicing RBPs in AML: SF3B1 and RBM39

A frequently mutated class of proteins in hematological malignancies is the spliceosome. For example, ~60% of MDS patients, and around half of secondary AML patients have mutations in the splicing machinery [114]. The most frequently mutated splicing proteins are SRSF2, U2AF1 and SF3B1, with reported frequencies in AML occurring 6-10%, 4-8%, and 3% respectively [115]. In MDS, SF3B1 mutations are strongly correlated with ringed sideroblasts (MDS-RS), and around 80% of MDS-RS patients have SF3B1 mutations [116]. The sequential acquisition of various mutations or re-arrangements leads SF3B1 mutant MDS-RS patients to progress into AML. In fact, it has been shown that MDS-RS with SF3B1 mutations in HSC populations can give these clones an advantage leading to persistent long term engraftment biased towards the myeloid lineage [116].

Another important protein involved in splicing that has been implicated in AML is RBM39, a serine/arginine-rich RNA binding protein. This RBP has been reported to be involved in alternative splicing, sharing sequence similarity with U2AF65 [117, 118] and has also been seen to be upregulated in various cancer types like lung, breast and colorectal cancer [118]. A recent CRISPR screen investigating RBP dependencies in

AML identified RBM29 as being required for AML [119]. RBM39 expression was found to be higher in AML patients than in normal hematopoietic cells. Depletion of RBM39 also resulted in a reduction of growth potential and an increase in apoptosis in multiple AML human cell lines [119]. *In vivo* experiments with the RN2 (MLL-AF9 NRAS G12D) mouse line showed that depletion of RBM39 prolonged survival [119]. Multiple omic strategies found that RBM39 loss altered splicing and led to dysregulation of the programs required for AML cell growth. For example RBM39 loss results in a downregulation of the HOXA9 program [119].

Chemical modulation of splicing factors has been an ongoing effort that has led to the identification of various naturally derived chemicals. Spliceostatin A (SSA) is one such inhibitor of SF3B1, that was originally derived from *Pseudomonas*. SSA interferes with snRNA U2 binding to the 3' splice site [120]. Subsequently additional natural chemical products have been identified for inhibition of SF3B1 utilizing similar mechanisms of actions. Such compounds include pladienolides, and GEX1 [120]. H3B-8800 is another splicing modulator which has had pre-clinical success, and acts by interacting with the SF3b complex [121]. It was shown that treatment with H3B-8800 inhibits splicing in both WT and mutant forms of SF3B1. It was also shown that H3B-8800 treatment in the human leukemia cell line, K562, cells had a reduction of tumor burden using *in vivo* xenograft models and this was in WT and mutant SF3B1 background [121]. In addition to SF3b complex, RBM39 has also been a target of chemical modulation in AML. Sulfonamides (like indisulam, E7820, and chloroquinoxaline sulfonamide) act as selective degraders of RBM39. Treatment with indisulam degrades not only RBM39 but also leads to downregulation of HOXA9 target gene protein expression like MYB [119]. Using *in vivo* xenograft models with AML cell lines, it was found that indisulam treatment

leads to a reduction in tumor burden as well as a delay in leukemia. This was also observed using PDX models [119].

Transport RBPs in AML: XPO1

XPO1, also known as CRM1, is the main nuclear exporter in humans and found to be frequently overexpressed in AML [122]. XPO1 is responsible for the transport of over 200 proteins, among which includes significant targets involved in oncogenesis like p53, p21, Rb, PI3K/AKT, and p27 [123, 124]. XPO1 overexpression has been linked to poor prognosis or resistance to chemotherapy in various solid tumors (ovarian, pancreatic, brain, and cervical cancer) as well as hematological cancers like AML. Because of this XPO1 became an attractive therapeutic target and has been the subject of various novel inhibitors and clinical trials. The first XPO1 inhibitor, leptomycin B (also known as elastocin), was a natural product of *Streptomyces* bacteria that worked by irreversibly blocking Cys528 in the nuclear export signal (NES) domain. However a phase I trial for this compound experienced profound cytotoxicity and was discontinued [124, 125]. Further exploration into inhibitors for nuclear transport led to the development of selective inhibitors of nuclear transport (SINE) compounds, which are reversible covalent molecules. Treatment with SINE compounds lead to inhibited tumor growth, cell cycle arrest, differentiation and induction of apoptosis across numerous solid and hematological cancers [124]. Selinexor or KPT-330 is among one of the most studied, and is involved in multiple clinical trials across various solid and hematological malignancy clinical trials [124]. Used as a monotherapy, Selinexor has proven to be safe and efficacious in patients with relapsed or refractory AML [126]. Out of 81 evaluated patients, 31% demonstrated stable disease (≤50% increase in bone marrow blasts from baseline) [126]. In addition to monotherapy strategies, Selinexor has also been used in

combination therapy. For example, a phase I clinical trial, with Selinexor and hypomethylation agent decitabine, in relapsed/refectory AML and older untreated patients with AML found and overall response rate of 40% [127]. In a separate phase I study combination of DNA-damaging agents cytarabine and mitoxantrone were used with Selinexor, in newly diagnosed or refractory/relapsed AML patients. In this study, half the patients achieved complete remission, with serious adverse effects occurring in 30% of patients. Despite the high number of toxicities experienced, most were manageable with supportive care, and only one was fatal. It is unclear if this effect was a result of the high dose of cytarabine or Selinexor. [128]. Overall, Selinexor mediated inhibition of XPO1 resulted in marked toxicity precluding its therapeutic potential in AML patients.

RNA Editing RBPs in AML: ADAR1

ADAR1 has been found to be involved in various cancers like lung cancer, cervical cancer, and AML. Investigation of ADAR1's role in AML found ADAR1 to have higher expression in patients compared to healthy controls [129]. Depletion of ADAR1 in a human AML cell line resulted in reduced cell growth, reduced colony formation potential and an increase in G0/G1 phase suggesting that ADAR1 controls AML cell proliferation capacity [129]. Further mechanistic investigation found that ADAR1 depletion also led to downregulation of several Wnt pathway effectors, like β-catenin, c-MYC, TCF4 and CCND2. All these same effects were observed *in vivo* using xenograft mouse models. It was found that ADAR1 loss resulted in reduced tumor burden and the resected tumors also had reduced levels of β-catenin, c-MYC, TCF4 and CCND2 [129]. Suggesting that ADAR1 is involved with the Wnt pathway and is required for AML growth. A separate study, investigating ADAR's role in myeloid differentiation found ADAR1 and ADAR2 expression is increased as cells differentiate [130]. In blast crisis chronic myeloid

leukemia (BC-CML), it has been shown that JAK2 signaling and BCR-ABL activate ADAR1, which leads to disruption of the LIN28B/let-7 self-renewal axis [131]. Depletion of JAK2 led to decreased let7 family miRNAs and this was also the case with BCR-ABL depletion. Upon forced expression of both JAK2 and BCR-ABL in CD34+ cord blood, colonies had enhanced colony formation potential, and treatment JAK2 inhibitor (SAR302503) and BCR-ABL inhibitor (dasatinib) decreased LSC self-renewal potential as shown by colony formation assay [131]. Upon inhibition of JAK2 and BCR-ABL it was also seen that ADAR1 expression was reduced. Further investigation found that treatment of cells with ADAR inhibitor 8-azadenosine (8-aza) restored let7 miRNA expression and that *in vitro* replating of BC-CML progenitors was reduced [131]. Transcriptional profiling of ADAR1 overexpressing in human cord blood CD34+ progenitors also demonstrated that ADAR1 regulates the stem cell program [131]. Thus, ADAR1 inhibitors represent a potential novel therapeutic strategy in AML.

Further work will be necessary to develop novel ADAR1 inhibitors for use in AML. Pre-print work investigating prostate cancer, has uncovered a new potential ADAR1 small molecule inhibitor, ZYS-1 [132]. ZYS-1 binds ADAR1's catalytic pocket and inhibits catalytic activity. In a pre-print study, ZYS-1 was shown to suppress prostate cancer growth *in vitro* and have anti-tumor effects *in vivo* [132]. This study also highlights the broad effects of this molecule, showing that it reduces cell proliferation in AML patient samples [132]. This suggests that ZYS-1 could represent a novel therapeutic for AML, however more pre-clinical investigation will be necessary to fully uncover the *in vivo* effects and mechanisms ZYS-1 is impacting.

Translation RBPs in AML: eIF4E, eIF4A

As described before, eIF4E plays a major role in translation initiation, by its interaction with 4E-BPs and the eIF4F translation initiation complex. Upon being released from 4E-BP proteins, through mTOR mediated phosphorylation of 4E-BPs, eIF4E can properly bind eIF4G and form the translation initiation complex. eIF4E has been shown to be overexpressed in various solid and hematological cancers, including breast cancer, colon cancer and AML [133]. In AML patient samples it has been seen those elevated levels of eIF4E cause a blockage in myeloid differentiation, and eIF4E's oncogenic mechanism involves its binding to m7G caps on mRNA and impacting their mRNA export and translation [133-135]. Thus, inhibition of eIF4E is of interest for AML therapeutic strategies. Ribavirin, a broad spectrum anti-viral drug, has been seen to have eIF4E inhibitor activity by acting as a mimic of the m7G cap and blocking eIF4E activity [135]. Pre-clinical investigation demonstrated ribavirin treatment reducing tumor burden in mouse models [133]. In a proof of principle clinical trial with ribavirin using 11 AML patients, it was found that 9% experienced complete remission with 18% experiencing partial remission, and no significant toxicity [135]. Despite the promising results of this clinical trial, all patients relapsed [136]. Upon deeper investigation, it was uncovered that sonic hedgehog transcription factors (GLI1 and UGT1A) are upregulated in resistant cells [136]. This resistance could be overcome by inhibition of GLI1 [136], revealing a combination strategy that could benefit some patients in overcoming relapse. Thus, more investigation will be necessary to uncover additional combination therapies that could be used along with ribavirin.

Additionally, eIF4E can also be regulated by phosphorylation of its Ser209 residue through MAP kinase-interacting kinases (MNK) (specifically MNK1 and MNK2). Phosphorylated eIF4E has been linked to tumor biology [137]. Phosphorylation of eIF4E promotes translation of mRNAs involved in cell proliferation and survival, some known to

enhance malignancy including c-MYC [138]. Because of this, inhibition of MNK1 and MNK2 is of interest for therapeutic strategy in targeting phosphorylation of eIF4E. A pre-clinical study for MNK1 and MNK2 inhibitor Tomivosertib (also known as eFT-508) in AML demonstrated effective suppression of eIF4E phosphorylation and reduced AML proliferation and survival in human AML cell lines, especially in those harboring FLT3 activating mutations [139]. In combination with venetoxlax, tomivosertib synergistically enhanced the anti-leukemic effect [139], however the exact mechanism for why this combination is synergistic remains to be uncovered.

Another component of the translation initiation machinery that has potential as a therapeutic strategy is eIF4A which is the ATP dependent RNA helicase that makes up part of the eIF4F translation initiation complex. It has been seen that eIF4A is highly expressed in AML patient samples compared to cord blood [140]. Treatment of AML cells with rohinitib (RHT) induced apoptosis *in vitro* in a dose dependent manner, and it was found that AML with FLT3-ITD were more sensitive to RHT treatments. Additionally, *in vivo* studies with a xenograft mouse model using human cell line MOLM13 showed a decreased tumor burden and prolonged survival upon RHT [140]. Interestingly, it was also demonstrated that RHT treatment was more sensitive in patient AML initiating cells (CD34+CD38-) than in normal HSPCs (CD34+CD38-), and *in vivo* PDX transplants with RHT pre-treated primary patient AML demonstrated a reduction in tumor burden [140].

MSI2's role in AML

MSI2 has been found to be overexpressed in various cancers like ovarian cancer [141], non-small cell lung cancer [142], colorectal cancer [143] and cervical cancer [144]. MSI2 overexpression has been linked to poor prognosis in various cancers, including multiple

hematological cancers [92, 145]. MSI2's role in hematological disease was first identified by uncovering a translocation in chronic myeloid leukemia (CML) that caused a MSI2-HOXA9 fusion, in which both MSI2's RRMs are retained [146]. Additional translocations have been identified, including MSI2-EVI1 rearrangement in various hematological malignant conditions [147], TTC40-MSI2 fusion in de novo AML [148], and PAX5-MSI2 fusion in B cell acute lymphoblastic leukemia (B-ALL) [149]. Exactly how these fusions contribute to disease remains to be understood. Clinically, it has been shown that high MSI2 levels in patients with CML or AML have worse prognosis and poorer outcomes [95, 150, 151].

Functional studies investigating MSI2's role in myeloid malignancies have uncovered that MSI2 is important for leukemia and LSCs. For example, in AML and BC-CML cell lines, hairpin knockdown of MSI2 leads to reduced cell growth, increased apoptosis and differentiation [95]. Additional work investigating MSI2's role in LSC function, using a Mx1-Cre MSI2 flox/flox ($Msi2^{fl/fl}$) mouse model, found MSI2 to be required for MLL+ LSCs [152]. Upon *Msi2* depletion, *in vivo* leukemia progression was delayed, and cells had a reduction in cKit expression, as well as an increase in differentiation, but no changes in cell cycle or apoptosis [152]. Secondary transplants were performed to assess functional LSC activity, and MSI2 depletion showed a delay in leukemia that was longer than the primary transplants, with no effects on leukemia cell homing to the bone marrow or spleen [152]. Transcriptional profiling was conducted to mechanistically uncover how *Msi2* impacts LSCs, and it was found that MSI2 depletion in LSCs caused a loss of the stem cell program and signaling enrichment for differentiation [152]. Additional characterization with HITS-CLIP data showed that MSI2 directly binds to and regulates MLL direct and indirect targets like *Hoxa9*, *Myc*, and *Ikzf2* [152]. Further work profiling MSI2's binding activity in human AML and LSCs has identified the exact MSI2

binding location on some of these transcripts (*Hoxa9* and *Ikzf2*) [98]. Luciferase reporter assays using mutated transcripts (HOXA9 and MYB 3'UTR) confirms that these binding sites are regulatory for protein expression [98]. As mentioned before, this study also identified that MSI2 is preferentially required in LSCs vs. HSPCs to maintain protein expression of certain proteins (such as HOXA9) [98], and presents a window of therapeutic intervention even in patients that present equivalent levels of MSI2 expression in leukemia and normal blood cells.

Chemical modulation of MUSASHI proteins is still in early in development; however, several efforts have been undertaken to identify potential MUSASHI inhibitors. High throughput chemical screens have made identification of chemical modulators possible. In one screen of over 30,000 compounds, oleic acid was identified as a MSI1 allosteric inhibitor, that interacted with MSI1's N-terminal RRM and produced conformational changes that prevented MSI1 RNA binding activity [153]. A separate screen using fluorescence polarization, -glossypol was identified as the top hit for MSI1 inhibition, and found it interacts with the RNA binding pocket of MSI1. Orally administered -glossypol in a colon cancer xenograft model showed anti-tumor effects [154]. A small chemical screen of 6208 compounds investigating small molecules that interrupted MSI1 and MSI2 RNA binding activity identified several potential inhibitors with high potency [155]. One of these compounds is the commercially available Ro 08-2750 (Ro) molecule. Follow-up investigation on Ro found that it directly binds to MSI2's RRM1 domain and interrupts RNA binding activity [156]. Additionally, treatment of mouse AML cells with Ro resulted in increased differentiation and apoptosis, as well reduced colony formation abilities and reduced expression of MSI2 regulated targets like HOXA9, cMYC and SMAD3 [156]. *In vivo* Ro treatment also reduced tumor burden in a MLL-AF9 mouse model [156]. In human AML cell lines Ro treatment had similar anti-leukemic effects

showing increased apoptosis and differentiation [156]. Importantly, in AML patient samples, Ro treatment at 5μM had reduced colony formation potential compared to CD34+ cord blood cells [156]. Despite its apparent effectiveness in several hematopoietic malignancies, its poor drug-like properties, modest potency, and selectivity precludes its clinical relevance. Thus, the development of novel MSI inhibitors is needed.

Table 1 Summary of Several RNA binding proteins in Normal Hematopoiesis and Leukemia with Therapeutic Potential

RBP	mRNA process	Role in normal hematopoiesis	Role in leukemia/LSCs	Therapeutic/Small molecule
METTL3	RNA m6A methylation	Important for embryonic and adult hematopoiesis, maintains functional HSCs and HSC cell fate. Regulates *Myc* m6A levels, regulating MYC expression.[52, 54-56]	Overexpressed in AML, depletion leads to a loss of AML maintenance with increased differentiation, apoptosis, and a delay in leukemia *in vivo* [107, 108]	STM2457, small molecule shown in complex with Mettl3-Mettl14 [111]
METTL14	RNA m6A methylation	METTL14 highly expressed in HPSCs compared to downstream progenitors and regulates differentiation of human CD34+ cord blood, depletion causes mild loss of HSC activity (not as severe as METTL3 loss) [58, 59]	Overexpressed in AML, depletion leads to prolonged survival *in vivo*, and reduced LSC frequency [59]	

RBM15	RNA m6A methylation	Maintains HSC reconstitution capabilities. Depletion leads to HSPC expansion and decreased B cell differentiation. [61, 62]	Chromosomal translocation RBM15-MKL1 found in AML patients, depletion leads to decreased proliferation and apoptosis in BC-CML [157-159]	NA
YTHDF2	RNA m6A methylation	Involved in maintaining HSCs, depletion leads to expansion of HSCs and increased transplantation potential *in vivo*. [66]	Overexpressed in AML, and essential in maintaining AML LSCs in vivo. [160]	YTHDF inhibitor ebselen (not yet tested in leukemia) [161]
YTHDF3	RNA m6A methylation	Depletion leads to impaired HSC reconstitution potential *in vivo*. Translationally impacts expression of CCND1 to regulate HSC self-renewal [68]	NA	
FTO	RNA m6A methylation	Overexpression of FTO in CD34+ cord blood cells upregulates CXCR4 and enhances migration, homing and engraftment [162]	Overexpressed in AML. Depletion results in reduced cell growth. Impacts expression of ASB2 and RARA, which have functional effects on AML [109]	Inhibitors: FB23, FB23-2 [112], CS1, CS2 [113] Upregulates Expression: Angiotensin II (AGII) [162]
SF3B1	Splicing	Heterozygous depletion causes mild effects in steady state HSCs, but compromises HSC transplantation potential *in vivo* and proliferation	Frequently mutated in MDS-RS and AML. [115, 116]	Spliceostatin A (SSA), pladienolides, GEX1, HEB-8800 [120, 121]

		capacities *in vitro* [72, 73]		
U2AF1	Splicing	Homozygous depletion of *U2af1* causes fatal bone marrow failure in mice, shows reduced HSPC compartment and HSCs have reduced functional reconstitution potential [74]	Frequently mutated in MDS and AML [75, 77]	AML U2AF1 mutant cells are sensitive to sudemycin [163]
SRSF2	Splicing	Homozygous depletion of SRSF2 results in defective fetal liver and adult hematopoiesis, demonstrating reduced HSC function upon transplantation [78, 79]	Frequently mutated in MDS and AML [115, 164]	NA
ZRSR2	Splicing	Ablation of ZRSR2 results in enhanced proliferation and HSC self-renewal activity *in vitro* and *in vivo* [82]	Frequently mutated in MDS and AML [115, 164]	NA
RBM39	Splicing	NA	Overexpressed in AML. Depletion results in reduced proliferation, and increased apoptosis. *In vivo* depletion causes a delay in leukemia [119]	Sulfonamides (indisulam, E7820, chloroquinoxaline sulfonamide) [119]

ADAR	RNA editing	Dispensable for embryonic hematopoiesis but required for adult hematopoiesis. Depletion of ADAR1 leads to decreased HSPC reconstitution potential [86, 87]	Overexpressed in AML patients, depletion results in reduced cell growth and colony formation [129-131]	8-azadenosine [131]
XPO1	Transport	NA	Overexpressed in AML, linked to poor prognosis/resistance to chemo. [122]	Leptomycin B [124, 125], SINE compounds (such as Selinexor). [124, 126-128]
4EBP1, 4EBP2	Translation	Simultaneous depletion of 4E-BP1 and 4E-BP2 increases protein synthesis in HSCs and causes loss of reconstitution potential [91]	NA	NA
eIF4E, eIF4A	Translation	NA	Overexpressed in AML and enhances translation of oncogenic associated transcripts [133-135, 140]	Ribavirin for eIF4E inhibition [135], and rohinitib for eIF4A inhibition[140]
MSI2	Translation	Essential for HSC function. Depletion of MSI2 leads to impaired self-renewal and altered cell fate decisions. [36, 95-97]	Overexpressed in AML, associated with worse prognosis. Depletion of MSI2 leads to reduced cell growth, apoptosis and differentiation in AML and BC-CML. Depletion in LSCs causes a loss of the stem cell program.[92, 95, 98, 145, 151, 152]	Gossypol, oleic acid Ro 08-2750 [155, 156]

Conclusions and Future Directions

Post-transcriptional regulation processes are involved in ensuring proper HSC and HSPC function, and several have implications in malignant hematology. This chapter highlights several key RBP's involved in normal and leukemic function (Table 1), including many that are also potential therapeutic targets for AML. However, despite the tremendous efforts to expand our knowledge of RBPs, several questions remain as to the exact mechanisms for RBP's binding specificity and how they interact with other proteins. In recent years, there has been advances to better understanding RBP binding profiles, however limitations of crosslinking techniques like UV crosslinking immunoprecipitation (CLIP) have made it impossible to understand RBP binding activity in rare stem cell populations. The development of the HyperTRIBE technique has expanded the capacity to study RBP activity, by allowing the use of small quantities of starting materials, profiling rare stem cell populations is now possible [98, 165]. In addition to this method, a more recent method developed called STAMP uses an RBP-APOBEC1 fusion which causes C to U edits and allows identification of RBP binding sites. Combination of this technique with ribosome-APOBEC fusion allows a profiling of ribosome association in addition to RBP binding, providing more in-depth information on how RBPs impact translational activity [166]. Further use of these RNA editing techniques will be necessary to gain a wider understanding of RBP's activity in stem cells.

Additionally, many RBPs remain uncharacterized in certain cell contexts and the extent to which the RBP network functions also remains to be fully explored. Because of their therapeutic potential in various hematological and solid tumors, it is essential to further

explore the impact RBPs play in regulating stem cell properties. In AML there has been some effort to better understand the RBP network. A CRISPR/Cas9 domain screen that identified RBM39's role in regulating AML maintenance also identified and validated several other RBPs including: DHX37, SUPT6H and HNRNPH1 [119]. Separately, our group conducted an *in vivo* shRNA screen investigating MSI2's interactome and identified various RBPs that are novel regulators of AML [167]. Among such hits was RBMX, which our group went to further investigate and verified its requirement in mouse and human AML. RBMX's influence on AML occurs through its transcriptional control of CBX5 and downstream chromatin regulation [168]. In addition to RBMX, another RBP among the top hits in the shRNA screen was synaptotagmin binding cytoplasmic RNA interacting protein (SYNCRIP). It was also verified that SYNCRIP acts as a novel AML regulator [167]. SYNCRIP's role in normal and malignant stem cells will be discussed in depth in the remaining chapters. These screen studies highlight the value of investigating the RBP network. Future work will be necessary to understand the full extent to how the RBP network functions in stem cells, in other words how RBPs interact with each other and the RNA transcripts that are impacted in normal and malignant hematological cells.

Chapter II: SYNCRIP is required to maintain long term HSPC self-renewal capacities and proteostasis in hematopoietic stem cells

Modified from: Herrejon Chavez, F., Luo, H., Cifani, P. et al. RNA binding protein SYNCRIP maintains proteostasis and self-renewal of hematopoietic stem and progenitor cells. Nat Commun **14, 2290 (2023). https://doi.org/10.1038/s41467-023-38001-x*

Introduction

RBPs are important regulators of post transcriptional RNA processes, and many have been identified as key regulators in normal and malignant hematopoiesis as discussed in chapter I. Among such RBPs, previous work conducted in our lab uncovered SYNCRIP as an important regulator of AML. SYNCRIP (also goes by HNRNP Q), is composed of and acidic residue-rich domain towards the N-terminus, three RRMs in the central region, an RGG (Arginine–Glycine–Glycine Repeat) domain towards the C-terminus, and two NLS (nuclear localization signal) domains flanking the RGG domain. SYNCRIP has various isoforms, but the two most abundant in the blood are the full-length isoform hnRNP Q3 (623 amino acids) and the smaller isoform hnRNP Q1 (562 amino acids) [167]. The structural difference between these two isoforms is that SYNCRIP 562 isoform lacks a portion of the C-terminus, where it loses a nuclear localization signal (NLS) and a section of the RGG domain [169]. Previous work in HeLa cells have identified that the larger isoform, SYNCRIP 623, localizes to the nucleus, and the smaller isoform, SYNCRIP 562, localizes to the cytosol [170]. In addition to localization, these two isoforms have been found to have differential splicing effects in HEK293T *survival motor neuron 2 (Smn2)* transcripts, where SYNCRIP 562 enhances inclusion of exon 7, but SYNCRIP 623 acts as a negative regulator of exon 7 inclusion [170]. In AML, overexpression of either of these isoforms in MLL-AF9 cells causes an increase in colony formation abilities. Additionally, overexpression of SYNCRIP 562 in leukemia

cells caused a more aggressive leukemia *in vivo* [167]. However, exactly how each isoform regulates mRNA processes in blood cells remains to be investigated.

SYNCRIP is an RBP that has been shown to regulate various post transcriptional mRNA processes such as splicing [171, 172], translation [167, 173, 174], transport [175, 176], and stability [177, 178]. Prior to the MSI2 interactome shRNA screen, no other studies had identified a role for SYNCRIP in blood stem cells. Instead SYNCRIP had been seen be involved in the GAIT complex in immune cells [179], in exosomal miRNA sorting in hepatocytes [175], and many studies have explored SYNCRIP's role in neurons, finding that it influences neuronal development and morphogenesis [173, 178, 180-182]. In recent years, a separate study investigating T-cell acute lymphoblastic leukemia (T-ALL) has also uncovered an important role for SYNCRIP in blood malignancies. However, this study identified that SYNCRIP, along with SNHG5, act as tumor suppressors in T-cell ALL [183]. Suggesting SYNCRIP's roles may differ depending on the cell context.

In our lab's initial exploration of SYNCRIP, it was found that SYNCRIP is dispensable for normal hematopoiesis [167]. This suggested a therapeutic potential SYNCRIP may have for AML patients. However, the experimental design at that time was to develop a SYNCRIP deficient mouse by CRISPR-Cas9 methods, that involved injections of gRNAs and Cas9 mRNA into mouse zygotes and then collection of fetal liver cells at embryonic day 14 [167]. These fetal liver cells were then transplanted into CD45.1 expressing adult recipient mice and CD45.2 chimerism was measured to determine the amount of engraftment in a primary and secondary transplant setting. In the primary transplant there was no difference in engraftment upon SYNCRIP depletion, and secondary transplants only showed a mild decrease in engraftment [167]. This suggested that SYNCRP largely doesn't influence normal hematopoiesis. However, upon further

investigation, it was found that these CRISPR-driven KO fetal liver samples were mosaic for WT SYNCRIP and resulted in outgrowth of residual WT expressing cells during leukemia transplants [167]. Therefore, the need to develop a better genetic mouse model was necessary. We were also interested in understanding SYNCRIP's role in adult hematopoiesis. Since then, our lab has developed a novel SYNCRIP conditional knockout mouse model to better understand SYNCRIP's role during adult normal hematopoiesis.

Results

SYNCRIP has modest effects during adult steady state hematopoiesis

Public data accessible through bloodspot database [184] shows *Syncrip* expression levels in the mouse hematopoietic system being higher in HSPCs and progenitors compared to downstream differentiated cells, and we confirmed this with RT-qPCR (**Figure 2.1A**). Interestingly, this is like MSI2's expression pattern which is also expressed higher in HSPCs compared to differentiated progenitors [95]. To assess SYNCRIP's role in adult normal hematopoiesis, we developed a *Syncrip* conditional KO mouse model, that was designed to place two flox-P sites flanking exon 3 and 4 of the *Syncrip* genomic locus (**Figure 2.1B**). Upon excision with Cre recombinase, a premature stop codon is generated, and the resulting product undergoes degradation via nonsense mediated decay (NMD). These *Syncrip* flox/flox (*Syncrip*$^{f/f}$) mice were crossed with *Mx1-Cre* mice to generate *Syncrip*$^{f/f}$ *Mx-1-Cre*+ (cKO) and *Syncrip*$^{f/f}$ *Mx-1-Cre*- (WT) control. To induce excision within the *Syncrip* alleles, 6-8 week-old mice underwent two rounds

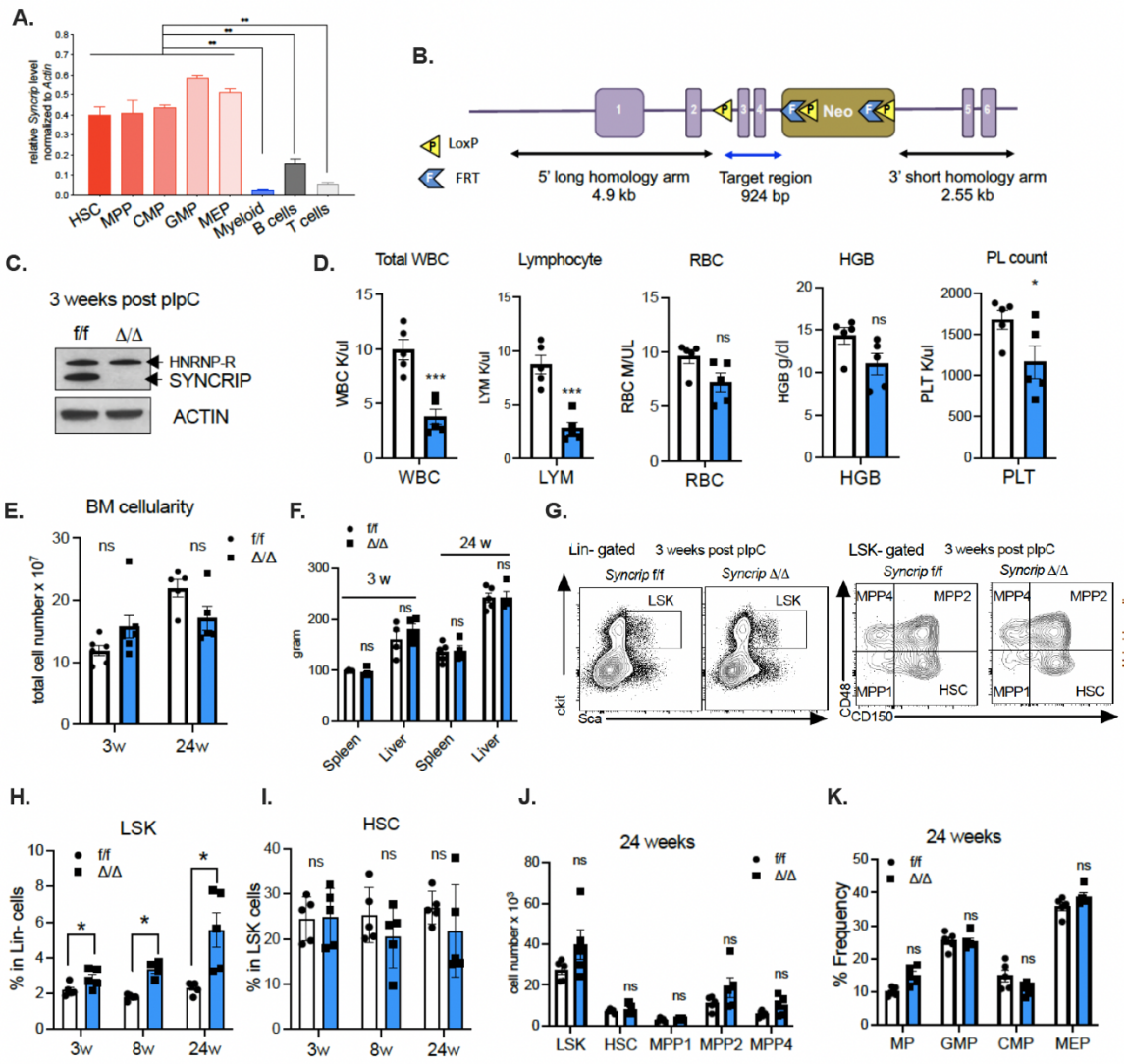

Figure 2.1: Syncrip is highly expressed in HSPCs and plays a mild role during steady state hematopoiesis

(A) qRT-PCR quantification of *Syncrip* mRNA expression across murine hematopoietic compartments. HSC – hematopoietic stem cells (Lin-Sca+ckit+ (LSK) CD48-CD150+); MPP – multipotential progenitor (LSK-CD48+/-CD150-); CMP – common myeloid progenitor (Lin-Sca+ckit- CD34+ FcγRII/III mid); GMP – granulocyte monocyte progenitor (Lin-Sca+ckit- CD34+ FcγRII/III high); MEP – megakaryocyte erythrocyte progenitor (Lin-Sca+ckit- CD34- FcγRII/III low); myeloid – (Mac1+Gr1+); B cells (B220+) and T cells (CD3+). **(B)** Diagram depicting the *Syncrip* locus and the targeting strategy to create *Syncrip* conditional knockout mouse (cKO). **(C)** Immunoblots showing efficiency knockout of SYNCRIP in bone marrow (BM) of knockout *Syncrip* Δ/Δ mice 3 weeks post pIpC injections. ACTIN was used as loading control. **(D)** Complete blood count (CBC) of *Syncrip* $^{f/f}$ and *Syncrip* $^{Δ/Δ}$ mice at 16 weeks post pIpC (n=5/phenotype). **(E)** Bone marrow cellularity in wild type *Syncrip* f/f (n=6) and knockout *Syncrip* Δ/Δ (n=5) mice at 3 weeks and 24 weeks post pIpC. **(F)** Spleen and liver weight from *Syncrip* $^{f/f}$ and *Syncrip* $^{Δ/Δ}$ mice 3- and

24 weeks post pIpC (n=4/genotype). **(G)** Representative flow analysis of hematopoietic stem and progenitor compartments from wild type *Syncrip* $^{f/f}$ and KO *Syncrip* $^{\Delta/\Delta}$ mice 3 weeks post pIpC. **(H)** Quantitative frequency of LSK (Lin_cKit+Sca-1+) cells within Lin- population from *Syncrip* $^{f/f}$ and *Syncrip* $^{\Delta/\Delta}$ mice at 3-, 8- and 24 weeks post pIpC (n=5/ genotype). **(I)** Quantitative frequency of HSC (LSK, CD150+CD48-) within LSK population from *Syncrip* $^{f/f}$ and *Syncrip* $^{\Delta/\Delta}$ mice at 3-, 8- and 24 weeks post pIpC (n=5/genotype). **(J)** Absolute number of HSC (LSK, CD150+CD48-) and MPP1 (LSK, CD150-CD48-), MPP2 (LSK, CD150+CD48+), and MPP4 (LSK, CD150-CD48+) in LSK population (n=5/ genotype). **(K)** Frequency of progenitor populations in *Syncrip* f/f and *Syncrip* Δ/Δ mice at 24 weeks post pIpC. MP-multi-progenitor (Lin-Sca+ckit); CMP; GMP and MEP.
All data represent mean $\pm$ s.e.m. p values were calculated by two-tailed t test unless specified. * $p<0.05$, ** $p<0.01$, *** $p<0.001$ and ns: not significant.

of poly(I:C) (pIpC) injection. With this method we obtained highly efficient depletion of SYNCRIP in bone marrow cells as demonstrated by SYNCRIP protein levels (**Figure 2.1C**). Note the antibody used for western blot assessment of SYNCRIP is nonspecific and additionally detects a separate RBP, hnRNP R, which is marked at a larger kDa size (**Figure 2.1C**). To understand *Syncrip's* role in adult hematopoiesis we first assessed the effects of *Syncrip* depletion on steady state hematopoiesis by examining the hematopoietic compartments of the WT *Syncrip*$^{f/f}$ and KO *Syncrip*$^{\Delta/\Delta}$ at multiple time points post pIpC injections. Complete blood count analysis at 24 weeks post pIpC revealed a reduction in total WBCs, lymphocytes, and platelets upon *Syncrip* depletion. However, we observed no significant reduction in RBCs and hemoglobin (HGB) (**Figure 2.1D**). Additionally, we observed no significant changes in bone marrow (BM) cellularity (**Figure 2.1E**) or spleen and liver weights (**Figure 2.1F**) at early (3 weeks) or late (24 weeks) times points post pIpC. There was also no reduction in the HSPC frequencies, in fact there was an increase in the HSPC (LSK, lin- sca1+ cKit+) population percentage (**Figure 2.1G-H**). However, this was not observed in the HSC (LSK, CD150+ CD48-) population (**Figure 2.1I**) nor was this observed in the absolute number of HSPCs (**Figure 2.1J**). There were also no changes in frequencies of the downstream progenitor populations (**Figure 2.1K**). This all aligns with the previously published claims stating

that SYNCRIP is largely dispensable for normal hematopoiesis [167]. With our cKO mouse we found that *Syncrip* depletion results in mild effects to lymphocyte counts but steady state hematopoiesis remains relatively preserved.

SYNCRIP is required for maintaining long term HSPC reconstitution potential

To test if SYNCRIP is required for HSC function and self-renewal, we conducted *in vitro* colony formation assays with (WT) *Syncrip*$^{f/f}$ and (KO) *Syncrip*$^{\Delta/\Delta}$ BM cells. Upon the first plating of cells, we observed a modest decrease in total colony numbers, as well as reduction in all population types (**Figure 2.2A**). Serially replating these cells shows a more drastic loss in colony number (**Figure 2.2B**), suggesting *Syncrip* is important for maintaining HSPC *in vitro* self-renewal potential. Next, we wanted to assess *Syncrip's* functional requirement for *in vivo* reconstitution, and to do this we transplanted BM cells from our (WT) *Syncrip*$^{f/f}$ and (KO) *Syncrip*$^{\Delta/\Delta}$ mice into lethally irradiated congenic CD45.1 recipient mice. Our (WT) *Syncrip*$^{f/f}$ and (KO) *Syncrip*$^{\Delta/\Delta}$ mice express CD45.2, therefore we can measure levels of these donor cells by gating around the CD45.2 population within the various compartments in the blood (**Figure 2.2C**). In a non-competitive primary transplant setting, SYNCRIP depletion shows a modest loss of chimerism in the BM at an early (8 week) timepoint, and a larger reduction at later (16 and 24 weeks) timepoints (**Figure 2.2D**). This was also observed in the peripheral blood (PB) (**Figure 2.2E**). Additional analysis also showed a partial reduction in myeloid and lymphoid cells at 16 weeks post pIpC (**Figure 2.2F**). Within the BM HSPC compartment, this similar trend of partial reduction in chimerism was observed at 16 weeks post pIpC, with a reduction in both HSC and MPP chimerism (**Figure 2.2G**). Inspection of the CD45.2 donor compartment showed no changes in HSPC (**Figure 2.2H**) or HSC (**Figure 2.2I**)

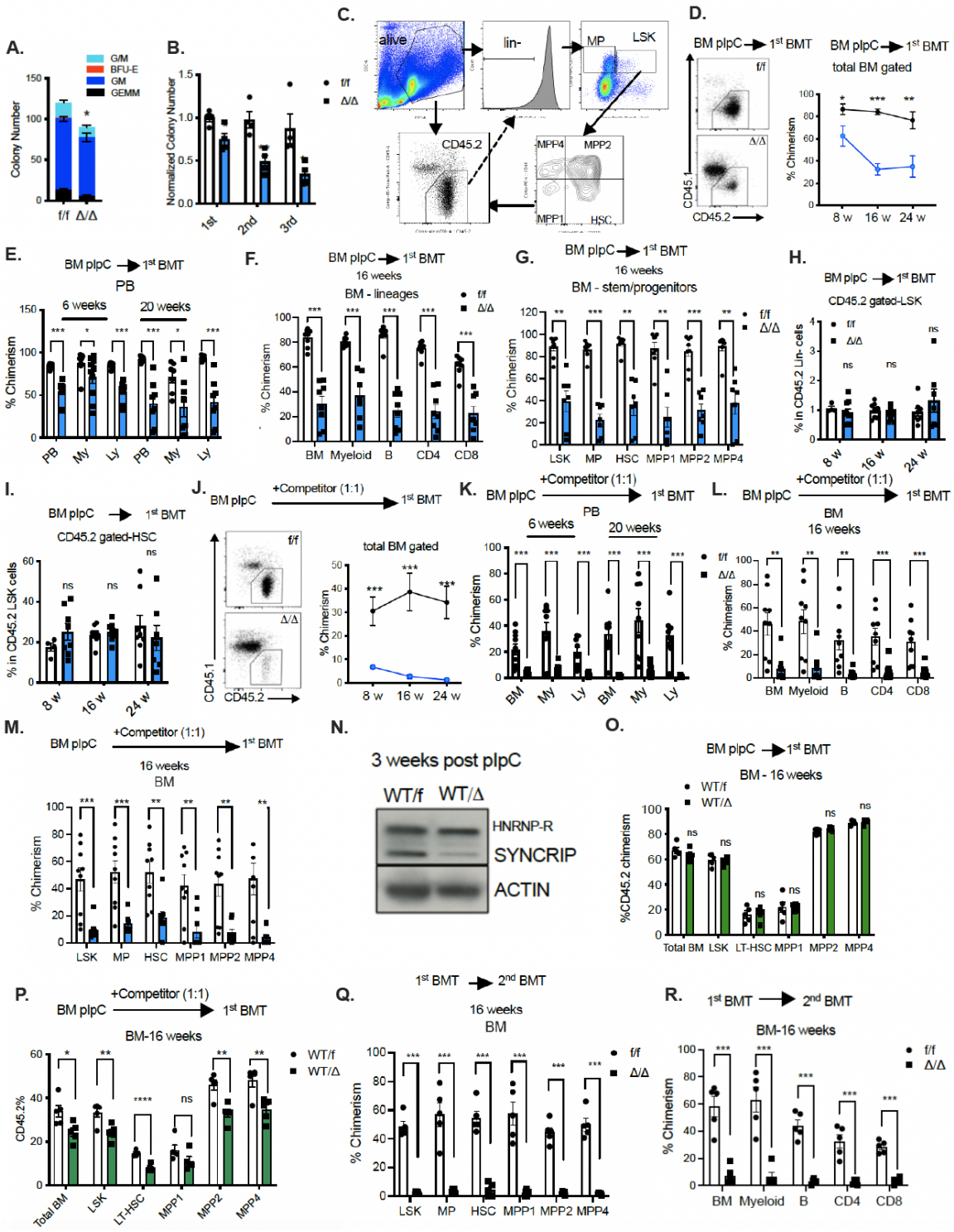

Figure 2.2: SYNCRIP is require for HSC self-renewal and long-term reconstitution potential

(A) The number of colonies formed from *Syncrip* f/f and *Syncrip* Δ/Δ BM cells. 10,000 BM cells were isolated 3 weeks post pIpC and plated in methoculture media for 7 days prior to scoring (n=4/genotype). **(B)** Normalized number of colonies formed in sequential 1st, 2nd and 3rd plating of cells described in (A). **(C)** Representative flow plots showing gating

strategy for analysis of CD45.2 chimerism in different stem and progenitor subpopulations. **(D)** Chimerism of donor-derived BM cells. Congenic CD45.1 recipient mice were noncompetitively transplanted with $2x10^6$ BM cells from either *Syncrip* f/f or *Syncrip* Δ/Δ 3 weeks post pIpC (n=2 donor, and n=10 recipients/genotype). Left plots: representative flow plots of total BM CD45.2 chimerism analysis at 8 weeks post-transplantation. Right Plot: Quantitative analysis of total BM chimerism at 8-, 16- and 24-weeks post-transplantation. **(E)** Donor cell engraftment in congenic CD45.1 recipient mice noncompetitively transplanted with $2x10^6$ BM cells from either *Syncrip* f/f or *Syncrip* Δ/Δ. Chimerism in peripheral blood (PB) cell populations: PB (total PB cells), My (Mac1+Gr1+ cells), Ly (CD19+ cells) at 6- and 20- weeks post transplantation (n=2 donor, and at 6 weeks n=10 recipients/genotype, at 20 weeks n=7 recipients/genotype). **(F)** Chimerism of donor-derived cells in different BM mature populations of recipient mice described in (D) at 16 weeks post-transplantation: Myeloid (Mac1+Gr1+ cells), B (B220+ cells), CD4 (CD4+ cells); CD8 (CD8+ cells). **(G)** Chimerism of donor-derived cells in stem and progenitor compartments of recipient mice described in (D) at 16 weeks post-transplantation: LSK (Lin_cKit+Sca-1+), MP (Lin_cKit+Sca-1), MPP1 (LSK, CD150-CD48-), MPP2 (LSK, CD150+CD48+), and MPP4 (LSK, CD150-CD48+) **(H-I)** Quantitative frequency of (H) LSK and (I) HSC cells within CD45.2+ Lin- and LSK populations, respectively, of recipient mice described in (D) at 8-, 16- and 24 weeks post transplantation. **(J)** Chimerism of donor-derived BM cells. Congenic CD45.1 recipient mice were competitively transplanted with $1x10^6$ BM cells from either *Syncrip* f/f or *Syncrip* Δ/Δ 3 weeks post pIpC and $1x10^6$ BM cells from a wild type CD45.1 mouse (n=2 donor, and n=10 recipients/genotype). Left plots: representative flow plots of total BM CD45.2 chimerism analysis at 8 weeks post-transplantation. Right plot: Quantitative analysis of total BM chimerism at 8-, 16- and 24-weeks post-transplantation. **(K-L)** Donor cell engraftment in congenic CD45.1 recipient mice competitively transplanted with $1x10^6$ BM cells from either *Syncrip* f/f or *Syncrip* Δ/Δ (n=2 donor, and n=10 recipients/genotype) and $1x10^6$ BM cells from a wild type CD45.1 mouse.(K) Chimerism in peripheral blood (PB) cell populations: PB (total PB cells), My (Mac1+Gr1+ cells), Ly (CD19+ cells) at 6- and 20- weeks post transplantation (n=2 donor, and at 6 weeks n=10 recipients/genotype, at 20 weeks n=9 recipients/genotype). (L) Chimerism in BM and different mature populations: Myeloid (Mac1+Gr1+ cells), B (B220+ cells), CD4 (CD4+ cells); CD8 (CD8+ cells) at 16 weeks (n=2 donor, and n=10 recipients/genotype). **(M)** Chimerism of donor-derived cells in stem and progenitor compartments of recipient mice described in (J) at 16 weeks post-transplantation. **(N)** Immunoblots showing efficiency reduction of SYNCRIP in bone marrow (BM) of heterozygous knockout *Syncrip* f/Δ mice 3 weeks post pIpC injections. ACTIN was used as loading control. **(O)** Chimerism of donor-derived cells in stem and progenitor compartments of primary transplantation of *Syncrip* f/f and *Syncrip* f/Δ recipient mice at 16 weeks post-transplantation. Congenic CD45.1 recipient mice were noncompetitively transplanted with $2x10^6$ BM cells from either *Syncrip* f/f or *Syncrip* f/Δ 3 weeks post pIpC (n=5 recipients/genotype). LSK (Lin- Sca-1+ cKit+), MP (Lin- Sca- cKit+), MPP1 (LSK, CD150-CD48-), MPP2 (LSK, CD150+CD48+), and MPP4 (LSK, CD150-CD48+). **(P)** Chimerism of donor-derived cells in stem and progenitor compartments of competitive transplant of *Syncrip* f/f and *Syncrip* f/Δ recipient mice at 16 weeks post-transplantation. Congenic CD45.1 recipient mice were competitively transplanted with $1x10^6$ BM cells from either *Syncrip* f/f or *Syncrip* f/Δ 3 weeks post pIpC and $1x10^6$ BM cells from a wild type CD45.1 mouse (n=5 recipients/genotype). **(Q)** Chimerism of donor-derived BM cells in secondary recipient at 16 weeks post-transplantation. $2x10^6$ BM cells from primary transplanted *Syncrip* $^{f/f}$ and *Syncrip* $^{Δ/Δ}$ (described in D) were isolated and injected into secondary recipient mice (n=2 donor, and n=10 recipients/genotype). **(R)** Donor cell

engraftment within different BM mature populations in secondary recipients at 16 weeks post-transplantation. $2x10^6$ BM cells from primary transplanted *Syncrip* f/f and *Syncrip* Δ/Δ (described in D) were isolated and injected into secondary recipient mice (n=2 donor, and n=10 recipients/genotype).
All data represent mean $\pm$ s.e.m. p values were calculated by two-tailed t test unless specified. * $p<0.05$, ** $p<0.01$, *** $p<0.001$ and ns: not significant.

frequencies. However, upon competitive transplantation with WT CD45.1 BM cells at a 1:1 ratio, we see a drastic loss of engraftment at all timepoints (**Figure 2.2J**). In the PB at early (6 week) and late (20 week) timepoints this drastic reduction in chimerism is also observed (**Figure 2.2K**), and within the myeloid and lymphoid cells in the BM there is a similar loss of chimerism (**Figure 2.2L**). Looking at the HSPC compartment and progenitor cells, we also observe a drastic loss of chimerism in the BM at 16 weeks post pIpC (**Figure 2.2M**). All of this suggests that *Syncrip* plays functional role in maintaining *in vivo* HSC reconstitution potential and without *Syncrip* cells are drastically out competed by WT cells during competitive transplants.

To rule out the effects of Cre toxicity (or Cre expression) being responsible for this phenotype, we conducted additional transplants using heterozygous (WT) *Syncrip*$^{f/f}$ and (KO) *Syncrip*$^{\Delta/f}$ mice. Using the same pIpC regimen as the homozygous mice, we're able to see reduction in SYNCRIP protein levels (**Figure 2.2N**). In a non-competitive transplant setting with these heterozygous cells, inspection in the BM demonstrated no changes in total BM chimerism or in any of the cells within the HSPC compartment (**Figure 2.2O**). This suggests that the phenotype we observed in the homozygous mice is due to the loss of *Syncrip* and not Cre expression or pIpC injection. Additionally, we conducted competitive transplants with these heterozygous cells and in this setting, we see mild reduction in chimerism in the total BM, HSCs and most MPP populations (**Figure 2.2P**). This is a very interesting finding, since it indicates that loss of one *Syncrip*

allele shows mild reduction in chimerism, indicating that SYNCRIP may have a dose dependent effect on HSPC function.

To test *Syncrip's* role in long term HSPC reconstitution potential, we harvested BM cells from primary transplant cells and conducted a secondary transplant in a non-competitive manner. In this secondary transplant setting we observed dramatic loss of chimerism in the *Syncrip* depleted condition at 16 weeks post pIpC in every population within the HSPC compartment (**Figure 2.2Q**) as well as in the total BM and myeloid and lymphoid populations (**Figure 2.2R**). In the WT condition, mice maintain ~30-60% donor chimerism upon the secondary transplantation, but loss of *Syncrip* results in almost no engraftment in the HSPC compartment or lineage populations. Altogether this data suggests that SYNCRIP plays an essential role in maintaining proper HSC and HSPC self-renewal and function *in vivo*.

SYNCRIPs functional requirement in HSPC reconstitution potential is cell autonomous

Given that our mouse model is not specific to depleting *Syncrip* in a single cell lineage, we wanted to assess if the functional requirement SYNCRIP has in maintaining HSC self-renewal and HSPC reconstitution potential is intrinsic or if it's due to external mechanism from having SYNCRIP loss in other cell types (like the bone marrow environment cells). To test if the effects are cell autonomous, we transplanted 6–8-week-old (WT) *Syncrip*$^{f/f}$ and (KO) *Syncrip*$^{\Delta/\Delta}$ BM cells into lethally irradiated congenic recipient mice. At 6 weeks post-transplant mice displayed equal levels of chimerism and were pIpC injected at this timepoint (using same regimen as described above), and 3 weeks post pIpC we observed efficient depletion of SYNCRIP protein (**Figure 2.3A**). Next, we

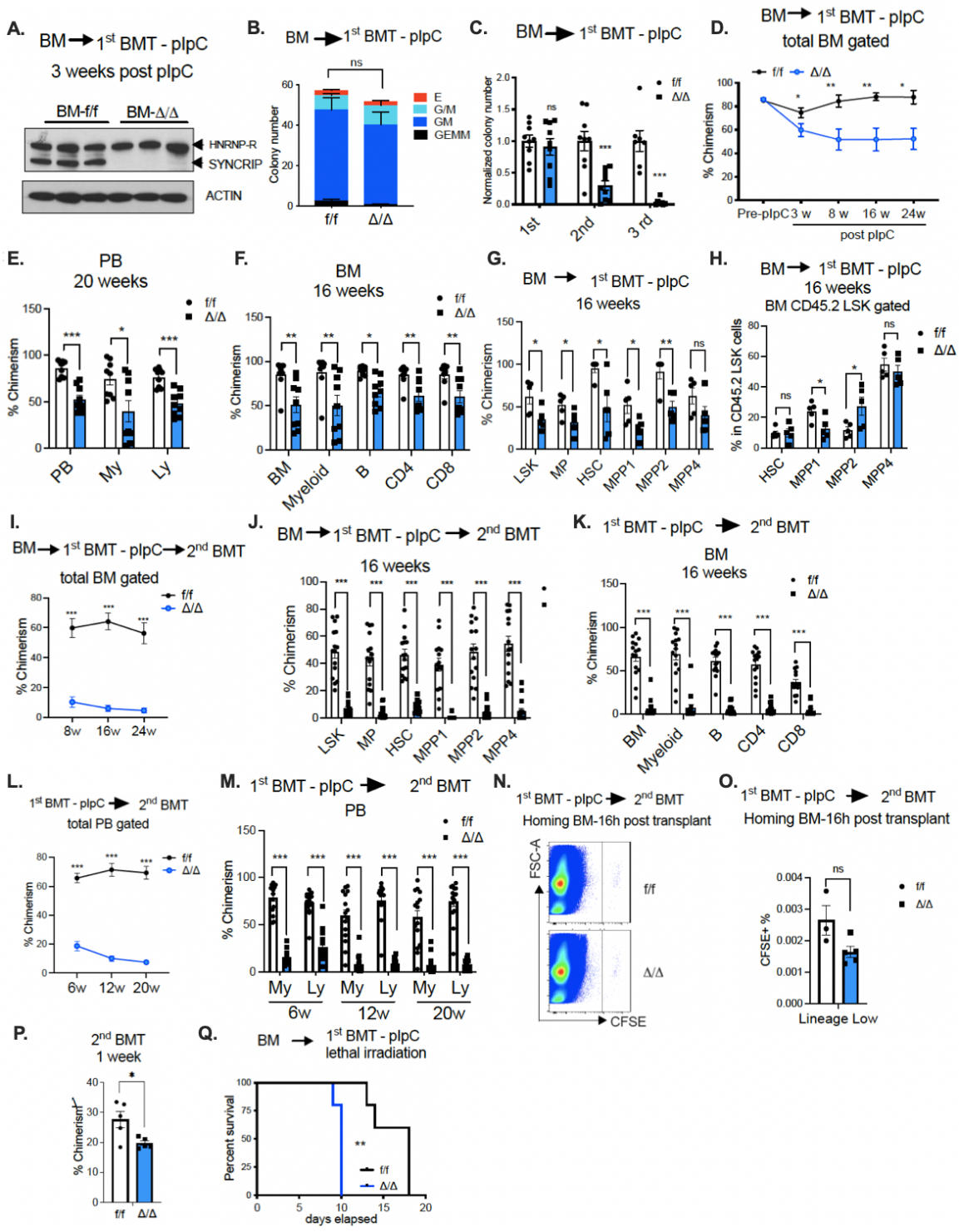

Figure 2.3: SYNCRIP's requirement in HSPC function is cell autonomous

(A) Immunoblots showing efficiency knockout of SYNCRIP in engrafted *Syncrip* Δ/Δ BM cells 3 weeks post pIpC injections. ACTIN was used as loading control. CD45.1 recipient mice were transplanted with $2x10^6$ BM cells from either WT *Syncrip* f/f Mx-1 Cre- or cKO *Syncrip* f/f Mx-1 Cre+. 6 weeks post transplantation, recipient mice were injected with pIpC

to induce deletion. **(B)** The number of colonies formed from *Syncrip* f/f and *Syncrip* Δ/Δ BM cells (described in Figure 2A). 10,000 BM cells were isolated 3 weeks post pIpC and plated in methoculture media for 7 days prior to scoring (n=9/genotype). **(C)** Normalized number of colonies formed in sequential 1st, 2nd and 3rd plating of cells described in (B). **(D)** Chimerism of donor-derived BM cells in recipient mice described in (A) at series time points: pre-pIpC, 3-, 8-, 16- and 24- weeks post pIpC (n=3 donor, and n=15 recipients/genotype at pre- and 3 weeks; n=9 at 8-, 16- and 24- weeks post pIpC). **(E)** Donor cell engraftment in PB of mice described in (A) at 20- weeks post transplantation. PB (total PB cells), My (Mac1+Gr1+ cells), Ly (CD19+ cells) (n=3 donor, and n=9 recipients/genotype). **(F)** Donor cell engraftment in BM of mice described in (A) at 16 weeks post transplantation. Myeloid (Mac1+Gr1+ cells), B (B220+ cells), CD4 (CD4+ cells); CD8 (CD8+ cells) (n=3 donor, and n=9 recipients/genotype). **(G)** Chimerism of donor-derived cells in stem and progenitor compartments of recipient mice described in (A) at 16 weeks post pIpC. **(H)** Quantitative summary of frequencies of HSC and MPPs cells within CD45.2+ LSK populations of recipient mice described in (A) at 16 weeks post pIpC. **(I)** Chimerism of donor-derived BM cells in secondary recipients at 8-, 16- and 24 weeks post-transplantation. $2x10^6$ BM cells from primary transplanted *Syncrip* f/f and *Syncrip* Δ/Δ (described in A) were isolated and injected into secondary recipient mice (n=3 donor, and n=15 recipients/genotype). **(J)** Chimerism of donor-derived cells in stem and progenitor compartments of secondary recipient mice (described in I) at 16 weeks post transplantation (n=3 donor, and n=15 recipients/genotype). **(K)** Donor cell engraftment within different BM mature populations in secondary recipients described in (I) at 16 weeks post-transplantation (n=3 donor, and n=15 recipients/genotype). **(L)** Donor cell engraftment in PB of secondary recipient mice (described in I) at 6-, 12- and 20 weeks post transplantation (n=3 donor, and n=15 recipients/genotype). **(M)** Donor cell engraftment in PB mature populations of secondary recipient mice described in (I) at 6-, 12- and 20 weeks post transplantation: My (Mac1+Gr1+ cells), Ly (CD19+ cells) (n=3 donor, and n=15 recipients/genotype). **(N)** Representative flow plots showing gating of CFSE positive LSK cells engrafted in bone marrow of secondary recipients at 16 hours post-transplantation (n=5/genotype). **(O)** Quantitative summary of data shown in (N) for homing of WT *Syncrip* f/f and KO *Syncrip* Δ/Δ. **(P)** Chimerism of donor-derived cells in total bone marrow cells of secondary recipient mice ($3.2x10^4$ LSK cells from primary transplanted mice were isolated and injected into secondary recipients) at 1 week post transplantation (n=7 donor, n=5 recipient/genotype). **(Q)** Kaplan-Meier analysis of survival of WT *Syncrip* f/f and KO *Syncrip* Δ/Δ mice following lethal irradiation (n=5 each).
All data represent mean ± s.e.m. p values were calculated by two-tailed t test unless specified. * $p<0.05$, ** $p<0.01$, *** $p<0.001$ and ns: not significant.

conducted *in vitro* assessment of SYNCRIP depletion in these cells, primary plating in colony formation assay shows that there is a mild (non-significant) decrease in colony formation (**Figure 2.3B**). However, upon serial plating (2nd and 3rd re-plating) we see dramatic loss of colony formation potential (**Figure 2.3C**). Suggesting that the *in vitro* defect in HSC self-renewal after *Syncrip* depletion is due to intrinsic factors not external influences.

To verify this phenotype is cell autonomous *in vivo*, we conducted non-competitive transplants as described in Figure 2.3A and tracked chimerism across multiple timepoints. We observed a continuous decrease in donor chimerism upon *Syncrip* KO over extended timepoints (8-24 weeks) (**Figure 2.3D**). This phenotype, very similar to our previous transplants, showed only a moderate reduction in chimerism. This reduced chimerism was also observed in the PB myeloid and lymphoid lineages (**Figure 2.3E**), as well as in the myeloid and lymphoid lineages in the BM (**Figure 2.3F**). This moderate reduction in chimerism was also observed in the HSPC compartment (**Figure 2.3G**). However, inspection of the donor HSCP compartment shows no decrease in frequencies in HSCs, MPP2, or MPP4 populations, but there is a reduced frequency of MPP1 cells. This is very interesting because our depletion of *Syncrip* didn't reduce the frequencies within the HSPC compartment in a setting without transplantation (Figure 2.1J), however this data suggests that the HSPCs that have undergone transplantation are more impacted by loss of SYNCRIP.

We further tested the response of SYNCRIP depletion to hematopoietic stress, by subjecting the SYNCRIP KO HSCs to repopulation stress in a secondary transplant. (WT) *Syncrip*$^{f/f}$ and (KO) *Syncrip*$^{\Delta/\Delta}$ cells harvested from primary transplanted mice described in Figure 2.3D and tracked chimerism in a similar manner. Very similar to the results we saw in Figure 2.2Q-R, we find that loss of SYNCRIP causes a dramatic loss of chimerism at during a secondary transplant (**Figure 2.3I**). This is observed in the HSPC compartment (**Figure 2.3J**) and myeloid and lymphoid lineages in the BM (**Figure 2.3K**). PB also shows this almost complete loss of chimerism (**Figure 2.3L**) in both the myeloid and lymphoid compartments (**Figure 2.3M**). Overall, this experiment suggests

that the HSC loss of self-renewal defect we see upon SYNCRIP loss is due to intrinsic effects and not exposure to any external mechanisms prior to any transplantation.

Next, we wanted to determine if the loss of chimerism was due to a homing defect upon SYNCRIP depletion. To test this question, we harvested (WT) *Syncrip*$^{f/f}$ and (KO) *Syncrip*$^{\Delta/\Delta}$ HSPC cells that had undergone a primary transplant, these cells were then stained with CFSE and transplanted into a secondary recipient. At 16 hours post transplantation the mice were euthanized, and BM cells harvested. The CFSE stained cells were visible through flow cytometry (**Figure 2.3N**) and showed a small trend, but not significant, reduction in homing capacity upon transplant (**Figure 2.3O**). Investigating the chimerism one week post-secondary transplant, we observed a modest reduction in chimerism (~10% reduction), which is unlike the dramatic reduction we observed at later timepoints (**Figure 2.3P**). This strongly suggests that the defects we see in HSC self-renewal and repopulation capacity are not due to defects in homing.

Lastly, we wanted to investigate the response of the *Syncrip*$^{\Delta/\Delta}$ KO cells to myeloablation, and whether they would be more sensitive to this type of stress. To explore this, we conducted a primary transplant with (WT) *Syncrip*$^{f/f}$ and (KO) *Syncrip*$^{\Delta/\Delta}$ and subsequently exposed the recipient mice to lethal irradiation. We tracked these mice and found that they had worse survival compared to the WT control mice, suggesting that SYNCRIP KO mice are more sensitive to stress induced by lethal irradiation (**Figure 2.3Q**). Altogether this data supports the important role SYNCRIP plays in normal hematopoiesis, and how SYNCRIP is required for proper HSC and progenitor function in response to stress, most potently in secondary transplantation and myelosuppression settings.

SYNCRIP moderately influences MPP cell cycling but doesn't alter HSC cycling or proliferation

To understand the underlying reasons why SYNCRIP depletion leads to decreased reconstitution potential and defects in self-renewal we investigated the known link between increased HSC activation (cell cycling/proliferation) leading to HSC exhaustion [16, 185-187]. We wanted to see if SYNCRIP depletion led to an increase in HSPC cell cycling or proliferation. We approached this question with multiple strategies. First, we looked at cell cycling with Hoechst and Pyronin Y (PY) staining and observed a shift in MPP1 cells. MPP1s have a reduction in the G0 phase, an increase in S/G2/M phase and no changes in G1 (**Figure 2.4A**). In the HSC population we observed a slight trend to increase S/G2/M phase, but it's not significant (**Figure 2.4B**). To better determine if SYNCRIP influences cell proliferation *in vivo*, we injected primary transplanted mice with BrdU, at 16hrs post transplantation we euthanized the animals and traced the BrdU incorporation in the cycling BM cells. Within the total BM as well as the HSPC compartment we noticed no significant changes in BrdU incorporation, including in HSCs and most MPPs. The only exception is the MPP2 population, which shows a moderate increase in BrdU incorporation (**Figure 2.4C**). All this suggests that there is a slight increase in cycling and proliferation in the MPP population, which could help explain the initial drop in engraftment we observe in the primary transplant setting. However, we don't observe any changes in the HSC cycling or proliferation, therefore this effect on MPPs doesn't explain the very dramatic loss of reconstitution potential/HSC self-renewal defect we observe in the secondary transplant.

To directly investigate if loss of *Syncrip* has any effect on division of HSCs we set up an *in vitro* live cell imaging time course using the CellRaft Air system. We sorted transplanted HSCs from (WT) *Syncrip*$^{f/f}$ and (KO) *Syncrip*$^{\Delta/\Delta}$ mice and plated them into

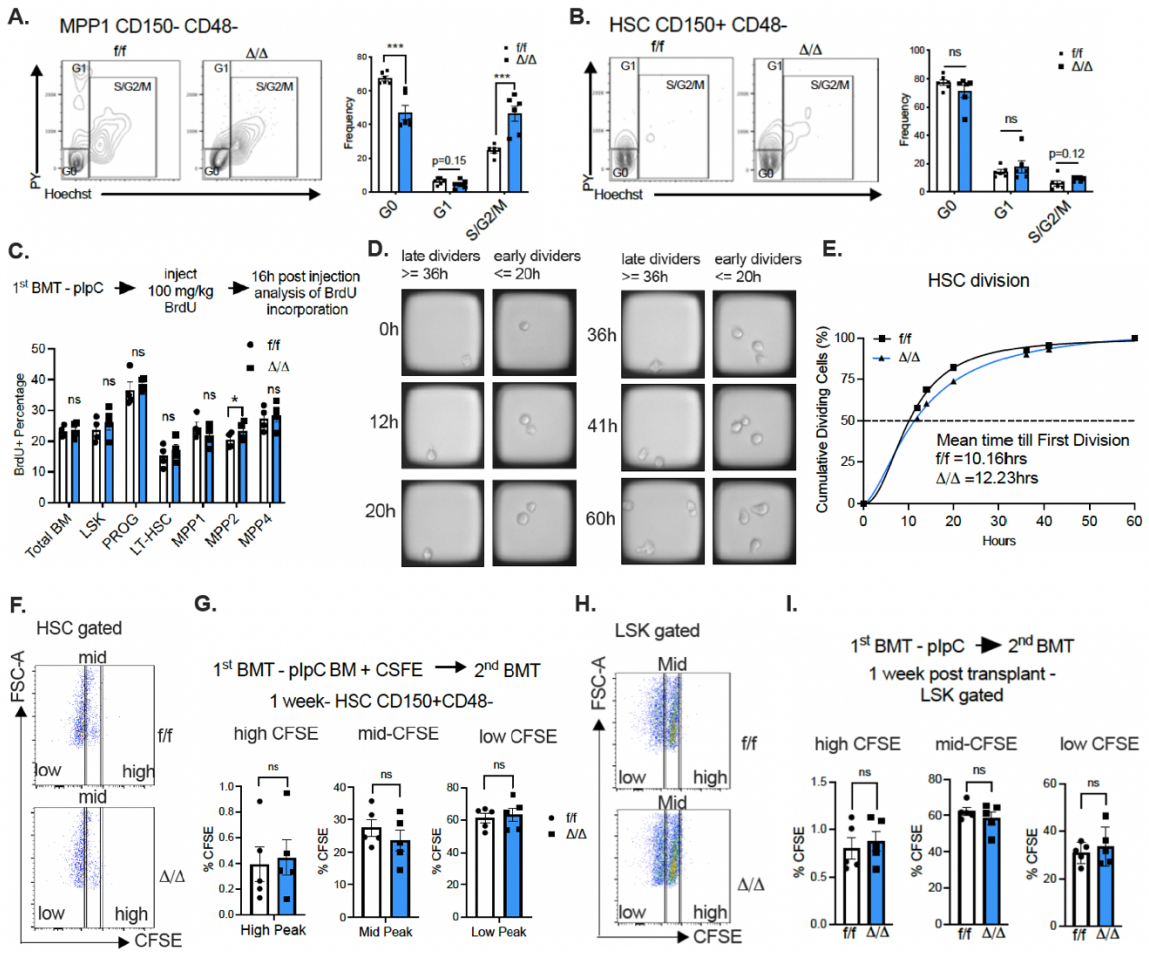

Figure 2.4: SYNCRIP's role on HSPC Cell Cycling and Proliferation

(A-B) Cell cycle analysis of (A) MPP1 (LSK, CD150-CD48) and (B) HSCs (LSK, CD150+CD48-) isolated WT *Syncrip* f/f and KO *Syncrip* Δ/Δ mice (n=6 each genotype) described in (Figure 2.3A). Left: Representative flow plots. Right: Quantitative analysis of cell cycle status. **(C)** Incorporation of BrdU pulse into different stem and progenitor compartments in bone marrow of WT *Syncrip* f/f and KO *Syncrip* Δ/Δ. **(D)** Representative images of *in vitro* HSC cell division imaged on CellRaft AIR System (Cell Microsystems), shown in brightfield. **(E)** Cumulative graphs tracking *in vitro* division of HSCs over the course of 60 hours using CellRaft AIR System (Cell Microsystems). **(F)** Representative flow plots showing gating strategy for analysis of CFSE stained HSC in recipient mice (described in Figure 2.3P) at 1 week post transplantation. **(G)** Representative flow plots showing gating strategy for analysis of CFSE stained HSC in recipient mice (described in F) at 1 week post transplantation. **(H)** Representative flow plots showing gating strategy for analysis of CFSE stained LSK in recipient mice (described in Figure 2.3P) at 1 week post transplantation. **(I)** Quantitative summary of data shown in (H). All data represent mean ± s.e.m. p values were calculated by two-tailed t test unless specified. * p<0.05, **p<0.01, ***p<0.001 and ns: not significant.

single wells on specialized CellRaft technology rafts. The wells were continuously live imaged using the CellRaft Air system for 60hrs to track the time it took them to first divide (**Figure 2.4D**). Although there is a slight difference in how long it took HSCs from each condition to divide (10.16hrs for *Syncrip*$^{f/f}$ and 12.23hrs for *Syncrip*$^{\Delta/\Delta}$), with the KO condition showing a longer time to first division, cumulatively all HSCs had undergone one division by 60hrs (**Figure 2.4E**). This suggests that SYNCRIP's role in regulating HSC divisions is very minimal and doesn't indicate that SYNCRIP would lead to an increase in HSC activation.

Finally, to further verify if SYNCRIP pays a role during HSC *in vivo* proliferation we CFSE stained LSK cells from primary transplanted mice and transplanted them into secondary recipients. One week after transplant the recipient mice were euthanized, and BM cells were harvested so we could track cell division. CFSE signal dilutes in cells as they proliferate, the CFSE signal is diluted into the daughter cells sequentially and can be visualized for multiple generations of cell divisions. We identified a high CFSE signal, indicating a small amount of CFSE dilution suggesting low amounts of proliferation. On the other hand, low CFSE signal indicates a large amount of CFSE dilution suggesting high amounts of proliferation. We also noticed a mid-level CFSE signal, which indicates some amount of proliferation (**Figure 2.4F, H**). In the HSC population we noticed *Syncrip* loss caused no changes in the high, mid, or low CFSE stained populations (**Figure 2.4G**). This was also the case in the HSPC (LSK) population (**Figure 2.4I**). All together this data supports all our pervious finding that *Syncrip* doesn't influence *in vivo* or *in vitro* HSC cell cycling and proliferation.

SYNCRIP is important for human cord blood HSPC self-renewal and cell growth

Given that we see SYNCRIP play an important role in mouse HSCs and MPPs, we also wanted to assess whether SYNCRIP influences human HSPCs. To test this, we isolated human cord blood HSPCs (CB-CD34+) and used hairpin lentivirus to reduce *Syncrip* expression. Western blot shows efficient depletion of SYNCRIP at 4 days post transduction for shRNA 1. At 14 days post transduction we see clear depletion of SYNCRIP in both shRNA 1 and shRNA 2 conditions (**Figure 2.5A**). Depletion of SYNCRIP in CB-CD34+ HSPCs demonstrated a reduction in colony formation ability, most clearly seen in the secondary serial re-plating (**Figure 2.5B**). We also observed a decrease in cell proliferation upon SYNCRIP reduction, however this was only observed at the later timepoints (day 17 and 19 post seeding) (**Figure 2.5C**). Apoptosis levels 4 days post transduction show an increasing trend when SYNCRIP is knocked down, however it is not significant (**Figure 2.5D**). This suggests that SYNCRIP plays a role in regulating *in vitro* CB-CD34+ self-renewal capacities, and cell growth. Additionally, we checked how SYNCRIP influences the various cell populations within the HSPC compartment using flow cytometry 4 days post transduction (**Figure 2.5E**). We noticed a trend for increased LT-HSC frequency in the SYNCRIP depleted conditions however it's not significant (**Figure 2.5F**). Absolute numbers also show that SYNCRIP depletion doesn't significantly change the LT-HSC population. (**Figure 2.5G**). Altogether this data suggests that SYNCRIP doesn't have a large effect on the frequency or number of HSPC cells at early timepoints, but it does influence the self-renewal and growth of human CB-CD34+ HSPCs at later timepoints.

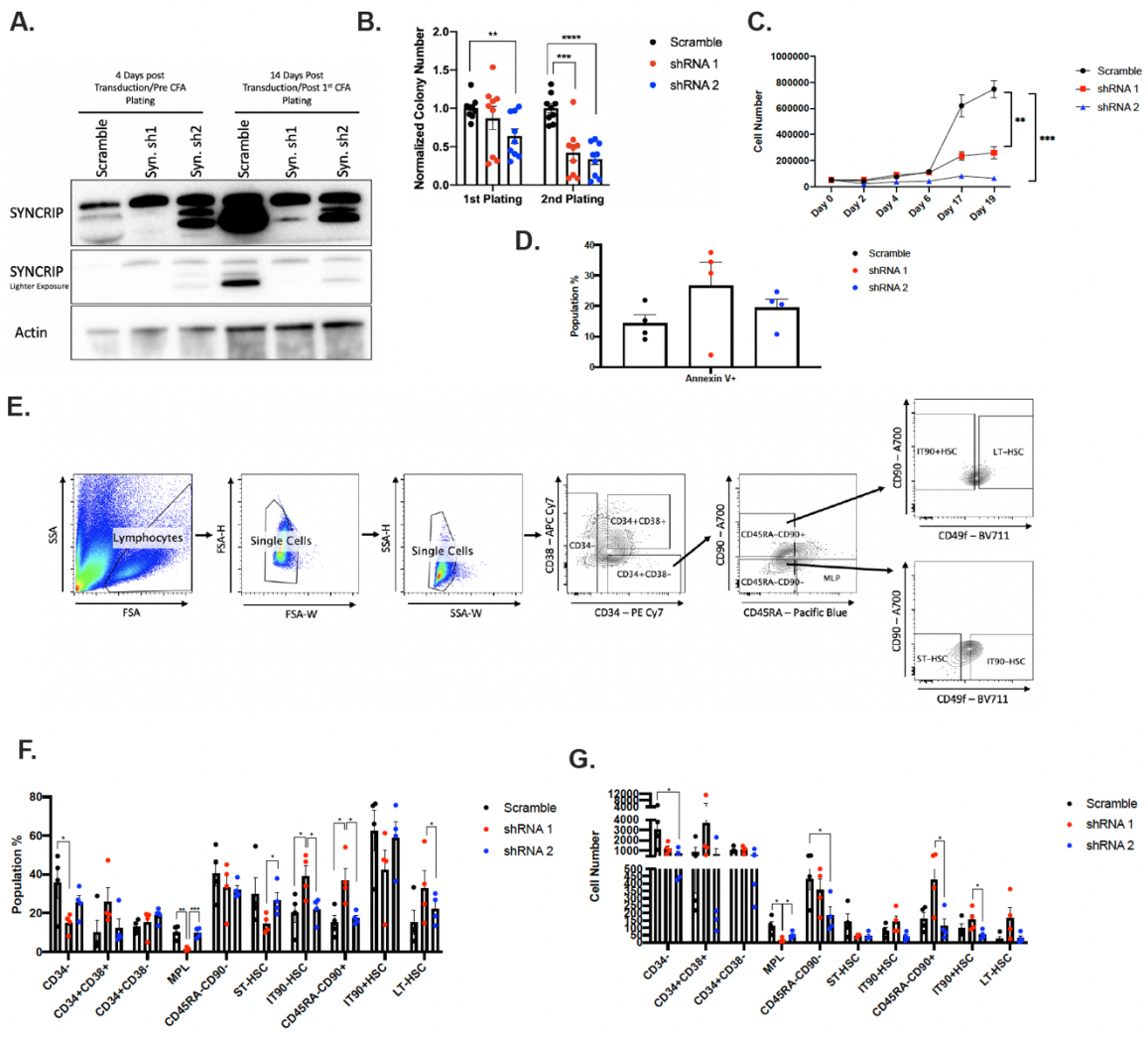

Figure 2.5: SYNCRIP's role in human CB-CD34+ HSPCs

(A) Western blot depicting SYNCRIP depletion. CB-CD34 cells were enriched, transduced twice with SYNCRIP hairpin lentivirus, and selected with 2ug/ml puromycin treatment for 24hrs prior to setup for any experiments. Blot's first three lanes are samples taken 4 days post transduction, prior to the colony formation assay (CFA). The last three lanes are samples taken 14 days post transduction, after the 1st plating of the CFA, and prior to the 2nd plating. ACTIN is used as a loading control. **(B)** CFA conducted with CB-CD34+ HSPCs described in (A). For 1st plating, 10000 cells were plated in methylcellulose media 4 days post transduction and scored 14 days after being seeded. For 2nd plating 10000 cells from 1st plating were seeded in methylcellulose media and scored 14 days post transduction. For both plating's, 0.5ng/ml puromycin was added to the methylcellulose media **(C)** Proliferation curve of CB-CD34+ HSPCs described in (A). 50000 cells were plated in cytokine supplemented IMDM media (along with 5ng/mL puromycin) and counted for of 19 days post seeding. **(D)** Apoptosis quantification of CB-CD34+ HSPCs described in (A), plot based on Annexin V and DAPI staining at 4 days post transduction. **(E)** Representative flow plots and gating strategy for CB-CD34+ HSPCs described in (A). **(F)** Quantification of HSPC population frequencies from CB-CD34+ HSPCs described in (A). **(G)** Quantification of HSPC absolute numbers from CB-CD34+ HSPCs described in (A).

All data represent mean ± s.e.m. p values were calculated by two-tailed t test unless specified. * p<0.05, **p<0.01, ***p<0.001.

Single Cell RNA-sequencing (scRNA-seq) reveals activation of unfolded protein response and chaperone pathways

To uncover how *Syncrip* loss impacts cell identity in hematopoietic cells, and to better understand the transcriptional changes amongst the various hematopoietic cell populations we performed single cell RNA sequencing (scRNA-seq) on primary transplanted, (WT) *Syncrip*$^{f/f}$ and (KO) *Syncrip*$^{\Delta/\Delta}$, sorted LK cells (Lin-, cKit+ cells) (from primary transplants as described in Figure 2.3A). Uniform Manifold Approximation and Projection (UMAP) and t-Distributed Stochastic Neighbor Embedding (t-SNE) analysis identified the previously characterized stem and progenitor clusters (including HSC, MPPs, erythroid, myeloid, and lymphoid progenitors) [188-190] (**Figure 2.6A-B**). Closer inspection revealed no significant changes in frequencies for any population in the HSPC compartment upon SYNCRIP depletion (**Figure 2.6C**). In the downstream progenitor populations, we observed some mild changes in frequency in the Mk, Ba, and Mo populations (**Figure 2.6D**). In addition to the previously characterized populations, an additional HSC-like population was identified with both t-SNE and UMAP which we have annotated as HSC-C1 (**Figure 2.6A-B**). Transcriptionally this HSC-C1 population is enriched for signatures associated with HSCs compared to MPPs (**Figure 2.6B**). Although there is no change in the HSC-C1 frequency upon SYNCRIP KO, inspection of the UMAP (**Figure 2.6E**) and T-SNE (**Figure 2.6F**) WT and KO plots revealed a shift in the HSC-C1 population.

Previous work has unveiled that HSCs can be functionally separated into two types of HSCs, a low output HSC that is quiescent and required for long term repopulation, and a

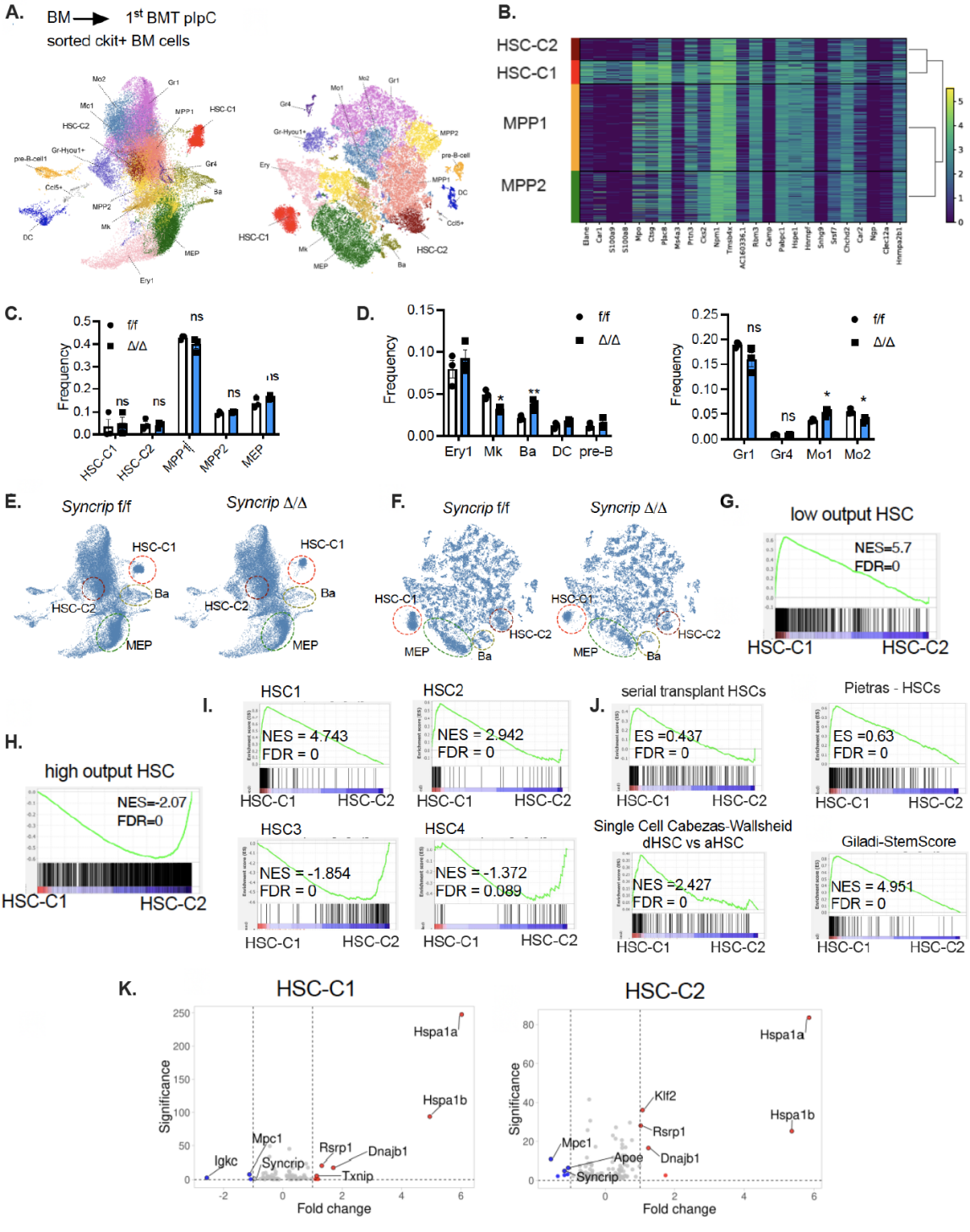
A.
BM
1st BMT plpC
sorted ckit+ BM cells
B.
HSC-C2
HSC-C1
MPP1
MPP2
C.
f/f
Δ/Δ
Frequency
ns
HSC-C1
HSC-C2
MPP1
MPP2
MEP
D.
Ery1
Mk
Ba
DC
pre-B
Gr1
Gr4
Mo1
Mo2
E.
Syncrip f/f
Syncrip Δ/Δ
F.
G.
low output HSC
NES=5.7
FDR=0
H.
high output HSC
NES=-2.07
FDR=0
I.
HSC1
NES = 4.743
FDR = 0
HSC2
NES = 2.942
FDR = 0
HSC3
NES = -1.854
FDR = 0
HSC4
NES = -1.372
FDR = 0.089
J.
serial transplant HSCs
ES =0.437
FDR = 0
Pietras - HSCs
ES =0.63
FDR = 0
Single Cell Cabezas-Wallsheid
dHSC vs aHSC
NES =2.427
FDR = 0
Giladi-StemScore
NES = 4.951
FDR = 0
K.
HSC-C1
HSC-C2
Significance
Fold change
Hspa1a
Hspa1b
Mpc1
Rsrp1
Dnajb1
Igkc
Syncrip
Txnip
Klf2
Apoe

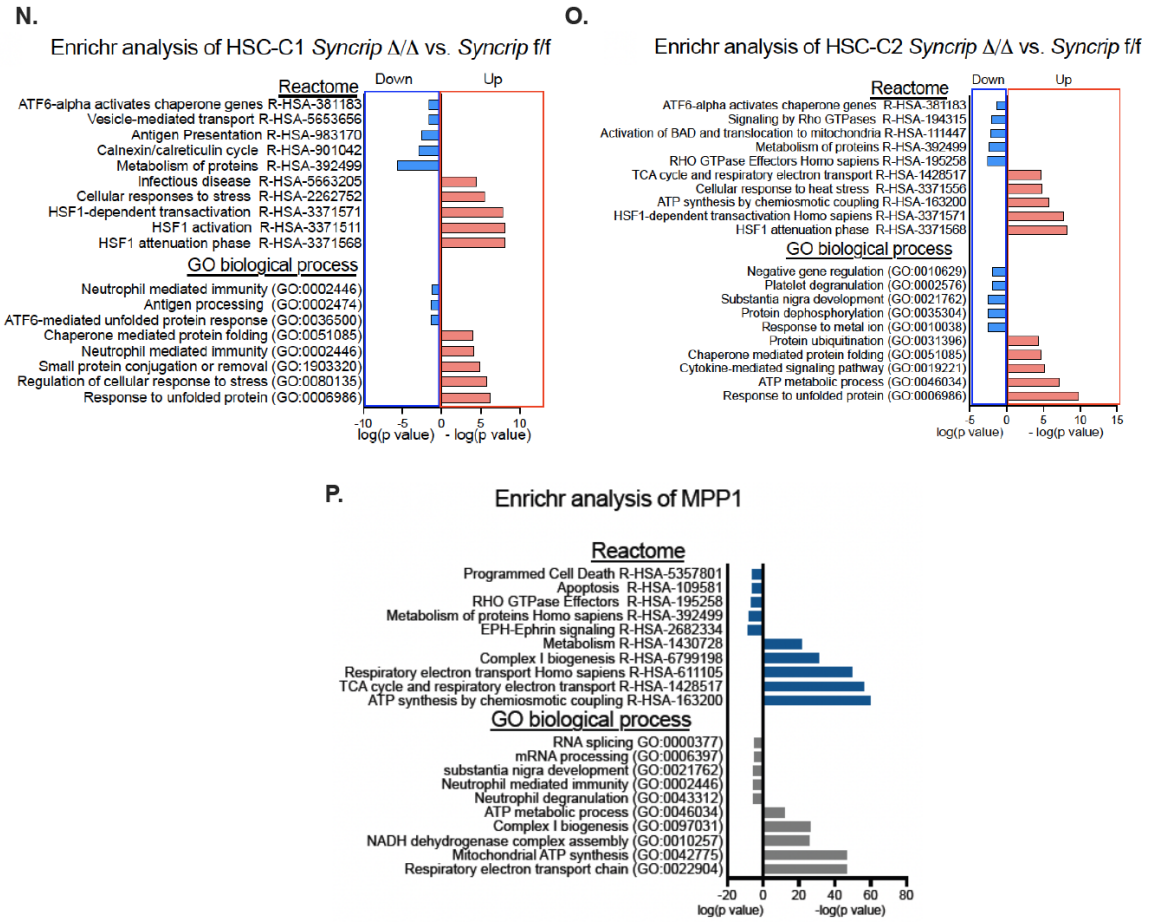

Figure 2.6: scRNA-seq uncovers an activated unfolded protein and chaperone response in Syncrip deficient HSCs

(A) Identification of hematopoietic cell populations within WT *Syncrip* f/f (n=3) and KO *Syncrip* Δ/Δ (n=3) Lin-ckit+ cells based on UMAP analysis (left plot) and t-SNE analysis (right plot) of Single cell RNA sequencing (scRNA-seq). **(B)** Gene expression heat map of the highly expressed genes in aHSC vs. HSC, MPP1 and MPP2 populations. **(C)** Quantitative summary of frequencies of different populations defined by scRNA-seq analysis in WT *Syncrip* f/f (n=3) and KO *Syncrip* Δ/Δ (n=3). Data represent mean ± s.e.m. p values were calculated by two-tailed t test unless specified. ns: not significant. **(D)** Quantitative summary of frequencies of different populations defined by scRNA-seq analysis in WT *Syncrip* f/f (n=3) and KO *Syncrip* Δ/Δ (n=3). Data represent mean ± s.e.m. p values were calculated by two-tailed t test unless specified. * p<0.05, **p<0.01, ns: not significant. **(E)** UMAP displays of all hematopoietic clusters of WT *Syncrip* f/f and KO *Syncrip* Δ/Δ scRNA-seq as described in (A). Cluster HSC-C1 shows the most shift. HSC-C2, Ba and MEP clusters were highlighted for comparison. **(F)** tSNE displays of all hematopoietic clusters of WT *Syncrip* f/f and KO *Syncrip* Δ/Δ scRNA-seq as described in (A). Cluster HSC-C1 shows the most shift. HSC-C2, Ba and MEP clusters were highlighted for comparison. **(G-H)** GSEA analysis of genes differentially expressed between HSC-C1 vs. HSC-C2 in WT *Syncrip* f/f mice for enrichment of gene signatures specific for low output and high output HSCs. **(I)** GSEA analysis of HSC-C1 transcriptome of KO *Syncrip*

Δ/Δ vs. WT *Syncrip* f/f against those of different HSC clusters defined in [191]. **(J)** GSEA analysis of HSC-C1 (vs. HSC-C2) transcriptome against signatures of serial transplant HSCs [191], primitive HSCs [192], dormant HSCs [193] and StemScore [189]. **(K)** Volcano plots showing genes differentially expressed between *Syncrip* f/f vs. *Syncrip* Δ/Δ within (left plot) HSC-C1 and (right plot) HSC-C2 clusters. The most differentially expressed genes are highlighted. **(L-M)** Enrichr analysis for GO biological processes and Reactome enrichment of significant (FDR <0.05) downregulated and upregulated genes within the HSC-C1 (L) and HSC-C2 (M) populations of *Syncrip* Δ/Δ vs. *Syncrip* f/f. X-axis: $-\log_{10}$(p value). Enrichment of downregulated targets was depicted as negative $\log_{10}$(p) and enrichment of upregulated targets was depicted as positive $\log_{10}$(p). **(N)** Enrichr analysis for GO biological processes and Reactome enrichment of significant (FDR <0.05) downregulated and upregulated genes within the MPP population of *Syncrip* Δ/Δ vs. *Syncrip* f/f. X-axis: $-\log_{10}$(p value).

high output HSC that differentiates to produce progeny [191]. We utilized gene set enrichment analysis (GSEA) to investigate if the transcriptional profile of our HSC-C1 population matched with these previously identified HSC populations. Interestingly, our GSEA analysis revealed that our HSC-C1 population is transcriptionally enriched for the low output HSC signature (**Figure 2.6G)** and the HSC-C2 population is enriched for the high output HSC signature (**Figure 2.6H**). We conduced further GSEA analysis to ensure that the HSC-C1 population is enriched for the previously identified “low output”, “reserve”, “dormant” HSC signatures identified by various other groups. In all our GSEA analysis’ we saw that the HSC-C1 population is enriched for primitive signatures (**Figure 2.6I**), and that it closely resembles HSCs characterized to have serial transplantation potential, self-renewing HSCs, and dormant HSCs (**Figure 2.6J**). Altogether this suggests that our HSC-C1 population represents an HSC with high self-renewal potential.

We next sought to explore the specific genes impacted by loss of *Syncrip* in both the HSC and aHSC populations. Upon close inspection of differentially expressed genes, we noticed upregulation of various chaperone associated proteins in both the HSC-C1 and HSC-C2 populations. Among such chaperone genes is *Hspa1a* (*Hsp70-1*), *Hspa1b*

(*Hsp70-2*) and *Dnajb1* (**Figure 2.6K**). Furthermore, pathway enrichment analysis by the Enrichr program (http://amp.pharm.mssm.edu/Enrichr/) [194] suggested strong activation of the unfolded protein response (UPR) in both HSC-C1 and HSC-C2 populations upon loss of *Syncrip*. Chaperone activation was also observed when SYNCRIP was depleted, predominantly in the form of HSF1 dependent pathways. We also found a reduction of Rho GTPase signaling upon loss of *Syncrip* in the HSC-C2 and MPP populations (**Figure 2.6L-M**). Very interestingly, this pattern of UPR and chaperone activation was not observed in MPPs, instead it appears to be unique to the HSC populations (**Figure 2.6N**). Overall, these data suggests that loss of SYNCRIP results in activation of unfolded protein stress, and a HSP1 dependent chaperone response. Based on what is known about HSCs requiring high protein quality to maintain proper self-renewal capacities [89], this activation of UPR indicates that SYNCRIP plays a role in protecting the cells from this type of stress and could be another contributor to the loss of self-renewal upon SYNCRIP depletion.

SYNCRIP plays a role in promoting protein homeostasis in HSCs

Based on our findings in Figure 2.6 that strongly suggested the unfolded protein response and chaperone pathways are activated upon loss of *Syncrip*, we wanted to know if SYNCRIP depleted HSCs were experiencing altered proteostatic states. To answer this question, we utilized the tetraphenylethene malemide (TMI) probe to measure unfolded protein in cells [89]. TMI is a cell-permeable dye that fluoresces upon binding to cysteine thiols [195], which are normally not exposed in folded proteins but become exposed as proteins become unfolded or if they're misfolded. Use of this probe on primary transplanted cells revealed that SYNCRIP depletion causes a trend towards increasing TMI signal, however it's not significant in either LSK cells or progenitors

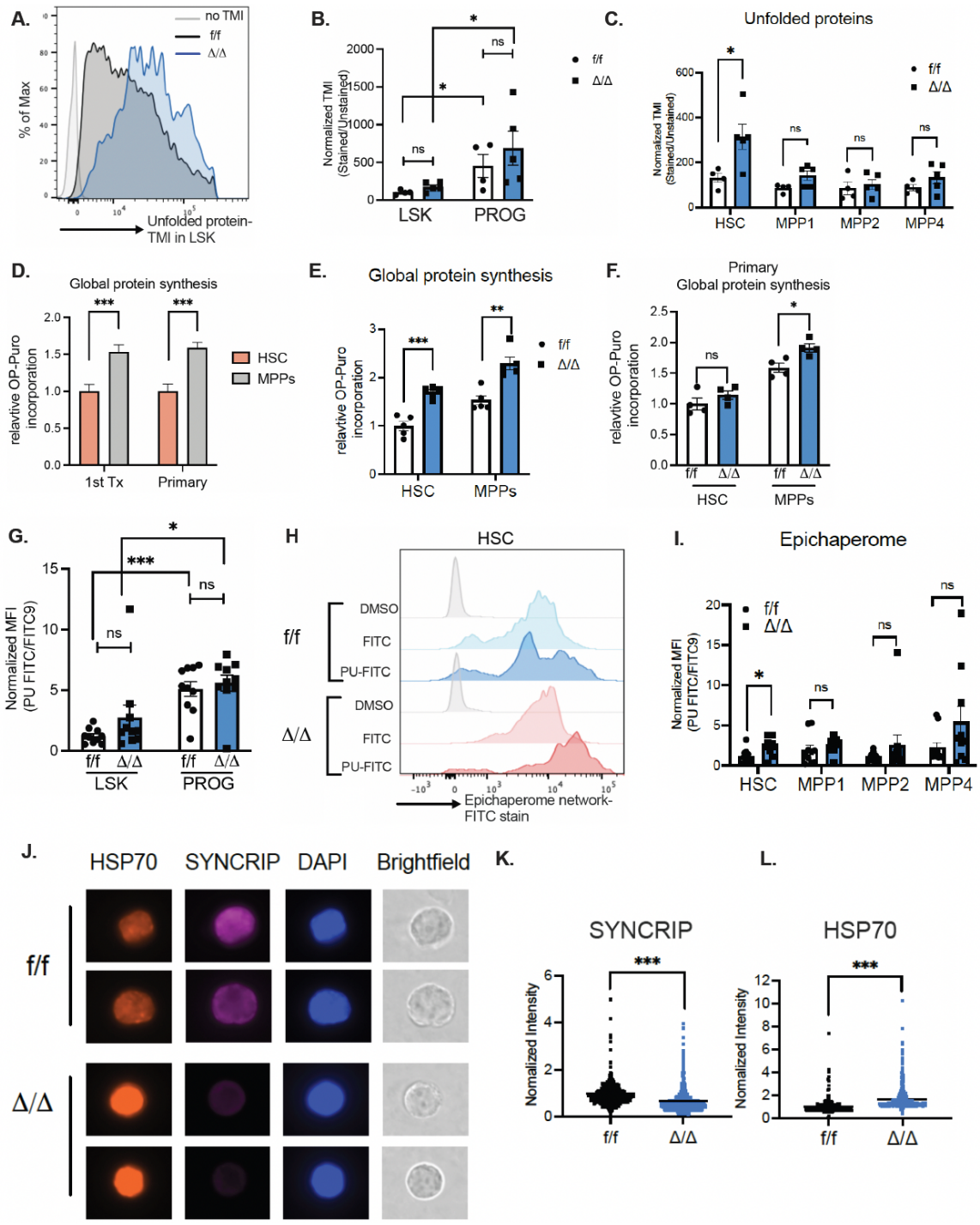
A.
no TMI
f/f
Δ/Δ
% of Max
Unfolded protein-TMI in LSK
B.
Normalized TMI (Stained/Unstained)
LSK
PROG
f/f
Δ/Δ
C.
Unfolded proteins
Normalized TMI (Stained/Unstained)
HSC
MPP1
MPP2
MPP4
D.
Global protein synthesis
relavtive OP-Puro incorporation
HSC
MPPs
1st Tx
Primary
E.
Global protein synthesis
relavtive OP-Puro incorporation
HSC
MPPs
F.
Primary
Global protein synthesis
relavtive OP-Puro incorporation
HSC
MPPs
G.
Normalized MFI (PU FITC/FITC9)
LSK
PROG
H
HSC
DMSO
FITC
PU-FITC
f/f
Δ/Δ
Epichaperome network-FITC stain
I.
Epichaperome
Normalized MFI (PU FITC/FITC9)
HSC
MPP1
MPP2
MPP4
J.
HSP70
SYNCRIP
DAPI
Brightfield
f/f
Δ/Δ
K.
SYNCRIP
Nomalized Intensity
L.
HSP70
Nomalized Intensity

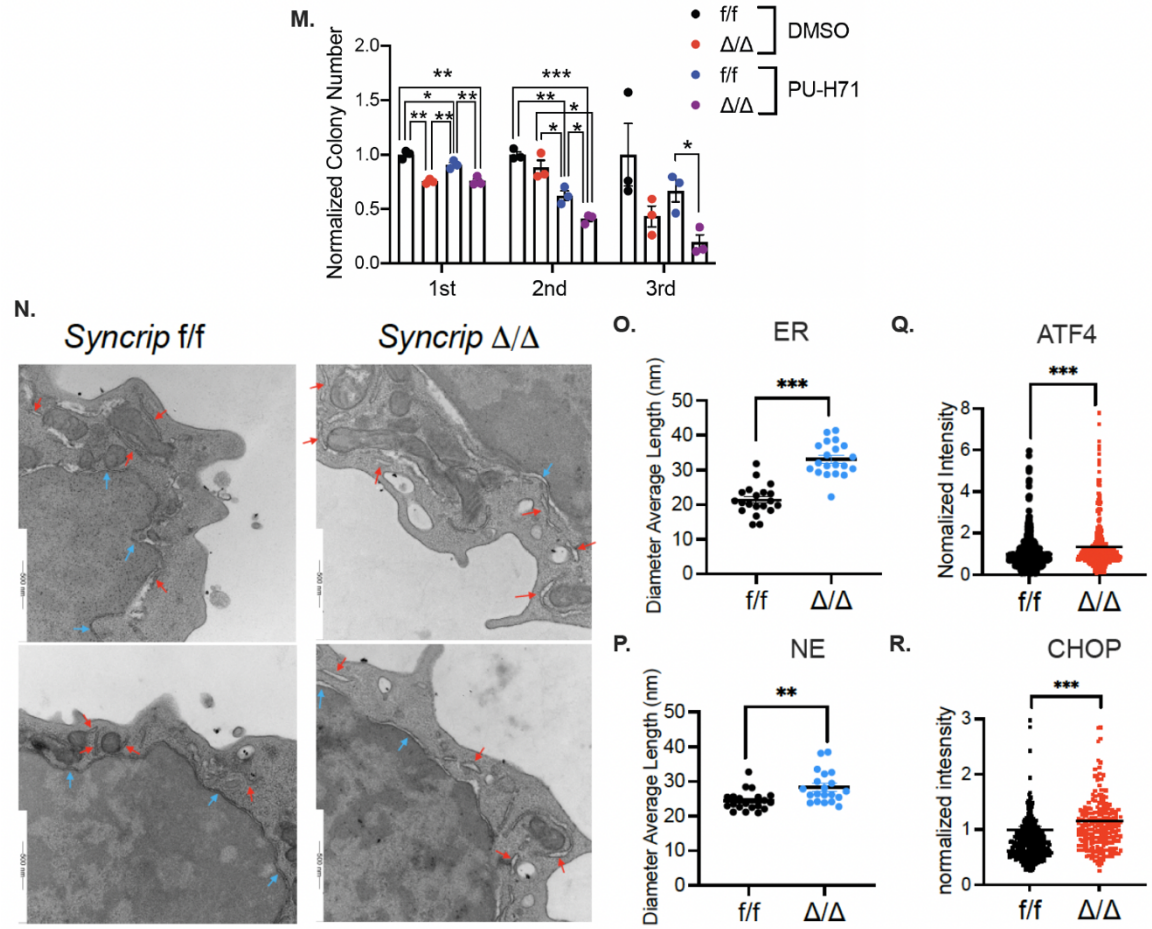

Figure 2.7: SYNCRIP maintains protein homeostasis in HSCs
(A) Representative histograms of TMI flow analysis of LSK (Lin-Sca+ckit+ cells) from *Syncrip* f/f vs. *Syncrip* Δ/Δ mice. **(B)** Quantitative summary of relative tetraphenylethene maleimide (TMI) fluorescent signals in LSK (Lin-Sca+ckit+ cells) and PROG (Progenitors-Lin-Sca-ckit+ cells) from *Syncrip* f/f (n=4) vs. *Syncrip* Δ/Δ (n=5). **(C)** Quantitative summary of relative tetraphenylethene maleimide (TMI) fluorescent signals in HSC, MPP1, MPP2 and MPP4. TMI signals were used to quantify the unfolded proteins in single hematopoietic cells in *Syncrip* f/f (n=4) vs. *Syncrip* Δ/Δ (n=5). **(D)** OP-Puro incorporation in HSC and MPP populations isolated from *Syncrip* f/f primary mice (n=4) (described in Figure 1) or *Syncrip* f/f 1st transplant recipient mice (n=5) (described in Figure 2.3A). OP-Puro incorporation was used to quantify the level of global protein synthesis in single hematopoietic cells. **(E)** OP-Puro incorporation in HSC (CD150+ CD48- LSK) and MPP (CD150- and CD150+CD48+ LSK) populations isolated from *Syncrip* f/f (n=5) vs. *Syncrip* Δ/Δ (n=5) 1st transplant recipient mice. OP-Puro incorporation was used to quantify the level of global protein synthesis in single hematopoietic cells. **(F)** OP-Puro incorporation in HSC (CD150+ CD48- LSK) and MPP (CD150- and CD150+CD48+ LSK) populations isolated from *Syncrip* f/f (n=5) vs. *Syncrip* Δ/Δ (n=5) primary mice. OP-Puro incorporation was used to quantify the level of global protein synthesis in single hematopoietic cells. **(G)** Quantitative summary of PU-FITC fluorescent signals normalized to FITC control in LSK and PROG. PU-FITC signals were used to quantify the epichaperome single hematopoietic cells in *Syncrip* f/f (n=10) vs. *Syncrip* Δ/Δ (n=10). **(H)** Representative histograms of PU-FITC flow analysis of HSCs from *Syncrip* f/f vs. *Syncrip* Δ/Δ. DMSO –

stain control; FITC – background signal control and PU-FITC corresponding to level of epichaperome in single hematopoietic cells. **(I)** Quantitative summary of PU-FITC fluorescent signals normalized to FITC control in HSC, MPP1, MPP2 and MPP4. PU-FITC signals were used to quantify the epichaperome signal of hematopoietic cells in *Syncrip* f/f (n=10) vs. *Syncrip* Δ/Δ (n=10). **(J)** Immunofluorescence (IF) staining of HSP70 and SYNCRIP in *Syncrip* f/f and *Syncrip* Δ/Δ HSCs (shown in brightfield). **(K-L)** Quantitative summary of normalized immunofluorescence reflecting SYNCRIP (K) and HSP70 (L) protein expression in *Syncrip* f/f and *Syncrip* Δ/Δ HSCs (n=4-5 each genotype; total cells *Syncrip* f/f n=324 and *Syncrip* Δ/Δ n=654). **(M)** Normalized number of colonies formed in sequential 1st, 2nd and 3rd plating of LSK cells isolated from *Syncrip* f/f and *Syncrip* Δ/Δ mice and treated with either vehicle- control or Epichaperome inhibitor PU-H17 (n=3/each condition). **(N)** Transmission electron microscopy (TEM) images of HSCs isolated from *Syncrip* f/f vs. *Syncrip* Δ/Δ mice. Red arrow: endoplasmic reticulum (ER); Blue arrow: nuclear envelope (NE). **(O-P)** Quantitative summary of diameter average length (nm) of ER (O) and NE (P). (n=7 each genotype; total cells *Syncrip* f/f n=20 and *Syncrip* Δ/Δ n=20). (**Q-R)** Quantitative summary of normalized immunofluorescence reflecting ATF4 (Q) and CHOP (R) protein expression in *Syncrip* f/f and *Syncrip* Δ/Δ HSCs (n=4-5 each genotype; total cells (Q) *Syncrip* f/f n=548 and *Syncrip* Δ/Δ n=477; (R) *Syncrip* f/f n=342 and *Syncrip* Δ/Δ n=266). All data represent mean ± s.e.m. p values were calculated by two-tailed t test unless specified. * p<0.05, **p<0.01, ***p<0.001 and ns: not significant.

(CMP, MEP, MEP, Lin- cKit+ sca1-) (**Figure 2.7A-B**). What we do observe is that regardless of SYNCRIP expression, progenitor cells have an increase in unfolded protein (**Figure 2.7B**), which reproduces previously published work using this TMI probe [89], and helps validate our results. Next, we investigated the how loss of *Syncrip* alters the TMI signal within the HSPC populations. We noticed an increase in TMI signal in HSCs, meaning that HSCs are accumulating unfolded proteins when SYNCRIP is depleted (**Figure 2.7C**). This effect is specific to HSCs, as we see no significant increase in TMI signal in the rest of the HSPC compartment. This supports our scRNA seq data and suggests that SYNCRIP is required to maintain high protein quality in HSCs. Since we observe a clear increase in unfolded protein in the HSC population, we next wanted to investigate how SYNCRIP influences global translation in HSPCs. Given that our lab's previously published work on SYNCRIP's role in leukemia showed an increase in global translation upon SYNCRIP depletion [167], we predicted that loss of *Syncrip* might also lead to some changes in HSPCs. To test this, we utilized OP-puro (OPP), a cell permeable analog of puromycin, that can incorporate in nascently translated peptides.

The incorporated OPP can be subsequently click conjugated to fluorescent azides and visualized by flow cytometry. In both primary transplanted mice and primary colony mice we observed more OPP incorporation in MPPs compared to HSCs, indicating more protein synthesis occurs in the MPP populations (**Figure 2.7D**). When we look at the effect of SYNCRIP depletion in the primary transplanted mice we observe a significant increase in OPP incorporation in both MPPs and HSCs (**Figure 2.7E**), therefore this suggests that loss of *Syncrip* increases global protein synthesis in transplanted HSPCs. We also looked at what occurs with OPP incorporation when SYNCRIP is depleted in primary colony mice, and in this context, we only observed a significant increase in global translation in the MPP population and not in the HSCs (**Figure 2.7F**). Altogether this data suggests that SYNCRIP plays an important role in regulating translation, and acts as a negative regulator of global translation in HSPCs.

To understand the upregulation of the chaperone expression and activation of the HSF1 pathway we investigated the hyperconnected network of chaperone proteins also known as the epichaperome, which is involved in various processes including facilitating proper protein folding. HSP90 is a chaperone that's been shown to act as a hub for the epichaperome network, and inhibition of HSP90 has been seen to disrupt the epichaperome [196]. Previous work investigating the epichaperome identified that some tumor cells utilize it as a survival mechanism and its expression can be used as a surrogate to indicate aberrant cellular stress [196]. PU-H71 is an inhibitor of HSP90 and has been demonstrated to selectively bind to the epichaperome [196]. PU-H71 conjugated to FITC (PU-FITC) can be used as a tool to identify the state of the epichaperome in cells. We used this chemical tool, along with its negative analog FITC probe, to evaluate the epichaperome in primary transplanted cells. First, we looked at epichaperome signal in HSPCs vs progenitors and observe an increase in signal in

progenitors (**Figure 2.7G**). Next, we looked to see what happens upon loss of *Syncrip,* and we observe no change in the HSPC compartment or progenitor cells (**Figure 2.7G**). However, deeper investigation into the HSPC compartment, we observed an increase in the epichaperome signal upon SYNCRIP depletion in the HSC population, with no significant changes in the rest of the HSPC compartment (**Figure 2.7H-I**). Additionally, we also validated our data from the scRNA-seq that had suggested higher expression of HSP70 chaperone protein. Immunofluorescent staining demonstrated an increase in HSP70 protein upon SYNCRIP depletion (**Figure 2.7J-L**). Studies in tumor cells, including leukemia, have shown that dysregulated epichaperome networks are more sensitive to HSP90 inhibition [196, 197], therefore we wanted to assess the effects of HSP90 inhibition in SYNCRIP depleted cells. We found that upon treatment with PU-H71 the *in vitro* colony replating defect becomes even further reduced in SYNCRIP depleted HSPC cells (**Figure 2.7M**). This suggests that SYNCRIP plays an important role in the chaperone network, and in its absence the normal protein folding program becomes aberrant.

Since it is known that increased protein production and accumulation of unfolded proteins leads to an increase in ER stress and activation of the unfolded protein response, we next sought to investigate if SYNCRIP influences the state of ER-stress in HSCs. To do this, we directly visualized ER-stress using transmission electron microscopy (TEM) on primary transplanted HSCs (**Figure 2.7N**). We see that *Syncrip* loss leads to a visible swelling of the ER (red arrows) and nuclear envelope (NE, blue arrows) (**Figure 2.7N**), which is quantifiable and significantly increased in diameter upon SYNCRIP depletion (**Figure 2.7O-P**). This indicates the presence of ER stress upon loss of *Syncrip*. Furthermore, we tested if the UPR is truly activated by checking the expression of downstream effectors ATF4 and CHOP, which are upregulated when the

PERK arm of the UPR is activated. Immunofluorescence in primary transplanted HSCs shows an increase in both ATF4 (**Figure 2.7Q**) and CHOP (**Figure 2.7R**), confirming our previous data and suggesting that upon loss of SYNCRIP HSCs build up ER stress. Overall, we see that SYNCRIP is involved in regulating global translation in HSPCs, and without its presence HSCs accumulate unfolded proteins, an altered epichaperome and ER stress. Suggesting that SYNCRIP plays a role in maintaining proteolytic balance specifically in the HSCs.

Discussion

RNA binding proteins are emerging as key regulators in maintaining HSCs by impacting properties such as self-renewal and cell fate decisions [36, 58, 66, 96, 188]. Here, our work demonstrates that the RBP SYNCRIP, which has previously been identified to be required for the leukemia stem cell program [167], plays an essential role in maintaining proteomic balance and long-term self-renewal capacity in HSCs under regenerative stress. Upon conditional ablation of SYNCRIP, we found a reduction to lymphocyte blood counts but an overall modest effect on adult blood development and steady state hematopoiesis. However, under conditions of regenerative stress we found a severe defect in HSPC self-renewal. We observed progressive loss in reconstitution potential during serial transplantation, which was nearly abolished by the second transplant. Indicating that SYNCRIP is important for HSC function.

Our single cell RNA sequencing with transplanted cells identified an HSC-C1 population that shows enrichment with the previously described low output HSC signature. Previous work has identified that these low output HSCs possess the highest self-renewing capacity and are responsible for repopulating activities in secondary recipient animals

[191]. Despite the importance of this most primitive HSC population, the molecular mechanisms underpinning its specification and maintenance is largely unknown [191]. However, all the current analysis with our work on these HSC-C1 cells is computational and limits what we can uncover from this population. Additional studies will be necessary to functionally assess this HSC-C1 population, and to truly understand how SYNCRIP influences this population's ability to reconstitute the blood compartment.

Previous work by others, has found protein homeostasis is maintained in a cell specific manner, where HSCs have lower protein synthesis rates than restricted progenitors [88]. HSCs are particularly sensitive to alternations in protein synthesis that even mild increases of protein synthesis reduce HSCs protein quality, resulting in an impairment of self-renewal [89, 91]. Transcriptional profiling of our SYNCRIP KO HSCs demonstrated an activation of the UPR. Further investigation confirmed an accumulation of unfolded protein when SYNCRIP was depleted. Additionally, loss of *Syncrip* let to an increase in nascent global protein synthesis. These results provide some mechanistic insight into why *Syncrip* loss leads to loss of self-renewal in HSCs. On the other hand, we observed an increase in MPP cell cycling suggesting that activation of these cells may be contributing to some loss of blood production during early engraftment. However, this cell cycling activation is not seen in the SYNCRIP KO HSCs, and therefore doesn't explain the severe defects in blood production seen in secondary transplants.

There are several pathways that HSCs utilize to protect themselves from proteotoxic stress such as the ubiquitin proteasome system [198], autophagy [21, 22], and the ER unfolded protein response [199, 200]. The purpose of these pathways is to relieve stressors by attenuating translation, removing or promoting proper folding of unfolded proteins, and, in the case of chronic stress, inducing apoptosis in HSCs [201]. Our

scRNA-seq analysis demonstrated a deregulated stress response unique to SYNCRIP KO HSC populations, which was characterized by HSF-1-dependent activation of heat shock proteins i.e., HSP70 and HSP90. We further validated increased expression of HSP70 protein as well as an accumulation of an epichaperome network in HSCs. Despite being previously characterized in cancer including acute myeloid leukemia as pro-survival mechanisms [196, 197], the formation of the aberrantly reorganized chaperone protein networks reflects an abnormal cellular state. Therefore, the enhanced epichaperome observed in SYNCRIP deficient HSCs strongly indicated an altered proteome. In addition, while HSF1 activation has been shown to help maintain proteostasis in cultured and aging HSCs [202], activation of HSF1 response in SYNCRIP KO HSCs is not sufficient to compensate for SYNCRIP's loss of function. In fact, we also observed activation of ER stress. Specifically, we observed an increase in ATF4 and CHOP protein expression associated with the PERK arm of the UPR, as well as morphological changes in the ER that suggest the presence of mild ER stress. Overall, despite activation of these stress response pathways, SYNCRIP KO HSCs failed to alleviate the proteotoxic stress to preserve self-renewing potential. This suggests a broad and essential role of SYNCRIP in safeguarding the healthy proteome in HSCs.

Contributions

Figure 2.1: *Syncrip* conditional knockout mouse was generated by MSKCC mouse genetics core facility. Characterization of steady state hematopoiesis was conducted mostly by Ly Vu with assistance from Alexandra Schurer and Ersilia Barin. Florisela conducted euthanasia and processing of final timepoints for 3w and 24w timed experiments, used for BM cellularity and organ weights.

Figure 2.2: Colony formation assays and transplantations with homozygous mice were conducted by Ly Vu with assistance from Alexandra Schurer and Ersilia Barin. Florisela performed all transplants and analysis with heterozygous mice.

Figure 2.3: Colony formation assays and transplantations from panels A-M and Q were conducted by Ly Vu with assistance from Alexandra Schurer and Ersilia Barin. Florisela conducted all CFSE transplants and 1-week secondary transplant, with assistance from Kathryn Chang.

Figure 2.4: Pyronin cell cycle experiments were conducted by Ly Vu. Florisela conducted all remaining cell proliferation experiments with assistance from Hanzhi Luo, Lindsey Kuehm, Michael Xiao, Aspen Pierson, Grace Han, and Kathryn Chang.

Figure 2.5: All human cord blood CD34+ experiments were performed by Florisela with training and essential advice from Angie Savino, Hanzhi Luo and Diu Nguyen.

Figure 2.6: scRNA-seq samples were sorted by Ly Vu and sequencing was conducted using the Weil Cornell Epigenomics Core Facility. Alli Pine conducted all scRNA-seq analysis with essential guidance from Christina Leslie. Alli also generated frequencies, plots and heatmaps. All GSEA and Enrichr was generated by Ly Vu.

Figure 2.7: TMI reagent was custom synthesized by Yuning Hong's group. All epichaperome probes and PU-H71 inhibitor were custom synthesized by Gabriela Chiosis' group and protocols were shared by Suhasini Joshi. Florisela conducted all flow cytometry TMI and epichaperome experiments, immunofluorescence, and colony formation assays. TEM was performed by Weil Cornell Microscopy and Image Analysis Core facility. Florisela prepared samples for TEM and analyzed TEM images with essential advice from Weil Cornell Microscopy and Image Analysis Core facility

Chapter III: SYNCRIP regulates cell polarity through direct regulation of CDC42 and maintains proper inheritance of cell fate determinants in HSCs

Modified from: Herrejon Chavez, F., Luo, H., Cifani, P. et al. RNA binding protein SYNCRIP maintains proteostasis and self-renewal of hematopoietic stem and progenitor cells. Nat Commun **14, 2290 (2023). https://doi.org/10.1038/s41467-023-38001-x*

Introduction

In chapters I and II, the importance of RBPs in the context of normal hematopoiesis is discussed. It's highlighted that RBPs play an essential role in regulating HSC self-renewal and repopulation function, through various post-transcriptional processes. However, to fully understand the impact RBPs have in the hematopoietic system we need to understand what transcripts they target, and if there are cell-context dependencies in each cell population. The gold standard methods of determining RBPs transcript interactions has been through crosslinking immunoprecipitation methods (such as eCLIP or iCLIP) followed by RNA-sequencing. However, these methods are technically challenging and require a large source of starting material, which is not feasible for rare populations of cells. Instead, recent studies have developed an alternative method called HyperTRIBE. First developed in Drosophila, HyperTRIBE utilizes the catalytic domain of ADAR, fused to an RBP of interest to generate RNA edits on transcripts from adenosine to inosine which is then read out as guanosine by RNA-seq methods (A-to-G) [165, 203]. Our group recently utilized this technology for use in mammalian cells, specifically with normal and malignant hematopoietic cells using MSI2 as the RBP of interest [98]. Within the normal hematopoietic system this study found that there is differential MSI2 binding within the HSPC compartment, specifically it was shown that MSI2 has modestly more binding activity in HSCs compared to MPPs [98].

This work suggested the RPB activity and transcript regulation is dependent on the cell context and may differ within the HSPC compartment populations.

Therefore, our goal in this chapter is to characterize SYNCRIP's binding activity within different cell contexts in the hematopoietic system. Additionally, we wanted to identify a functional downstream target of SYNCRIP binding, that influences the SYNCRIP depletion defect with HSC self-renewal. To do so, we utilized a multi-omics approach taking advantage of transcriptional and translational changes upon *Syncrip* loss and overlapping this with SYNCRIP's direct binding targets in HSPCs.

Results

Mapping SYNCRIP's Direct Binding Targets in HSPCs Using HyperTRIBE

To understand how SYNCRIP deficiency leads to a defect in HSPC self-renewal observed in chapter II, we needed to characterize its transcriptional targets in HSPCs. To do this, we utilized the HyperTRIBE technology which fuses an RBP to the catalytic domain of ADAR and leads to A-to-I editing which can be read out as A-to-G in RNA-sequencing. Because this technique allows for low input material, we are successfully able to trace SYNCRIP binding activity in HSPC populations. Fused protein SYNCRIP-ADAR (S-ADAR) and control vector (EV) were expressed in HSCs (LSK CD150+ CD48-) and MPPs (non-HSC-LSK, including MPP1, MPP2 and MPP4), cells were sorted for RNA-seq based on GFP positivity 48hrs post transduction. GSEA analysis confirmed the sorted populations for HSC (**Figure 3.1A**) and MPPs (**Figure 3.1B**). We observed increased editing frequency in both HSC and MPP populations with the S-ADAR condition compared to the EV (**Figure 3.1C**). To identify S-ADAR mediated editing

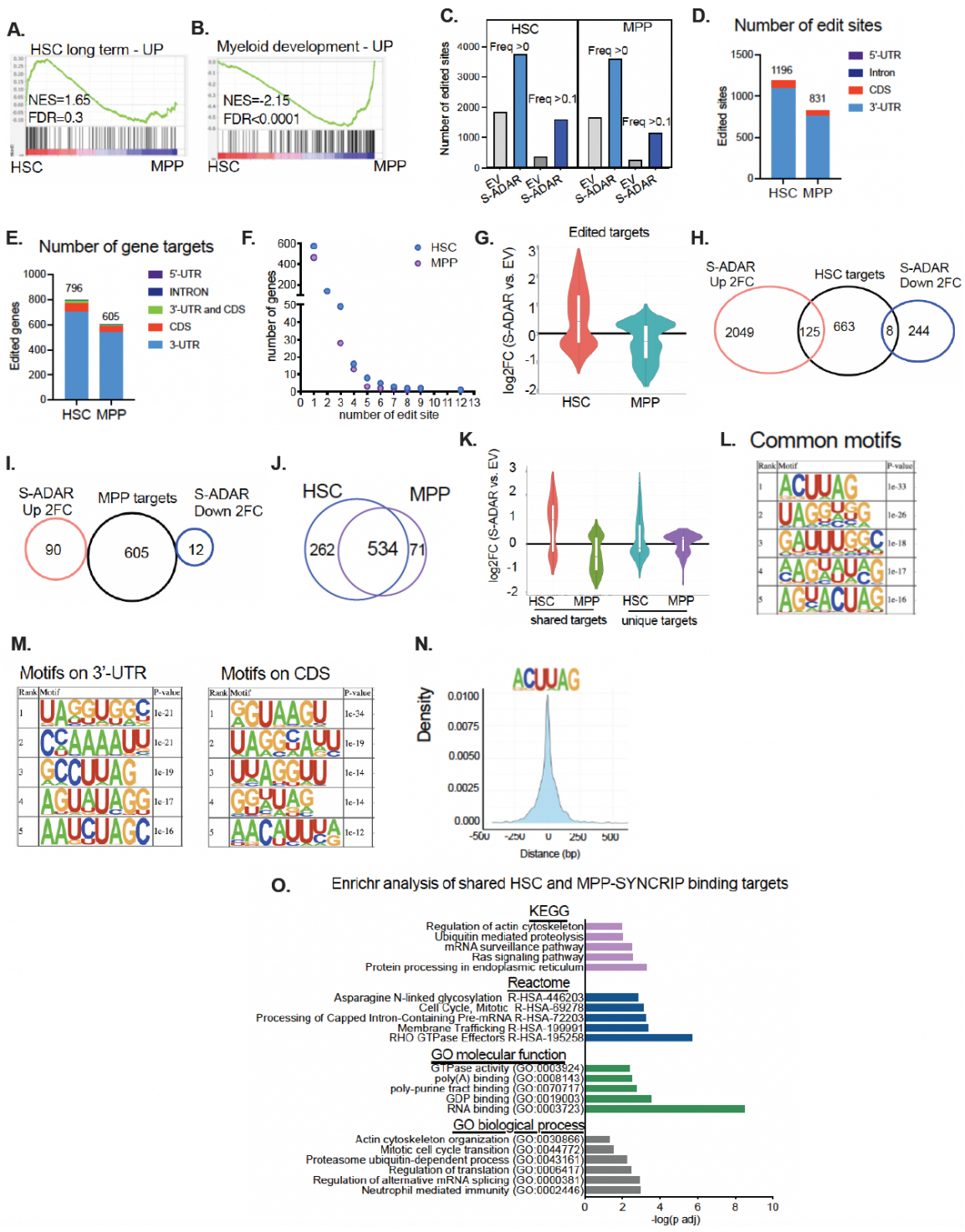

Figure 3.1 Mapping SYNCRIP binding activity in HSCs and MPPs
(A-B) GSEA analysis showing enrichment of genes differentially regulated in HSCs vs. MPP cells transduced with EV control. **(C)** Number of total ADAR-mediated edit sites with no cutoff (Frequency (Freq) >0) and with cutoff (Freq >0.1) in in HSC (left) and MPP (right) cells transduced with either control- empty vector (EV) or SYNCRIP-ADAR (S-ADAR). **(D)** Number of SYNCRIP-HyperTRIBE significant edit sites (FDR <0.05 and differential editing

frequency (SYNCRIP-ADAR vs. control) ≥ 0.1) and their genic locations in HSC and MPP cells. **(E)** Number of target genes with edited sites in (D) in HSC and MPP. **(F)** Distribution of number of genes with corresponding number of edit sites in HSC and MPP. **(G)** Violin plots showing level of mRNA expression (FDR <0.05, log2FC SYNCRIP-ADAR vs. control – S-ADAR vs. EV) of SYNCRIP direct targets identified in HSC and MPP. **(H)** Venn diagram showing overlapping of SYNCRIP targets in HSCs with genes differentially upregulated (2174 genes) and downregulated (252 genes) in HSCs transduced with S-ADAR vs. EV. **(I)** Venn diagram showing overlapping of SYNCRIP targets in MPP with genes differentially upregulated (90 genes) and downregulated (12 genes) in MPP cells transduced with S-ADAR vs. EV. **(J)** Venn diagram showing overlapping of SYNCRIP target mRNAs identified in HSC and MPP: 534 shared targets, 262 HSC unique targets and 71 MPP unique targets. **(K)** Violin plots showing level of mRNA expression (FDR <0.05, log2FC S-ADAR vs. EV) of shared targets, HSC unique targets and MPP unique targets defined in (J). **(L)** De novo motif search identifies SYNCRIP specific binding motifs enriched in mRNA targets with edited sites in both coding regions (CDS) and 3'-UTR. **(M)** De novo motif search identifies SYNCRIP specific binding motifs enriched in mRNA targets with edited sites in (right) coding regions (CDS) and (left) 3'-UTR. **(N)** Probability density function (PDF) plots showing the distance from edits sites to the nearest SYNCRIP motifs as depicted. **(O)** Enrichr analysis for GO biological processes, GO molecular function, Reactome and KEGG enrichment of HSC and MPP shared SYNCRIP target genes. X-axis: $-\log_{10}$(p value).

events, we applied a strict standard of FDR < 0.05 and differential editing frequency >0.1, which has been established by the original developers of this technology [165, 203] and has been validated by our group [98]. In HSCs we observed a total of 1196 edit sites, and MPPs had 831 sites, both showing most of the editing occurring at the 3'UTR region, with some editing in the CDS region (**Figure 3.1D**). This suggests that SYNCRIP is mostly binding to transcript regions in the 3'UTR, however this does not dictate if SYNCRIP's binding to the 3'UTR is influencing any post-transcriptional activity. Additionally, we observed 796 HSC and 605 MPP gene targets, with the majority also being exclusively bound in the 3'UTR and a small fraction also having CDS binding activity (**Figure 3.1E**). Like MSI2, we observe SYNCRIP has more edit sites and gene targets in HSCs compared to MPPs. In both HSCs and MPPs we observe that most transcripts have less than 4 editing sites, with very few that have more (**Figure 3.1F**). We also plotted the number of editing events against the expression levels of the transcripts in S-ADAR vs EV transduced HSCs and MPPs and found no significant

correlation (**Figure 3.1K**), indicating that the editing we observed is not linked to the level of transcript expression. Comparison of SYNCRIP targets and differentially expressed genes when S-ADAR is expressed HSCs shows very few overlaps with upregulated and downregulated transcripts (**Figure 3.1H**). We see no overlap with between MPP targets, upregulated and downregulated S-ADAR genes (**Figure 3.1I**). We also compared the overlap between HSC and MPP targets and found that SYNCRIP shares 534 targets between both populations (**Figure 3.1J**). Additionally, we found there is no correlation between number of editing events and expression of unique MPP or HSC targets (**Figure 3.1K**). These data suggest that SYNCRIP's preference for binding is independent of mRNA abundancy.

Next, we wanted to assess SYNCRIP's binding motifs since no consensus SYNCRIP binding motif has been identified despite SYNCRIP being known to recognize various RNA sequences such as poly(A), UACU splicing element, and GGCU/A sequence in miRNA [171, 174, 175]. Using our SYNCRIP HyperTRIBE global assessment of SYNCRIP binding activity, customized de novo HOMER analysis [98] helped to identify SYNCRIP unique binding motifs. Across the targets the common motifs identified include ACUUAG and UAGGUGG (**Figure 3.1L**). We also identified the motifs unique to the 3'UTR, which has a top hit of UAGGUGGC, and the CDS region with top hit GGUAAGU (**Figure 3.1M**). All identified motifs were mapped within 250bp of edit sites (**Figure 3.1N**). Among the SYNCRIP binding sequences identified, we repeatedly notice the UAG motif which is known as MSI2's consensus binding motif. This is interesting since work from our group has previously identified SYNCRIP and MSI2 share transcript targets in leukemia cells [167]. Finally, we wanted to explore the molecular and cellular programs SYNCRIP regulates in HSPCs. Enrichment analysis for the 536 shared HSC MPP targets allowed us to see what pathways are associated with SYNCRIP (**Figure**

3.1O). Within these hits we see similar pathways we observed in our scRNA-seq dataset, such as protein processing in the ER, ubiquitin processes, and Rho GTPase activity. Interestingly we also observe a lot of RNA binding, translation, and cytoskeleton pathways.

Characterizing the Pathways SYNCRIP influences in HSCs

To better understand how SYNCRIP depletion leads to reduced HSC self-renewal we continued to explore the pathways SYNCRIP is involved with and how SYNCRIP influences transcript and protein abundance. First, we performed transcriptional profiling by conduction RNA-seq on HSCs sorted from transplanted *Syncrip* Δ/Δ and *Syncrip* f/f recipient mice. We observed 499 genes that are upregulated and 561 that are downregulated upon *Syncrip* loss (FDR < 0.05, Log2FC > 1) (**Figure 3.2A**). Using GSEA analysis we found *Syncrip* KO HSCs are not enriched for myeloid development and instead they appear to have enrichment for HSC signatures (**Figure 3.2B**), which is interesting because these cells have reduced self-renewal capacity. This suggests the cells could be trying to transcriptionally compensate to overcome the loss of *Syncrip*. Pathway analysis with Enrichr reveals some similarities with the pathways seen in the HyperTRIBE targets, mostly with translation and translation associated pathways (ribosome biogenesis) (**Figure 3.2C**). Overlap of this dataset with shared HSC and MPP HyperTRIBE targets shows very little overlap between direct targets with the upregulated and downregulated genes when SYNCRIP is KO (**Figure 3.2D**). Expanding this to all the HSC HyperTRIBE targets also shows low amounts of overlap with differentially expressed genes (**Figure 3.2E**). This suggests that SYNCRIP doesn't transcriptionally regulate most of the mRNA transcripts it binds to.

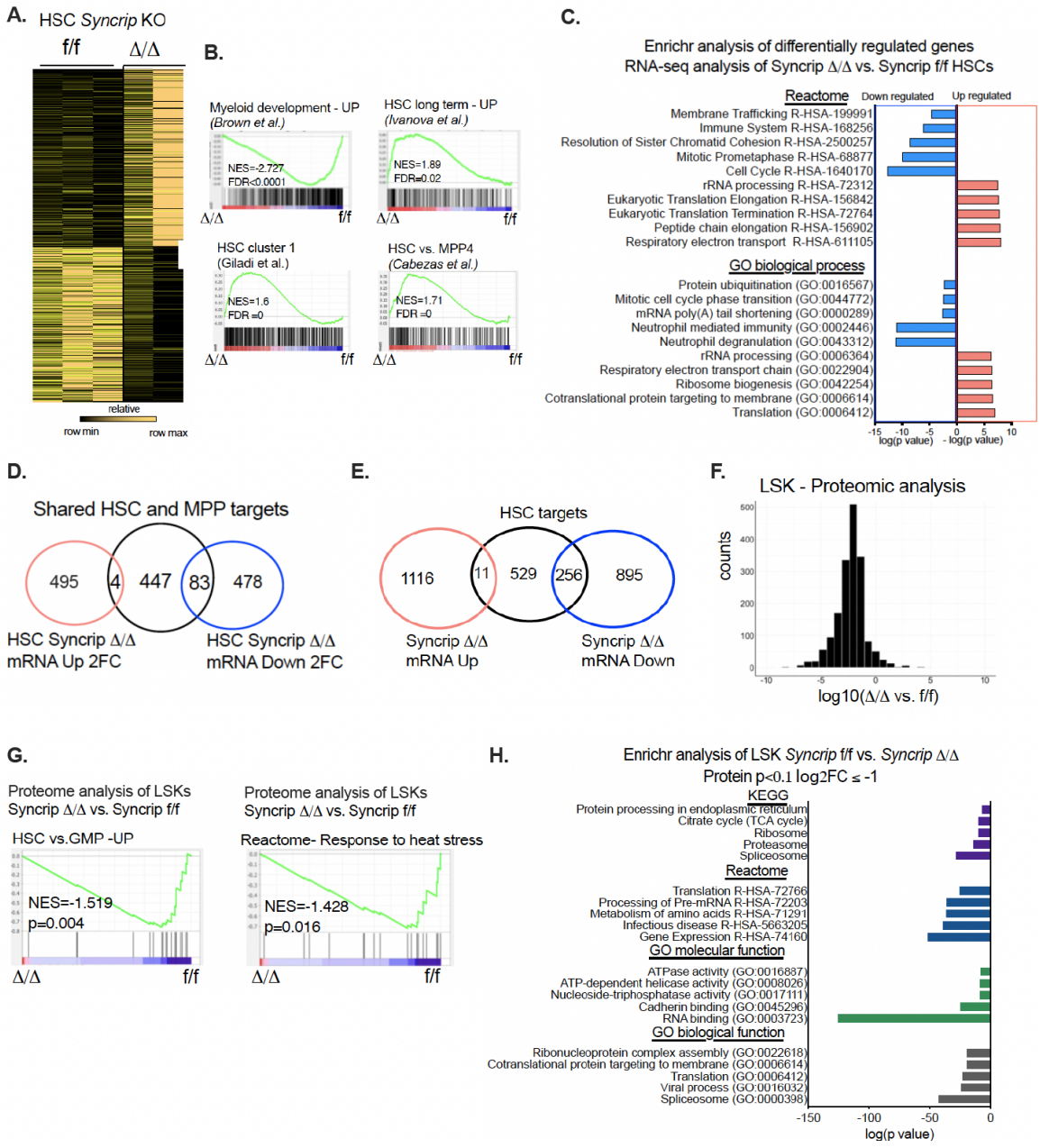
A.
HSC Syncrip KO
f/f
Δ/Δ
relative
row min
row max
B.
Myeloid development - UP
(Brown et al.)
NES=-2.727
FDR<0.0001
HSC long term - UP
(Ivanova et al.)
NES=1.89
FDR=0.02
HSC cluster 1
(Giladi et al.)
NES=1.6
FDR =0
HSC vs. MPP4
(Cabezas et al.)
NES=1.71
FDR =0
Δ/Δ
f/f
C.
Enrichr analysis of differentially regulated genes
RNA-seq analysis of Syncrip Δ/Δ vs. Syncrip f/f HSCs
Reactome
Down regulated
Up regulated
Membrane Trafficking R-HSA-199991
Immune System R-HSA-168256
Resolution of Sister Chromatid Cohesion R-HSA-2500257
Mitotic Prometaphase R-HSA-68877
Cell Cycle R-HSA-1640170
rRNA processing R-HSA-72312
Eukaryotic Translation Elongation R-HSA-156842
Eukaryotic Translation Termination R-HSA-72764
Peptide chain elongation R-HSA-156902
Respiratory electron transport R-HSA-611105
GO biological process
Protein ubiquitination (GO:0016567)
Mitotic cell cycle phase transition (GO:0044772)
mRNA poly(A) tail shortening (GO:0000289)
Neutrophil mediated immunity (GO:0002446)
Neutrophil degranulation (GO:0043312)
rRNA processing (GO:0006364)
Respiratory electron transport chain (GO:0022904)
Ribosome biogenesis (GO:0042254)
Cotranslational protein targeting to membrane (GO:0006614)
Translation (GO:0006412)
-15 -10 -5 0 5 10
log(p value) - log(p value)
D.
Shared HSC and MPP targets
495
4
447
83
478
HSC Syncrip Δ/Δ
mRNA Up 2FC
HSC Syncrip Δ/Δ
mRNA Down 2FC
E.
HSC targets
1116
11
529
256
895
Syncrip Δ/Δ
mRNA Up
Syncrip Δ/Δ
mRNA Down
F.
LSK - Proteomic analysis
counts
log10(Δ/Δ vs. f/f)
G.
Proteome analysis of LSKs
Syncrip Δ/Δ vs. Syncrip f/f
HSC vs.GMP -UP
NES=-1.519
p=0.004
Proteome analysis of LSKs
Syncrip Δ/Δ vs. Syncrip f/f
Reactome- Response to heat stress
NES=-1.428
p=0.016
Δ/Δ
f/f
H.
Enrichr analysis of LSK Syncrip f/f vs. Syncrip Δ/Δ
Protein p<0.1 log2FC ≤ -1
KEGG
Protein processing in endoplasmic reticulum
Citrate cycle (TCA cycle)
Ribosome
Proteasome
Spliceosome
Reactome
Translation R-HSA-72766
Processing of Pre-mRNA R-HSA-72203
Metabolism of amino acids R-HSA-71291
Infectious disease R-HSA-5663205
Gene Expression R-HSA-74160
GO molecular function
ATPase activity (GO:0016887)
ATP-dependent helicase activity (GO:0008026)
Nucleoside-triphosphatase activity (GO:0017111)
Cadherin binding (GO:0045296)
RNA binding (GO:0003723)
GO biological function
Ribonucleoprotein complex assembly (GO:0022618)
Cotranslational protein targeting to membrane (GO:0006614)
Translation (GO:0006412)
Viral process (GO:0016032)
Spliceosome (GO:0000398)
-150 -100 -50 0
log(p value)

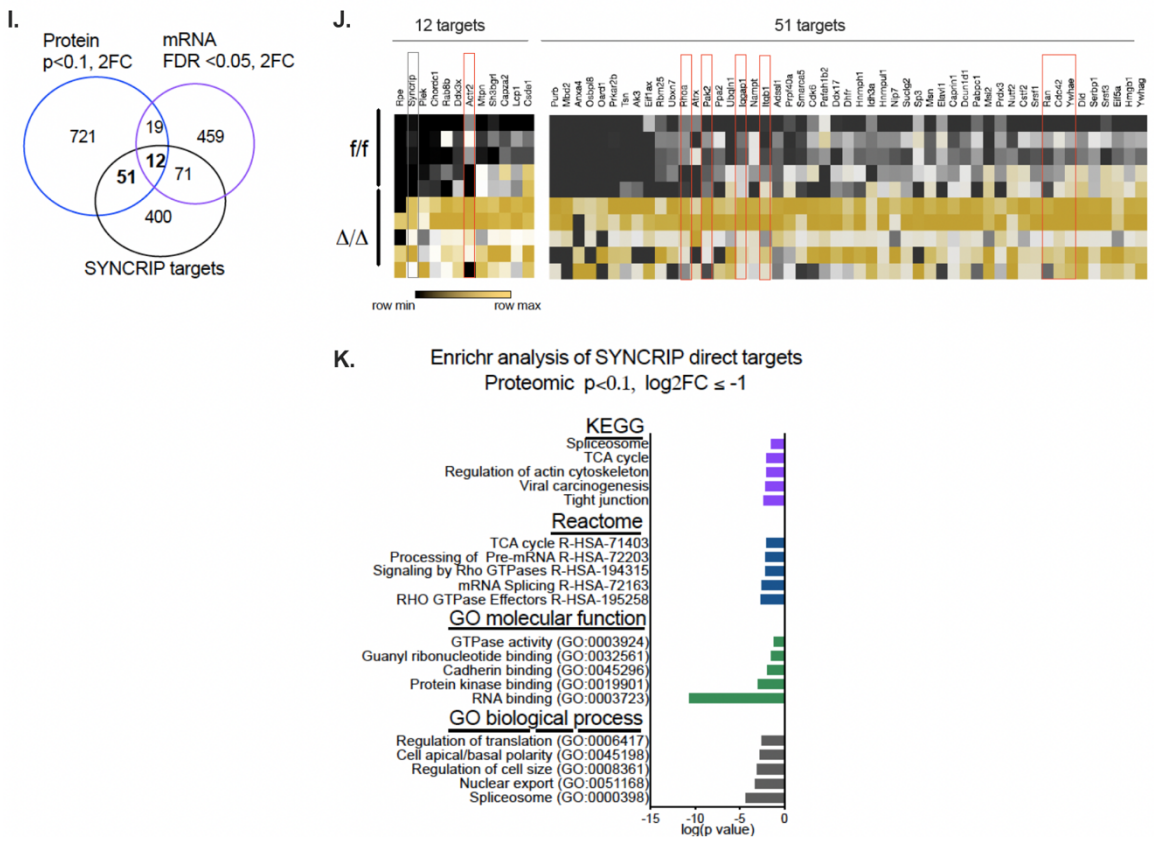

Figure 3.2: Characterizing the Pathways SYNCRIP Influences
(A) Gene expression heat map of the top upregulated and downregulated genes (fold change ≥ 2, FDR <0.05) from RNA sequencing analysis of HSCs (LSK $CD150^{+}CD48^{-}$) isolated from 1st transplant recipient WT *Syncrip* f/f (n=3) and KO *Syncrip* Δ/Δ (n=2) mice described in Figure 2.3A. **(B)** GSEA analysis showing enrichment of targets differentially regulated in HSCs of KO *Syncrip* Δ/Δ vs. WT *Syncrip* f/f for gene expression signatures pertaining to Myeloid development, and long term HSCs. **(C)** Enrichr analysis for GO biological processes and Reactome enrichment of significant (FDR <0.05) downregulated and upregulated genes in *Syncrip* deficient HSCs. X-axis: $-\log_{10}$(p value). Enrichment of downregulated targets was depicted as negative $\log_{10}$(p) and enrichment of upregulated targets was depicted as positive $\log_{10}$(p). **(D)** Venn diagram showing overlapping of shared SYNCRIP target mRNAs with genes significantly (FDR <0.05, FC≥ 2) upregulated (499 genes) and downregulated (561 genes) in *Syncrip* deficient HSCs. **(E)** Venn diagram showing overlapping of SYNCRIP target mRNAs in HSCs with genes whose expression levels are altered (FDR <0.05, FC≥0) in *Syncrip* deficient HSCs. **(F)** Absolute counts representing the abundance of proteins distributed across the range of $\log_{10}$foldchange in LSK cells isolated from *Syncrip* Δ/Δ vs. *Syncrip* f/f 1st transplant recipient mice (n=5 replicates of total 15 mice/genotype) described in Figure 2.3A. **(G)** GSEA analysis showing negative enrichment of proteins significantly downregulated in *Syncrip* f/f LSK cells for gene expression signatures (left) upregulated in HSC vs. GMP, (right) Reactome - Cellular response to heat stress. **(H)** Enrichr analysis for GO biological processes, GO molecular function, Reactome and KEGG enrichment of SYNCRIP target genes whose proteins are

downregulated in *Syncrip* deficient LSKs. X-axis: $\log_{10}$(p value). **(I)** Venn diagram showing overlapping of SYNCRIP direct target mRNAs (534 genes) with mRNAs significantly downregulated ((FDR <0.05, FC≤-2: 561 genes) in *Syncrip* deficient HSCs and genes of which protein levels are significantly downregulated (FDR <0.1, FC≤-2: 803 genes). **(J)** Heat map depicting relative protein levels of 12 and 51 overlapping genes highlighted in (I) in *Syncrip* Δ/Δ vs. *Syncrip* f/f LSKs. Red boxes highlight GTPase/cytoskeleton associated targets. **(K)** Enrichr analysis for GO biological processes, GO molecular function, Reactome and KEGG enrichment of SYNCRIP target genes whose proteins are downregulated in *Syncrip* deficient LSKs. X-axis: $\log_{10}$(p value).

Since SYNCRIP doesn't strongly influence the transcriptional expression of most its binding targets, we next sought out to explore if it influences protein abundance by performing mass spectrometry on sorted LSK cells from transplanted *Syncrip* Δ/Δ and *Syncrip* f/f recipient mice. We quantified over 2000 proteins per condition (FDR < 0.01) and found the vast majority of proteins have a reduction in abundance when SYNCRIP is depleted (**Figure 3.2F**). In contrast to our transcriptional analysis, the proteomic GSEA analysis reveals that the KO LSKs are not enriched for and HSC or cellular response to stress signatures (**Figure 3.2G**). This suggest that at the protein level, the SYNCRIP KO HSPCs have lost stemness and abilities to respond to stress, in line with the phenotype we observe. Pathway analysis with Enrichr reveals upon loss of *Syncrip* we have a reduction in pathways associated with RBPs (spliceosome, RNA binding activity), translation components and protein processing in the ER (**Figure 3.2H**).

Next, we wanted to identify potential hits that are SYNCRIP direct binding targets and are transcriptionally and or translationally regulated. To do this we overlapped various omics data sets, we overlapped our shared HSC/MPP HyperTRIBE targets with our HSC RNA seq and HSPC proteomics. We got 12 targets that overlapped in all three datasets, and 51 that are direct SYNCRIP binding hits and only change in protein quantity suggesting these are translationally regulated by SYNCRIP (**Figure 3.2I**). Within

these 63 hits we observed many that are involved in RHO GTPase pathways (highlighted by red boxes) and many that are RNA binding proteins, including MSI2 (**Figure 3.2J**). Additionally, pathway enrichment analysis with these hits reveals several pathways associated with Rho GTPase activity and regulation of cytoskeleton, as well as RNA binding activity and the spliceosome (**Figure 3.2K**). Of interest, we noted several GTPase's showing reduced protein abundance upon SYNCRIP depletion, such as CDC42, RHOA and RAN. This suggest SYNCRIP may be linked to cellular polarity and cytoskeletal organization by regulating the expression of certain GTPase proteins.

SYNCRIP regulates cell polarity by influencing CDC42 expression

Previous work has identified various members of the GTPase family are important in regulating HSPC properties such as cell survival, proliferation, adhesion, and migration [204]. CDC42 is one such GTPase that is known to regulate cell polarity, cytoskeletal organization and is important in maintaining HSC self-renewal, quiescence, homing and lodging [45, 205, 206]. Given that CDC42 was identified as a direct SYNCRIP binding target and shows protein abundance reduction via our mass spectrometry analyses, we decided to focus our attention on how control of CDC42 expression by SYNCRIP impacts HSCs. First, we validated that loss of SYNCRIP led to a reduced expression of CDC42 protein by conducting immunofluorescence staining, and we confirm that loss of SYNCRIP leads to a reduced expression of CDC42 in HSCs (**Figure 3.3A-C**). As previously mentioned, CDC42 is connected to cell polarity and cytoskeletal organization, because of this we next decided to investigate how SYNCRIP loss influenced tubulin polarity in HSCs. We observed a moderate reduction in TUBULIN expression (**Figure**

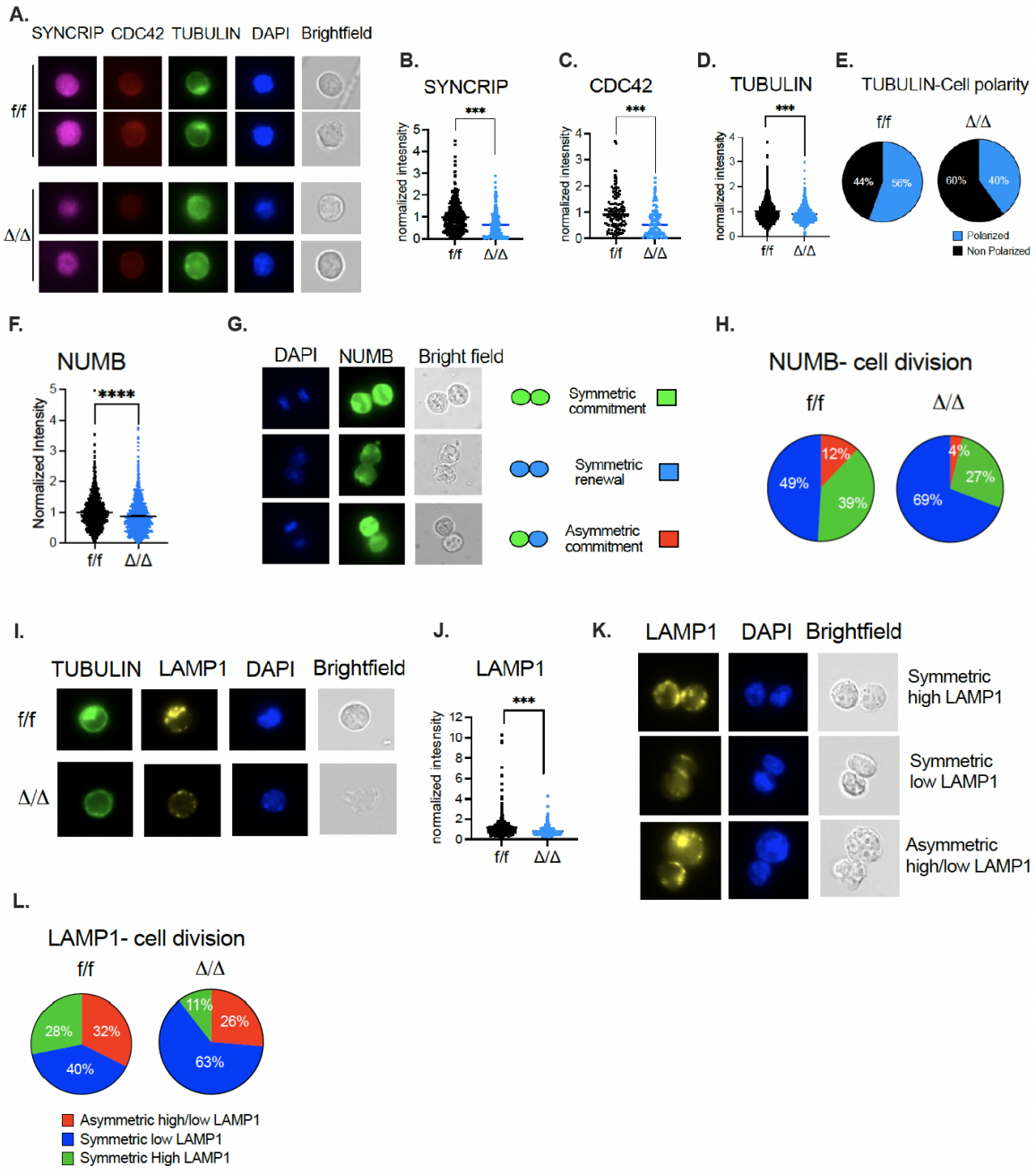

Figure 3.3: SYNCRIP influences cell polarity through regulation of CDC42 expression

(A) Representative images of immunofluorescence (IF) staining of SYNCRIP (left; note antibody also detects HNRNP-R), CDC42 (middle) and TUBULIN (right) in *Syncrip* f/f and *Syncrip* Δ/Δ HSCs (shown in brightfield). **(B-D)** Quantitative summary of normalized IF intensity reflecting the protein levels of (B) SYNCRIP and (C) CDC42 and (D) TUBULIN in *Syncrip* f/f and *Syncrip* Δ/Δ HSCs. **(E)** Quantitative summary of percentage of polarized vs. unpolarized HSCs based on TUBULIN polarization (n=4-5 each genotype; total cells *Syncrip* f/f n=99 and *Syncrip* Δ/Δ n=175). **(F)** Quantitative summary of normalized IF intensity reflecting the protein levels of NUMB in *Syncrip* f/f and *Syncrip* Δ/Δ HSCs. **(G)** Representative images of paired NUMB immunofluorescence (IF) staining daughter assay

performed with *Syncrip* f/f and *Syncrip* Δ/Δ HSCs. DAPI (left), NUMB (middle) and brightfield (right). **(H)** Quantitative summary of percentage of doublet cells in each type of cell division: symmetric commitment, symmetric renewal and asymmetric commitment (n=4-5 each genotype; total daughter pairs *Syncrip* f/f n=108 and *Syncrip* Δ/Δ n=52). **(I)** Representative images of immunofluorescence (IF) staining of TUBLIN, LAMP1 and DAPI in *Syncrip* f/f and *Syncrip* Δ/Δ HSCs (shown in brightfield). **(J)** Quantitative summary of normalized IF intensity reflecting the protein levels of LAMP1 in *Syncrip* f/f and *Syncrip* Δ/Δ HSCs. **(K)** Representative images of paired LAMP1 immunofluorescence (IF) staining daughter assay performed with *Syncrip* f/f and *Syncrip* Δ/Δ HSCs. LAMP1 (left), DAPI (middle) and brightfield (right). **(L)** Quantitative summary of percentage of doublet cells in each type of cell division: symmetric distribution of LAMP1 (symmetric LAMP1 low; symmetric LAMP1 high) and asymmetric distribution of LAMP1 (asymmetric LAMP1 high/low) (n=4-5 each genotype; total pairs *Syncrip* f/f n=110 and *Syncrip* Δ/Δ n=165). LAMP1 daughter cells with intensities Log2FC $\geq \pm 0.6$ were considered asymmetric, while cells with intensities Log2FC $< \pm 0.6$ were scored as symmetric. All data represent mean $\pm$ s.e.m. p values were calculated by two-tailed t test unless specified. * $p<0.05$, ** $p<0.01$, *** $p<0.001$ and ns: not significant.

3.3D) and we also observed a decrease in tubulin cell polarity in HSCs. Suggesting that SYNCRIP loss does impact cell polarity through its regulation of CDC42. For cells to divide symmetrically or asymmetrically (for proper distribution of fate determinants) they must establish proper cell polarity and cytoskeletal organization. As mentioned in chapter I, distribution of certain proteins and organelles act as markers of cell fate decisions in HSCs. Given the cell polarity defect we observe in SYNCRIP KO HSCs we wanted to know if SYNCRIP loss also impacted the abundance and distribution of cell fate determinates. First, we checked the expression of NUMB, a marker of differentiation, and we observed *Syncrip* loss led to a reduction in NUMB expression in HSCs (**Figure 3.3F**). Next we wanted to evaluate if SYNCRIP altered the patterns of NUMB inheritance in dividing HSCs, where the distribution of NUMB is used as a surrogate for three possibilities: symmetric renewal (both NUMB low), symmetric commitment (both NUMB high) and asymmetric cell division (one low and one high NUMB) [36, 207, 208]. We found that SYNCRIP depletion altered the distribution of NUMB in dividing HSCs, where we see a loss of asymmetric cell divisions and

symmetric commitment, with an increase in symmetric renewal divisions (**Figure 3.3H**). Besides NUMB, lysosomes have been shown to be asymmetrically divided in HSCs [35]. Since they are an important component of the degradation machinery and contribute to the removal of misfolded proteins and macromolecules [209]. We conducted additional immunofluorescence and daughter cell assays to investigate if SYNCRIP influences LAMP1 (marker of lysosomes and endosomes) distribution. First, we observe that SYNCRIP loss mildly reduces LAMP1 expression (**Figure 3.3I-J**). Importantly, when we looked at cell distribution of LAMP1 in dividing HSCs, we saw a similar trend that we saw with NUMB. We see a reduction in LAMP1 asymmetric division, and symmetric division with high LAMP1 expression. We also see an increase in symmetric division with low LAMP1 (**Figure 3.3K-L**). Altogether, this data suggests that SYNCRIP regulates cell polarization, and partitioning of cell fate determinants through direct regulation of CDC42 abundance.

SYNCRIP influences partitioning of unfolded proteins in HSCs

It has been suggested, cell division in HSPCs may enable cells to dilute out unfolded or misfolded proteins to maintain proteostasis [89]. Given our observation that SYNCRIP deficient HSCs accumulate unfolded protein, we next wanted to investigate if SYNCRIP loss leads to altered distribution of unfolded protein in dividing HSCs. Using the same TMI probe used in Figure 2.8, we conducted immunofluorescence staining using transplanted *Syncrip* Δ/Δ and *Syncrip* f/f HSCs. With immunofluorescence we first confirm the increase of unfolded protein in HSCs upon SYNCRIP depletion (**Figure 3.4A**). Additionally, we observed positive correlations between TMI expression and LAMP1 in WT and KO cells, with a shift towards the right in KO cells, indicating an increase in TMI and decrease in LAMP1 upon SYNCRIP KO. (**Figure 3.4B**). We

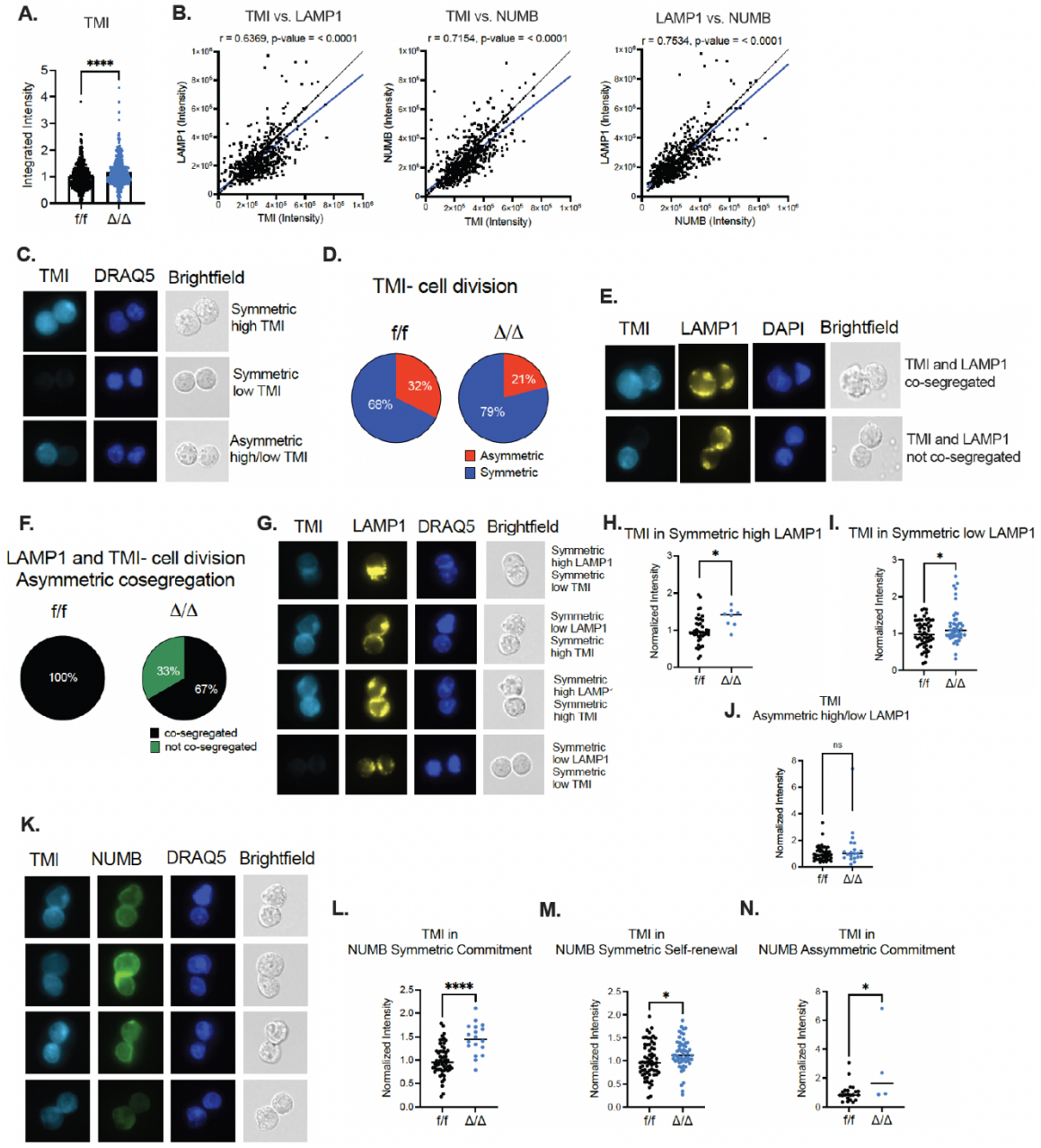

Figure 3.4: SYNCRIP influences partitioning of unfolded protein

(A) Quantitative summary of normalized IF intensity reflecting the levels of TMI in HSCs *Syncrip* f/f n=565 and *Syncrip* Δ/Δ n=378. **(B)** Correlation between TMI signals and LAMP1 and NUMB protein levels. **(C)** Representative images of paired TMI immunofluorescence (IF) staining daughter assay performed with *Syncrip* f/f and *Syncrip* Δ/Δ HSCs. TMI (left), DAPI (middle) and brightfield (right). **(D)** Quantitative summary of percentage of doublet cells in each type of cell division: symmetric distribution of TMI and asymmetric distribution of TMI (n=4-5 each genotype; total pairs *Syncrip* f/f n=71 and *Syncrip* Δ/Δ n=38). TMI daughter cells with intensities Log2FC ≥ ±0.6 were considered asymmetric, while cells with intensities Log2FC < ±0.6 were scored as symmetric. **(E)** Representative images of

paired TMI and LAMP1 immunofluorescence (IF) staining daughter assay performed with *Syncrip* f/f and *Syncrip* Δ/Δ HSCs. TMI (left), LAMP1 (middle) and brightfield (right). **(F)** Quantitative summary of percentage of doublet cells in asymmetric cell division where TMI and LAMP1 are co-segregated or not co-segregated. (n=4-5 each genotype; total pairs *Syncrip* f/f n=10 and *Syncrip* Δ/Δ n=6). **(G)** Representative images of immunofluorescence (IF) staining of TMI and LAMP1 in paired daughter assay performed with *Syncrip* f/f and *Syncrip* Δ/Δ HSCs. TMI (left); LAMP1 (middle), DRAQ5 (right) and brightfield. **(H)** Quantitative summary of normalized IF intensity reflecting the levels of TMI in doublet cells with symmetric high LAMP1 level in *Syncrip* f/f n=40 and *Syncrip* Δ/Δ n=8. **(I)** Quantitative summary of normalized IF intensity reflecting the levels of TMI in doublet cells with symmetric low LAMP1 level in *Syncrip* f/f n=56 and *Syncrip* Δ/Δ n=48. **(J)** Quantitative summary of normalized IF intensity reflecting the levels of TMI in doublet cells with asymmetric high/low LAMP1 level in *Syncrip* f/f n=46 and *Syncrip* Δ/Δ n=20. **(K)** Representative images of immunofluorescence (IF) staining of TMI and NUMB immunofluorescence (IF) staining in paired daughter assay performed with *Syncrip* f/f and *Syncrip* Δ/Δ HSCs. TMI (left); NUMB (middle), DRAQ5 (right) and brightfield. **(L-N)** Quantitative summary of normalized IF intensity reflecting the levels of TMI in doublet cells of NUMB paired daughter assay (L) NUMB symmetric commitment *Syncrip* f/f n=57 and *Syncrip* Δ/Δ n=18; (M) NUMB symmetric self-renewal *Syncrip* f/f n=64 and *Syncrip* Δ/Δ n=54 and (N) NUMB asymmetric commitment *Syncrip* f/f n=22 and *Syncrip* Δ/Δ n=4. All data represent mean ± s.e.m. p values were calculated by two-tailed t test unless specified. * $p<0.05$, ** $p<0.01$, *** $p<0.001$ and ns: not significant.

observed similar positive correlation trends when comparing TMI vs NUMB expression, and LAMP1 vs NUMB expression (**Figure 3.4B**). Interestingly we also observed that TMI was distributed in several patterns in dividing HSCs which include symmetric division with high TMI content, symmetric division with low TMI content, and asymmetric division (one high TMI and one low TMI cell) (**Figure 3.4C**). Next, we assessed how SYNCRIP loss influenced distribution of unfolded protein in dividing HSCs. Like LAMP1 and NUMB, we observe a reduction in asymmetric division of unfolded protein when SYNCRIP is depleted in HSCs (**Figure 3.4D**). Given that LAMP1 is a part of the degradation machinery, we wanted to investigate the relationship between LAMP1 and unfolded protein distribution in HSCs during cell division. We co-stained dividing cells with TMI and LAMP1 and observed that WT cells always have LAMP1 and TMI coinheritance into the same daughter cell during asymmetric division (**Figure 3.4E**). This

means that high content of LAMP1 is co-segregated into the TMI high daughter HSC, and low content LAMP1 is co-segregated into the low TMI daughter HSC. However, this pattern is altered upon SYNCRIP depletion, and we see the presence of dividing pairs that have high LAMP1 content being co-segregated into the low TMI HSC daughter cell, and low LAMP1 content being co-segregated into the high TMI HSC daughter cell (**Figure 3.4E-F**). Next, we evaluated the co-stained symmetric pairs and found various patterns that can occur including high LAMP1 with low TMI, low LAMP1 with high TMI, high LAMP1 with high TMI, and low LAMP1 with low TMI (**Figure 3.4G**). Closer inspection on the TMI expression of the various symmetric LAMP1 high (**Figure 3.4H**) and low (**Figure 3.4I**) pairs reveals a significant increase in TMI when SYNCRIP is depleted, but this is not observed in LAMP1 asymmetric pairs (**Figure 3.4J**). Additionally, we also explored the relationship between TMI and NUMB by co-staining pairs (**Figure 3.4K**). In these pairs, we observe elevated TMI signals in all NUMB distribution conditions (**Figure 3.4L-N**). Of interest, is that we observe an increase in TMI signal in the NUMB symmetric self-renewing pairs upon SYNCRIP depletion (**Figure 3.4M**), this indicates that unfolded protein is accumulating in the HSCs marked for self-renewal. Altogether, these data suggest that loss of SYNCRIP results in defects in partitioning of unfolded proteins and may impact the HSCs ability to dilute out the unfolded proteins onto progenitors during asymmetric division. This may further worsen the stress conditions within the SYNCRIP deficient HSCs.

Functional role of CDC42 in SYNCRIP Depleted HSCs

Given that we see SYNCRIP deficiency led to a loss of CDC42 protein expression and tubulin cellular polarity, we wanted to functionally assess if CDC42 loss was responsible for the self-renewal defect we see in SYNCRIP deficient HSPCs. To test this, we

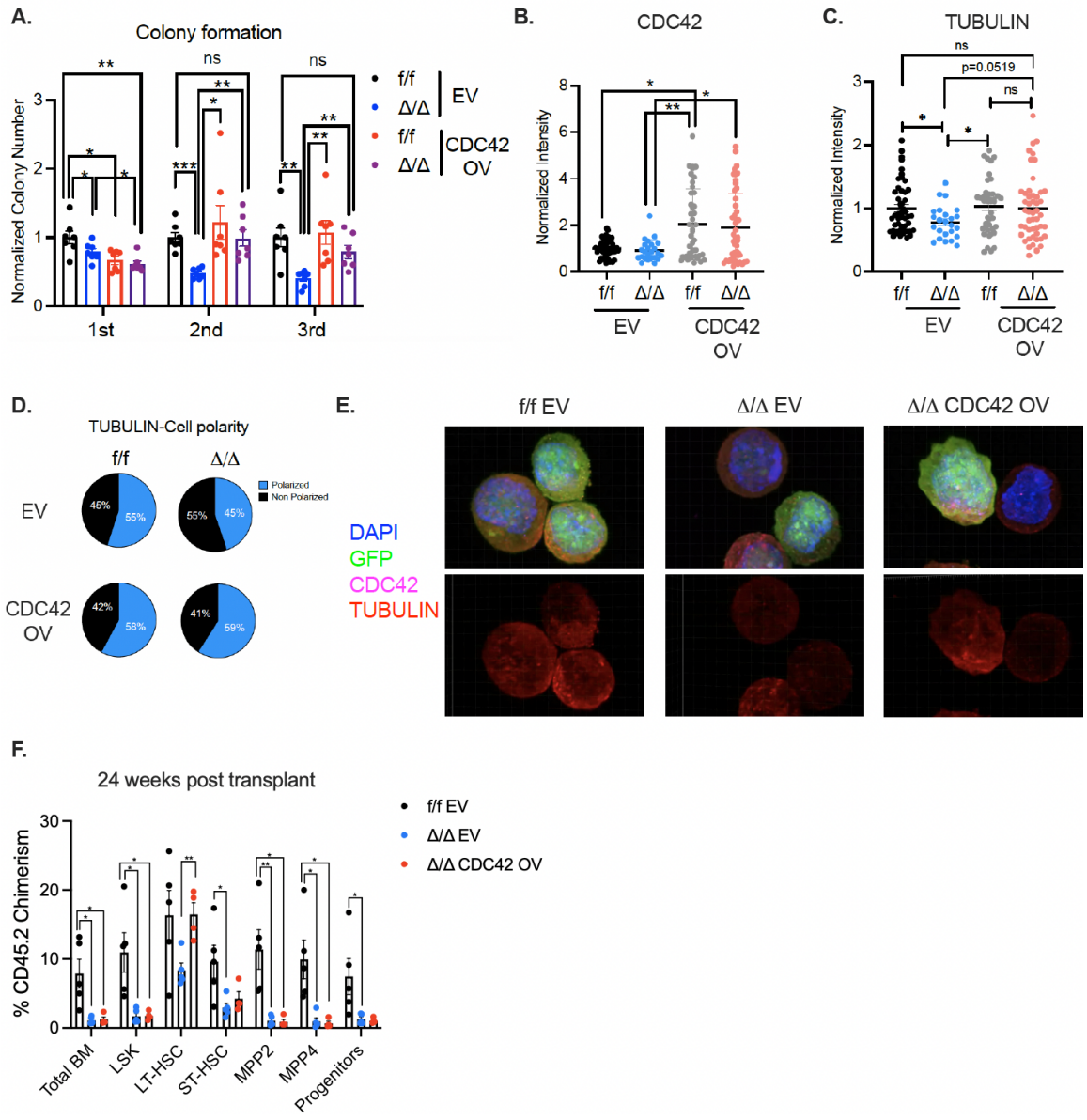

Figure 3.5: SYNCRIP KO in HSPCs Defect Partially Rescued by CDC42
(A) Normalized number of colonies formed in sequential 1st, 2nd and 3rd plating of LSK cells isolated from *Syncrip* f/f and *Syncrip* Δ/Δ mice and transduced with either empty vector control (EV) or vector expressing CDC42 (CDC42-OV) (n=7/each condition). **(B-C)** Quantitative summary of normalized IF intensity reflecting the protein levels of (B) CDC42 and (C) TUBULIN in *Syncrip* f/f and *Syncrip* Δ/Δ LSK cells transduced with either empty vector control (EV) or vector expressing CDC42 (CDC42-OV) as described in (A). **(D)** Quantitative summary of percentage of polarized vs. unpolarized cells described in (A) based on TUBULIN polarization (total cells *Syncrip* f/f-EV n=20; *Syncrip* Δ/Δ-EV n=29; *Syncrip* f/f-CDC42 OV n=22; and *Syncrip* Δ/Δ CDC42 OV n=19). **(E)** Representative images for CDC42 Rescue in LSK cells described in (D). Images show GFP expression in green, tubulin in red, CDC42 in magenta and DAPI counterstain in blue. Only cells with

GFP integrated intensities > 100000 were used for quantification in (D). **(F)** Donor-derived chimerism of LSK cells isolated from *Syncrip* f/f and *Syncrip* Δ/Δ mice and transduced with either empty vector control (EV) or vector expressing CDC42 (CDC42-OV) as described in (A) in primary recipients (n=5 mice/each condition). All data represent mean $\pm$ s.e.m. p values were calculated by two-tailed t test unless specified. * p<0.05, **p<0.01, ***p<0.001 and ns: not significant.

transduced HSPCs (LSK cells) from *Syncrip* KO and *Syncrip* WT with concentrated retrovirus with either empty vector (EV) or CDC42 overexpression (OV). We first assessed the ability of CDC42 overexpression in rescuing the *in vitro* colony formation defect we observed in Figure 2.2B. Interestingly, upon CDC42 OV we see a partial rescue in colony formation abilities in the SYNCRIP deficient HSPCs during secondary and tertiary serial plating as compared to the EV SYNCRIP depleted condition (**Figure 3.5A**). Immunofluorescence from these cells confirms that the CDC42 OV condition has an increase in CDC42 compared to the EV condition (**Figure 3.5B**). Additionally, we also observe that CDC42 OV restored tubulin abundance (although it is not significant, p-value = 0.0519) (**Figure 3.5C**). We also observed that CDC42 OV rescued the tubulin polarity defect observed in SYNCRIP KO HSPCs (**Figure 3.5D-E**). This data suggests that CDC42 is partially responsible for the *in vitro* SYNCRIP self-renewal defects we observe in HSPCs, however it is not sufficient to fully rescue the effect and thus SYNCRIP must be influencing additional functional targets.

Lastly, we wanted to see if CDC42 was also functionally responsible for the *in vivo* self-renewal defect we observe with SYNCRIP deficient HSPCs. To address this, we transduced HSPCs (LSK cells) from *Syncrip* KO and *Syncrip* WT with concentrated retrovirus with either empty vector (EV) or CDC42 overexpression (OV) (we didn't test the f/f CDC42 OV condition *in vivo*). After 48hrs post transduction, we transplanted $1x10^4$ transduced HSPCs into primary CD45.1 recipients. After 24 weeks post transplantation we read-out long term engraftment and observed that in the total bone marrow CDC42

OV doesn't rescue the KO defect (**Figure 3.5F**). However, we do observe that CDC42 OV rescued the engraftment defect in the LT-HSC population but it's unclear why this doesn't result in rescue of the total bone marrow (**Figure 3.5F**). Therefore, this data suggests that the SYNCRIP deficient self-renewal defect we observe in HSPCs isn't entirely a result of SYNCRIP's influence on CDC42 expression. In fact, our multi-omics identified various other SYNCRIP binding targets that may have functional roles, including multiple other RBPs and Rho GTPases. It is possible that a single target isn't responsible for this phenotype we observe with SYNCRIP depletion, and instead it's a result of multiple pathways being dysregulated. Altogether, these data do suggest SYNCRIP in part regulates *in vitro* HSC function through its translational control of CDC42.

Discussion

To identify relevant targets and downstream functional pathways of SYNCRIP in HSCs, we employed a multi-omic approach where we incorporated techniques tailored for low input materials derived from HSCs. These include HyperTRIBE technology to map SYNCRIP's direct mRNA targets, HSC transcriptomic profiling and HSPC proteomic profiling. We found that direct binding of SYNCRIP to its mRNA targets generally does not impact their abundance, strongly suggesting that SYNCRIP might play a more dominant role in post-transcriptional gene expression regulation. We uncovered a direct link between SYNCRIP with several functional pathways associated with GTPase activity and cytoskeleton organization. We further confirmed that SYNCRIP translational control impacted expression of Rho GTPase CDC42, which is well characterized to be essential for HSCs [205, 206, 210]. CDC42 deficient HSCs have been shown to cause defects in engraftment [206]. Additionally, it has been observed that changes in CDC42

activity or expression creates cytoskeletal polarity defects in HSCs [40, 205, 211]. The establishment of cell polarity by CDC42 also helps regulate cell division and segregation of cell fate determinants [43, 45]. It has been recently described that lysosome are asymmetrically inherited with asymmetrical inheritance of lysosomes predicting differentiated multipotent progenitor cells [35]. Lower lysosomal inheritance is associated with co-inheritance of differentiation markers such as CD71, suggesting cells with HSC daughter cells with low levels of lysosomes are primed to differentiate [35]. Additionally, HSC quiescence has been linked to greater abundance of large lysosomes, however this same study also identified that repression of lysosomal activation preserves HSC quiescence and potency [20]. We observed SYNCRIP depletion decreasing cell polarization, LAMP-1 marker associated lysosomes as well as asymmetric inheritance of lysosomes. Another important aspect of cell polarization and asymmetric cell division is the dilution of misfolded proteins from HSCs into differentiating daughter cells, to preserve HSCs from experiencing loss of self-renewal associated with accumulating misfolded protein. Using the TMI probe in HSCs we observed a reduction of asymmetric division of unfolded protein upon SYNCRIP loss, as well as abnormal patterns of distribution of TMI co-stained with LAMP1 and NUMB paired daughter cells. This suggests SYNCRIP deficient HSCs have a defect in their ability to properly dilute out the unfolded protein, in particular we observed accumulation of TMI in cells destined for self-renewal (as marked by NUMB). Important to note that these cell polarity assays were conducted in an *in vitro* setting and although they suggest that SYNCRIP plays a role in maintaining polarity and distribution of cell fate determinants, it is important to consider this limitation. *In vivo* asymmetric division remains a challenging to assess, therefore it is difficult to know if SYNCRIP's effect on polarity is also reflected *in vivo*.

In summary, our work demonstrates SYNCRIP's essential role in maintaining the reserve HSCs self-renewal under regenerative stress. We also demonstrate a mechanism for how an RBP maintains HSC proteostasis and cell polarity through CDC42 regulation axis, further advancing to the current understanding of how RBPs and post transcriptional regulation influence stem cell properties.

Contributions

Figure 3.1: HyperTRIBE constructs were designed by Diu Nguyen and HyperTRIBE experiments were performed by Ly Vu. HyperTRIBE analysis was conducted by Karen Chu, with essential guidance from Christina Leslie. Karen also generated HyperTRIBE characterization plots and performed homer motif analysis. GSEA and Enrichr plots were generated by Ly Vu.

Figure 3.2: HSC RNA seq was conducted by Ly Vu, utilizing Basepair for analysis. Paolo Cifani conducted mass spectrometry with essential guidance from Alex Kentsis. Enricher and GSEA plots were mostly generated by Ly Vu, with Florisela assisting on HSC RNA-seq GSEA.

Figure 3.3: Florisela performed all immunofluorescence and daughter cell assays, with essential advice from Hanzhi Luo and Yuanming Cheng. MSKCC Molecular Cytology core wrote the FIJI scripts to analyze immunofluorescence images.

Figure 3.4: TMI reagent was custom synthesized by Yuning Hong's group. Florisela conducted all immunofluorescence daughter cell assay experiments, using MSKCC Molecular Cytology FIJI scripts to run analysis.

Figure 3.5: Florisela performed all CDC42 rescue experiments. MSKCC Molecular Cytology set up confocal imaging settings and wrote the custom script to analyze these confocal images. *In vivo* rescue was performed with essential assistance from Hanzhi Luo.

Chapter IV: SYNCRIP is Required for Leukemia Stem Cell Self-Renewal

Introduction

Chapters II and III focus on SYNCRIP's role within the normal hematopoietic system, but another aspect we're also interested in exploring is SYNCRIP's role under conditions of malignant transformation. As discussed in chapter I, many RBPs have been recognized to play a role in leukemia and AML. However, not every RBP has been fully characterized. Previous work from our group identified SYNCRIP as a novel regulator of AML through an shRNA screen investigating MSI2's interactome [167]. In murine cells, hairpin depletion of SYNCRIP led to an increase in differentiation, increase in apoptosis, and an increase in survival in recipient mice [167]. In humans, *Syncrip* mRNA expression is upregulated in AML (under various oncogenic backgrounds) when compared to normal hematopoietic cells. Human cell lines and human patient samples also show an overexpression of SYNCRIP compared to CB-CD34+ HSPC cells [167]. Hairpin knockdown of SYNCRIP in human AML cell lines, show a reduction in cell growth and an increase in apoptosis [167]. Additionally, transplantation of SYNCRIP depleted AML patient samples resulted in a reduction of engraftment in mice, and HOXA9 expression correlated with the efficiency of SYNCRIP shRNA depletion. Altogether this study suggested that SYNCRIP plays an important role in regulating AML.

Deeper investigation into SYNCRIP's binding targets uncovered multiple shared targets with MSI2, including *Myc*, *Hoxa9*, and *Ikzf2* [167]. SYNCRIP depletion results in a reduction of HOXA9 protein, but no change in the transcript levels. Follow up with an AHA incorporation assay showed that SYNCRIP was translationally influencing HOXA9

expression. Additionally, HOXA9 retroviral overexpression in SYNCRIP-depleted murine MLL-AF9 cells partially rescued the colony formation defect [167]. Interestingly, MSI2 retroviral overexpression could only partially rescue the colony formation defect and restore the expression of HOXA9 [167]. This highlights the functional importance of the relationship between MSI2 and SYNCRIP and its impact on HOXA9 translational regulation. A major question remaining after this study is how SYNCRIP regulates HOXA9 translation and translation in general, as SYNCRIP is also shown to act as a negative regulator of global protein synthesis in leukemia cells [167]. This suppressive role on translation is not unique to leukemia as shown in chapter II, where SYNCRIP depletion results in enhanced global protein synthesis in HSPCs (Figure 2.8E). Therefore, this effect may be independent of cell context and a general feature of SYNCRIP's influence on translation. However, further work is required to fully understand how SYNCRIP represses global protein synthesis, and why certain targets like HOXA9 are translationally enhanced.

In addition to this regulation of HOXA9, transcriptomic profiling of SYNCRIP-depleted murine cells 4 days post hairpin transduction revealed a loss of the HSC signature, MLL-AF9 direct targets, LSC gene signature, and HOXA9/MEIS1 program [167]. Altogether, this suggested that SYNCRIP plays a role in regulating the leukemia stem cell program. However, our group's previous study didn't functionally assess this, nor did we have the tools to fully characterize *Syncrip's* role in an adult stem cell setting. With the development of our conditional knockout mouse model discussed in chapter II and HyperTRIBE technique discussed in chapter III, we are now able to assess *Syncrip's* functional role and activity in LSCs. Thus, the goal of this chapter is to explore how *Syncrip* functionally impacts LSCs, and to characterize more of its direct mRNA targets in AML.

Results

SYNCRIP is required for *in vivo* leukemia initiation

To determine SYNCRIP's effects on leukemia stem cells, we utilized our SYNCRIP conditional knockout mouse model described in Figure 2.1B. Use of this conditional model better captures the human leukemia hierarchical system and allows for more efficient deletion of *Syncrip* than the previously methods used [167]. The first question we wanted to address is whether SYNCRIP is required for leukemia initiation. To do this, we pIpC injected our *Syncrip* f/f and Syncrip Δ/Δ mice and, at 3w post pIpC we sorted LSK cells and transduced them with MLL-AF9 retrovirus. These cells were sorted for GFP+ and then transplanted into lethally irradiated recipients (**Figure 4.1A**). Bone marrow cells collected prior to transformation show efficient SYNCRIP depletion (**Figure 4.1A**). We tracked the transplanted mice for leukemia progression and observed a significant delay in leukemia upon SYNCRIP depletion, where f/f mice have a median survival of 81 days, and Δ/Δ mice have a median survival of 110 (p-value = 0.0277) (**Figure 4.1B**). This suggests that SYNCRIP is required for leukemia initiation. Next, we wanted to see if the long-term self-renewal capacity of the leukemia stem cells are impacted by *Syncrip* loss, so we performed sequential transplants into secondary, tertiary, and quaternary recipients. In all these transplants we observed a similar effect, where SYNCRIP depletion caused a delay in leukemia progression (**Figure 4.1C-E**). However, we also observe that this delay becomes increasingly shorter after each transplant (**Figure 4.1B-E**). This is unusual because we'd expect a defect in LSC self-renewal would cause the delay to increase. Despite this effect, we do see *Syncrip* loss leading to a delay in leukemia in each transplant, indicating that SYNCRIP is important

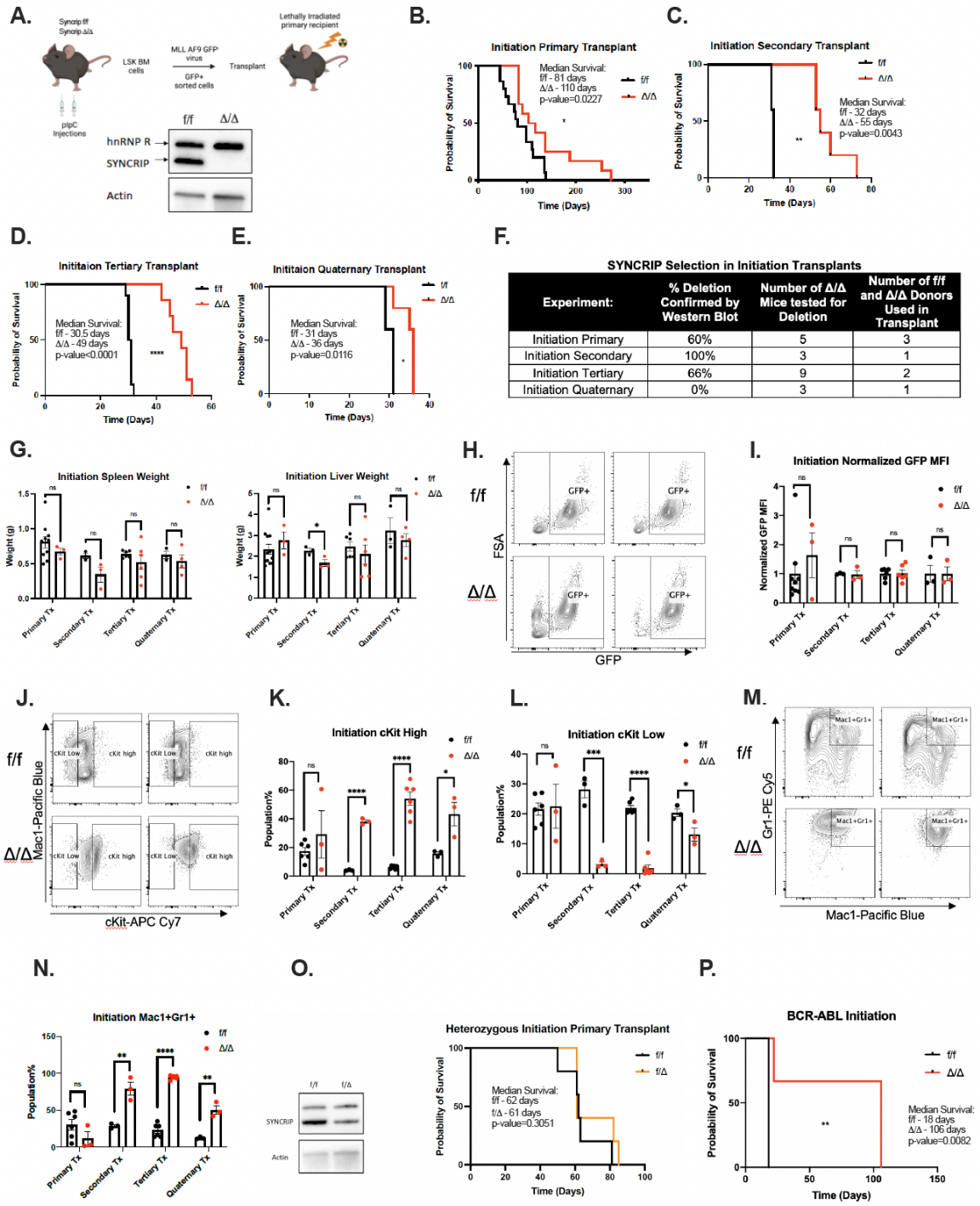

Experiment:	% Deletion Confirmed by Western Blot	Number of Δ/Δ Mice tested for Deletion	Number of f/f and Δ/Δ Donors Used in Transplant
Initiation Primary	60%	5	3
Initiation Secondary	100%	3	1
Initiation Tertiary	66%	9	2
Initiation Quaternary	0%	3	1

Figure 4.1: SYNCRIP is required for in vivo leukemia initiation
(A) Schematic of leukemia initiation transplant set up. Briefly Syncrip f/f and Syncrip Δ/Δ were injected with pIpC, and 3 weeks post injection LSK (lin-Sca1+cKit+) cells were harvested and transduced with MLL-AF9 retrovirus. Cells were GFP+ sorted and 200K cells were then transplanted into primary lethally irradiated B6 recipients. Western blot shows whole bone marrow cells from Syncrip f/f and Syncrip Δ/Δ 3 weeks post pIpC injection. ACTIN was used as a loading control. **(B)** Kaplan-Meier analysis of leukemia initiation primary transplant. Transplant was set up according to (A), f/f n=15, Δ/Δ n=13.

(C) Kaplan-Meier analysis of leukemia initiation secondary transplant. Recipient mice were injected with 100K GFP+ cells from primary transplant, after undergoing sublethal irradiation, f/f n=5, Δ/Δ n=5. **(D)** Kaplan-Meier analysis of leukemia initiation tertiary transplant. Recipient mice were injected with 100K GFP+ cells from secondary transplanted mice, after undergoing sublethal irradiation, f/f n=10, Δ/Δ n=7. **(E)** Kaplan-Meier analysis of leukemia initiation quaternary transplant. Recipient mice were injected with 100K GFP+ cells from tertiary transplanted mice, f/f n=5, Δ/Δ n=5. **(F)** Table showing the SYNCRIP selection occurring in the various initiation transplants. Representative western blots are shown in Figure 4.4. **(G)** Leukemia initiation spleen and liver weights for primary, secondary, tertiary, and quaternary transplants. Primary transplant f/f n=10, Δ/Δ n=3, secondary transplant f/f n=3, Δ/Δ n=3, tertiary transplant f/f n=6, Δ/Δ n=6, quaternary transplant f/f n=3, Δ/Δ n=4. **(H)** Representative flow plots for GFP expression in f/f and Δ/Δ conditions, plots are from secondary transplantation setting. **(I)** Normalized GFP MFI quantification of (H) from primary, secondary, tertiary and quaternary. Each transplant was normalized to its corresponding f/f control. Primary transplant f/f n=9, Δ/Δ n=3, secondary transplant f/f n=3, Δ/Δ n=3, tertiary transplant f/f n=6, Δ/Δ n=6, quaternary transplant f/f n=3, Δ/Δ n=3. **(J)** Representative flow plots for ckit expression in secondary transplant. **(K)** Quantification of (J) for ckit high expressing population in primary, secondary, tertiary, and quaternary transplants. Primary transplant f/f n=6, Δ/Δ n=3, secondary transplant f/f n=3, Δ/Δ n=3, tertiary transplant f/f n=6, Δ/Δ n=6, quaternary transplant f/f n=3, Δ/Δ n=3. **(L)** Quantification of (J) for ckit low expressing population in primary, secondary, tertiary, and quaternary transplants. Primary transplant f/f n=6, Δ/Δ n=3, secondary transplant f/f n=3, Δ/Δ n=3, tertiary transplant f/f n=6, Δ/Δ n=6, quaternary transplant f/f n=3, Δ/Δ n=3. **(M)** Representative flow plots for Mac1 and Gr1 expression in secondary transplant. **(N)** Quantification of (M) for Mac1+Gr1+ population in primary, secondary, tertiary, and quaternary transplants. Primary transplant f/f n=6, Δ/Δ n=3, secondary transplant f/f n=3, Δ/Δ n=3, tertiary transplant f/f n=6, Δ/Δ n=6, quaternary transplant f/f n=3, Δ/Δ n=3. **(O)** Western blot of whole bone marrow harvested from f/f and f/Δ mice to check efficient SYNCRIP depletion 3 weeks post pIpC. ACTIN is use as loading control (left) **and** Kaplan-Meier analysis of leukemia initiation primary heterozygous transplant (right). Transplant was set up same as described in (A), except using donor cells from *Syncrip* f/f and *Syncrip* f/Δ mice. **(P)** Kaplan-Meier analysis of BCR-ABL leukemia initiation transplant, f/f n=5, Δ/Δ n=3.
All data represent mean ± s.e.m. p values were calculated by two-tailed t test unless specified. * $p<0.05$, ** $p<0.01$, *** $p<0.001$ and ns: not significant.

for maintaining LSC long term self-renewal capacities. Additionally, it is important to note that we observed SYNCRIP selection in several of these transplants, for example in the primary transplant the SYNCRIP deletion efficiency was only 60% while in the secondary it was 100% (**Figure 4.1F**). This highlights the clonal selection that occurs when SYNCRIP is expressed, suggesting it outcompetes clones that are SYNCRIP depleted. Additionally, this also indicates that leukemia can still form without the presence of SYNCRIP. Spleen and liver weights from each of these transplants show a decreasing

trend (though not significant) (**Figure 4.1G**), suggesting that *Syncrip* loss may be mildly reducing tumor burden in these organs.

Next, we wanted to explore what may be causing the delay in leukemia upon SYNCRIP depletion and we started by evaluating if these mice had a difference in MLL-AF9 expression, which we could evaluate based on GFP expression. We observed that there was no significant difference in GFP+ MLL-AF9 expression in the bone marrow between *Syncrip* f/f and *Syncrip* Δ/Δ conditions (**Figure 4.1H-I**), indicating that the delay we observe isn't a result of MLL-AF9 expression. We then investigated the cKit expression in these cells. Previous work investigating MSI2's role in LSCs has shown that MSI2 loss resulted in a decrease cKit high expressing cells [152]. Since cKit is a marker of hematopoietic stem cells we decided to look at how it's expression changes upon *Syncrip* loss. However, unlike MSI2, upon SYNCRIP depletion we see an increase in cKit high expressing cells starting at the secondary transplant (**Figure 4.1J-K**) and we observe a decrease in cKit low cells (**Figure 4.1L**). We also looked at myeloid differentiation and observe an increase in Mac1+Gr1+ cells starting at the secondary transplant (**Figure 4.1M-N**). This increase in differentiation is expected since it's already been shown that reduction of SYNCRIP causes increased differentiation [167], but the cKit expression results are unexpected. This indicates that SYNCRIP depletion causes an increase in stemness as well as differentiation, at the cell surface marker level. Alternatively, this abnormal cell marker expression could also be a byproduct of some sort of clonal selection or additional transformation may have occurred between the primary and secondary transplant. However further investigation may be required to fully understand the clonal expansion upon *Syncrip* loss.

We also wanted to ensure the delay in leukemia we observe is a result of *Syncrip* loss and not a consequence of Cre recombinase expression. To test this question, we used *Syncrip* f/f and *Syncrip* f/Δ heterozygous mice to perform the same MLL-AF9 transformation and transplantation. After 3 weeks post pIpC, we observe reduction of SYNCRIP protein expression, accounting for ~50% depletion compared to control (**Figure 4.1O**). LSK cells from these mice were transduced with MLL-AF9 and transplanted into recipients. We saw no difference in leukemia progression upon heterozygous SYNCRIP depletion (**Figure 4.1O**), indicating that the delay we observed in homozygous mice is a result of *Syncrip* loss and not Cre recombinase expression. Additionally, this also suggests that only 50% depletion of SYNCRIP is not sufficient to prolong survival in MLL-AF9 leukemia recipients.

In addition to MLL-AF9 AML we also wanted to see if SYNCRIP's effects are broader across other myeloid leukemias. Therefore, we also tested the requirement for *Syncrip* in BCR-ABL driven leukemia initiation. In this setting we also observed a delay in leukemia progression upon SYNCRIP depletion (**Figure 4.1P**). This indicates that SYNCRIP's role in myeloid leukemia's is broad and not limited to only one type of oncogenic transformation. Altogether, these data show that *Syncrip* plays an important role in leukemia initiation and maintaining LSC self-renewal.

SYNCRIP is required for in vivo leukemia maintenance

Given that we saw *Syncrip* is required for leukemia initiation, we also wanted to know if *Syncrip* is important for leukemia maintenance. To investigate this, we used a similar method as described in Figure 4.1A, where LSK cells from *Syncrip* f/f and Syncrip Δ/Δ mice were harvested, transduced with MLL-AF9 retrovirus, and transplanted into lethally

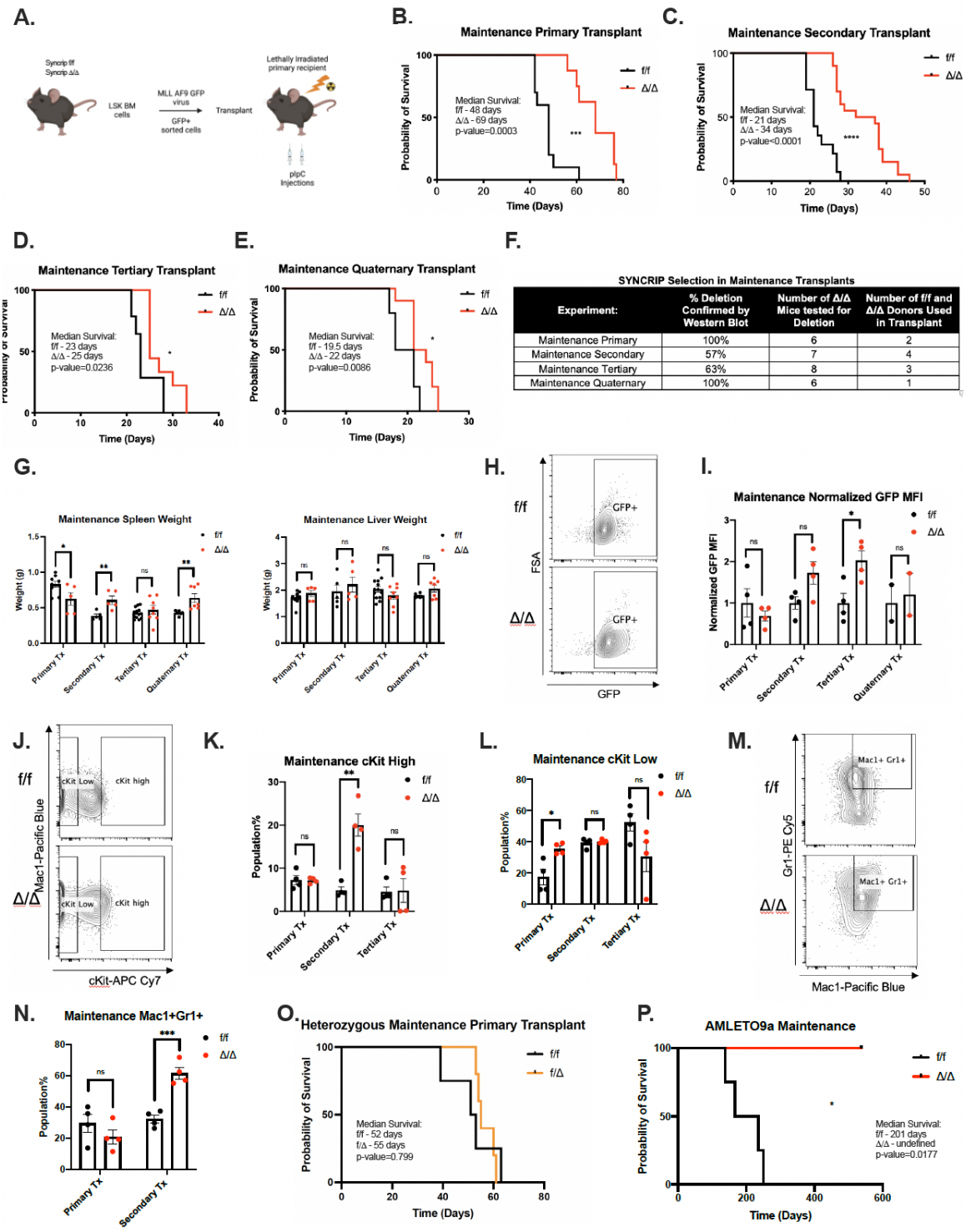

Figure 4.2: SYNCRIP is required for in vivo leukemia maintenance

(A) Schematic of leukemia maintenance transplant set up. Briefly Syncrip f/f and Syncrip Δ/Δ LSK (lin-Sca1+cKit+) cells were harvested and transduced with MLL-AF9 retrovirus. Cells were GFP+ sorted and 200K cells were then transplanted into primary lethally

irradiated B6 recipients. After 2 weeks post transplantation, mice were injected with pIpC and tracked for leukemia progression. **(B)** Kaplan-Meier analysis of leukemia maintenance primary transplant. Transplant was set up according to (A), f/f n=10, Δ/Δ n=8. **(C)** Kaplan-Meier analysis of leukemia maintenance secondary transplant. Recipient mice were injected with 100K GFP+ cells from primary transplant, after undergoing sublethal irradiation, f/f n=14, Δ/Δ n=20. **(D)** Kaplan-Meier analysis of leukemia maintenance tertiary transplant. Recipient mice were injected with 100K GFP+ cells from secondary transplanted mice, after undergoing sublethal irradiation, f/f n=14, Δ/Δ n=9. **(E)** Kaplan-Meier analysis of leukemia maintenance quaternary transplant. Recipient mice were injected with 100K GFP+ cells from tertiary transplanted mice, after undergoing sublethal irradiation, f/f n=10, Δ/Δ n=10. **(F)** Table showing the SYNCRIP selection occurring in the various maintenance transplants. Representative western blots are shown in Figure 4.4. (G) Leukemia maintenance spleen and liver weights for primary, secondary, tertiary, and quaternary transplants. Primary transplant f/f n=9, Δ/Δ n=5, secondary transplant f/f n=5, Δ/Δ n=5, tertiary transplant f/f n=13, Δ/Δ n=8, quaternary transplant f/f n=6, Δ/Δ n=7. **(H)** Representative flow plots for GFP expression in f/f and Δ/Δ conditions, plots are from secondary transplantation setting. (**I**) Normalized GFP MFI quantification of (H) from primary, secondary, tertiary and quaternary. Each transplant was normalized to its corresponding f/f control. Primary transplant f/f n=4, Δ/Δ n=4, secondary transplant f/f n=4, Δ/Δ n=4, tertiary transplant f/f n=4, Δ/Δ n=4, quaternary transplant f/f n=2, Δ/Δ n=2. **(J)** Representative flow plots for ckit expression in secondary transplant. **(K)** Quantification of (J) for ckit high expressing population in primary, secondary, tertiary, and quaternary transplants. Primary transplant f/f n=4, Δ/Δ n=4, secondary transplant f/f n=4, Δ/Δ n=4, tertiary transplant f/f n=4, Δ/Δ n=4. **(L)** Quantification of (J) for ckit low expressing population in primary, secondary, tertiary, and quaternary transplants. Primary transplant f/f n=4, Δ/Δ n=4, secondary transplant f/f n=4, Δ/Δ n=4, tertiary transplant f/f n=4, Δ/Δ n=4. **(M)** Representative flow plots for Mac1 and Gr1 expression in secondary transplant. **(N)** Quantification of (M) for Mac1+Gr1+ population in primary, secondary, tertiary, and quaternary transplants. Primary transplant f/f n=4, Δ/Δ n=4, secondary transplant f/f n=4, Δ/Δ n=4. **(O)** Kaplan-Meier analysis of leukemia maintenance primary heterozygous transplant. Transplant was set up same as described in (A), except using donor cells from *Syncrip* f/f and *Syncrip* f/Δ mice. **(P)** Kaplan-Meier analysis of AML-ETO9a leukemia maintenance transplant, f/f n=4, Δ/Δ n=3.
All data represent mean ± s.e.m. p values were calculated by two-tailed t test unless specified. * p<0.05, **p<0.01, ***p<0.001 and ns: not significant.

irradiated recipients. However, we waited until mice had engrafted the MLL-AF9 transduced cells prior to pIpC injection and excision of *Syncrip* (**Figure 4.2A**). We tracked leukemia progression in these primary transplanted recipients and saw a delay in leukemia upon loss of *Syncrip,* with f/f mice having a median survival of 48 days, while Δ/Δ mice showed a median survival of 68 days (p-value=0.0003) (**Figure 4.2B**). This indicates that *Syncrip* is also required for leukemia maintenance. Next, we tested how maintenance of LSC function was impacted by *Syncrip* loss, by performing sequential

transplants in secondary, tertiary, and quaternary recipients (**Figure 4.2C-E**). Very similar to the results we got for leukemia initiation transplants, we observed a delay in leukemia that progressively got shorter in each transplant (**Figure 4.2B-E**). Suggesting a similar mechanism may be taking place in the two settings. Additionally, we also observed that SYNCRIP depletion efficiency varied between the different transplants, for example we observed that in the primary transplant there was 100% SYNCRIP deletion but in the secondary transplant we observed only a 57% deletion efficiency (**Figure 4.2F**). This again highlights our hypothesis that clones with SYNCRIP expression can outcompete the SYNCRIP depleted cells and suggests that leukemias without SYNCRIP are capable of being maintained.

We continued to characterize these leukemia transplants and observed that the spleen and liver weights didn't show a clear trend. In the primary transplant we see a reduction in spleen weight but not in the remaining transplants. We also see no change in liver weights (**Figure 4.2G**). Same as the leukemia initiation setting, we also checked for MLL-AF9 expression by tracking GFP in the various transplants. In the leukemia maintenance, for the most part we don't see a significant difference in GFP expression, however we do observe a significant increase in GFP MFI upon SYNCRIP depletion in the tertiary transplant (**Figure 4.2H-I**). However, despite this increase in GFP MLL-AF9 expression we still see a delay in the leukemia progression, suggesting SYNCRIP has a potent effect in leukemia maintenance. We also tracked changes in cKit expression and observed an increase in the cKit high population at the secondary transplant (**Figure 4.2J-K**) but the cKit low population trends varied between the different transplants (**Figure 4.2L).** Although the shift in cKit expression in the leukemia maintenance transplants isn't as dramatic as we saw with the leukemia initiation transplants, we do see an increase in cKit high population in the secondary transplant. Additionally, we also

observed differentiation changes at the secondary transplant, which showed an increase in Mac1+Gr1+ cells (**Figure 4.2M-N**). These results are very similar to what we saw in the leukemia initiation setting, suggesting SYNCRIP may be impacting both scenarios in a mechanistically similar fashion. Altogether these data show that SYNCRIP is required for leukemia maintenance and LSC self-renewal.

To determine that SYNCRIP's role on leukemia maintenance is not a result of Cre recombinase expression, we conducted a similar transplant as described in Figure 4.2A using heterozygous mice. We transduced *Syncrip* f/f and *Syncrip* f/Δ LSK cells with MLL-AF9 retrovirus and transplanted them into lethally irradiated primary recipients. With the heterozygous donor cells, we observed no difference in leukemia progression (**Figure 4.2O**). This suggests that Cre expression is not responsible for the delay in leukemia observed upon SYNCRIP depletion. This also suggests a dose dependency on this phenotype, meaning that to see a delay in leukemia, a greater than 50% reduction of SYNCRIP is required.

In addition to MLL-AF9 we also wanted to see if SYNCRIP is required for maintenance in a different myeloid leukemia background like AML-ETO9a. In this setting we observed a similar effect, where SYNCRIP depletion caused a delay in leukemia progression (**Figure 4.2P**). In fact, all the SYNCRIP depleted mice never developed leukemia symptoms. This indicates that SYNCRIP's impact on leukemia maintenance is not specific to one oncogenic background and its requirement is broader. It could also suggest that SYNCRIP might be more essential in leukemia models that rely on the HSCs as the cell of origin. Although additional experiments are needed to strengthen this hypothesis.

Transcriptomic profiling of LSCs shows HOXA9 program is not downregulated

To explore the mechanisms behind the delay in leukemia caused by SYNCRIP depletion, we conducted transcriptomic profiling of sorted LSCs (GFP+, highest 10% cKit expressing cells) from the primary maintenance experiment described in Figure 4.2B. We observed a signature of 169 downregulated, and 414 upregulated genes (p-adj < 0.05, Log2FC > 1) (**Figure 4.3A**). Interestingly, in the SYNCRIP KO condition we observed significant upregulation of *Hspa1b* and *Hspa1a,* both of which had Log2FC > 3.5 (**Figure 4.3B**), this is very similar to what we observed in SYNCRIP depleted HSCs and suggests a similar molecular mechanism. Gene set enrichment analysis (GSEA) of these transplanted LSCs showed that upon *Syncrip* loss, the myeloid development program is not being enriched (**Figure 4.3C**). Instead, we see these SYNCRIP KO LSCs transcriptionally express a stem cell maintenance signature (**Figure 4.3D**). Very unexpectedly, we observed that the SYNCRIP depleted LSCs are not transcriptionally downregulating the HOXA9 and MEIS1 program (**Figure 4.3E**). This comes as a surprise since previous work using MLL-AF9 leukemia with shRNA knockdown of SYNCRIP at 4 days post transduction had shown a significant downregulation of the HOXA9 and MEIS1 program [167]. However, because these cell's come from a transplant that has potentially undergone clonal selection, these results suggest that a compensatory mechanism has developed to promote the expression of HOXA9 in the absence of SYNCRIP expression. This may also explain the shortening in leukemia delay we observe upon SYNCRIP depletion during sequential transplantations.

Further exploration into the mechanisms enhanced by SYNCRIP depletion in these transplanted LSCs led us to conduct additional GSEA analysis, and we found

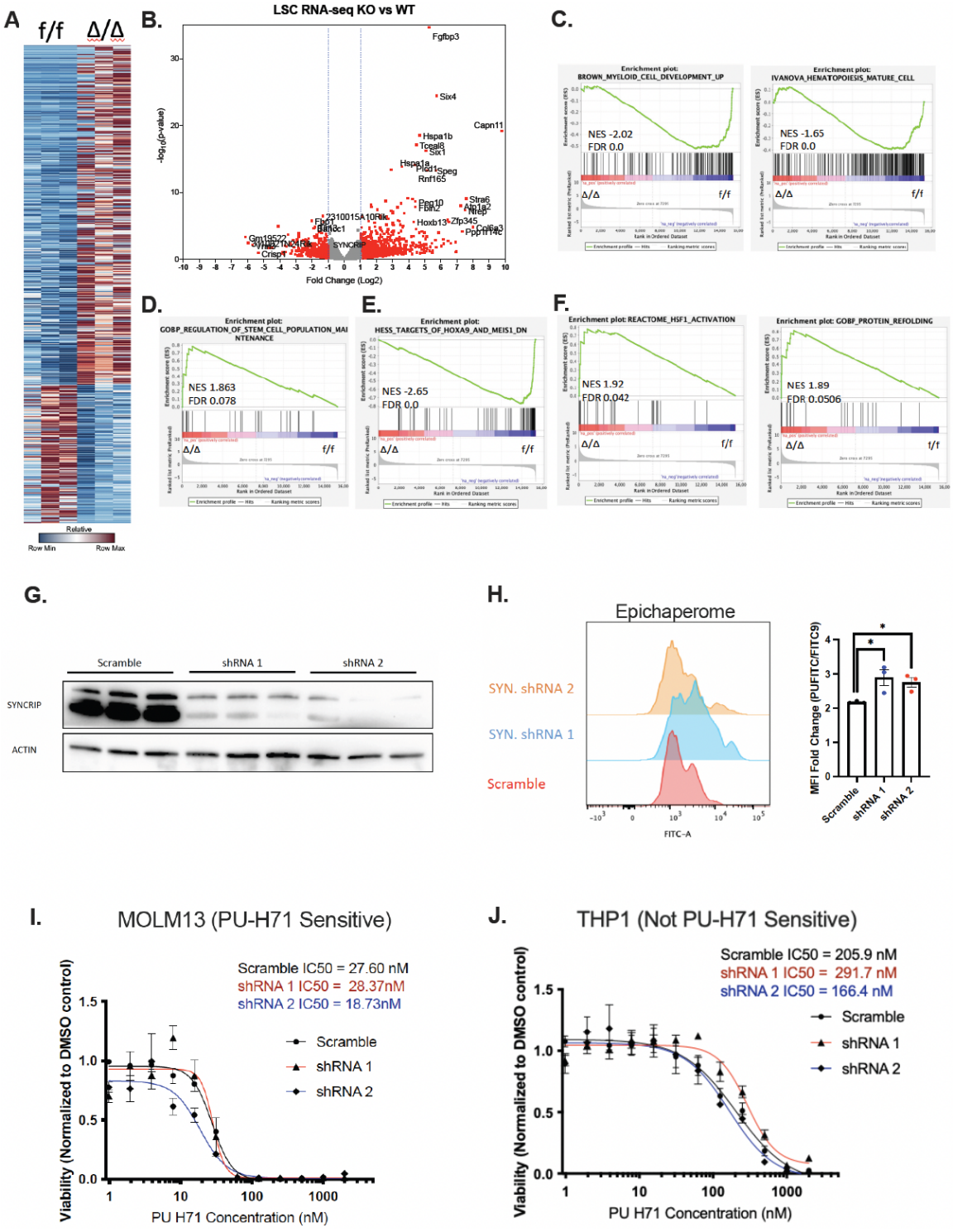

Figure 4.3: Transcriptomic Profiling of Transplanted LSCs shows HOXA9 program is not downregulated

(A) Gene expression heat map of the top upregulated and downregulated genes (fold change ≥ 2, FDR <0.05) from RNA sequencing analysis of LSCs (GFP+, top 10% cKit expressing cells) isolated from primary maintenance transplant WT *Syncrip* f/f (n=3) and KO *Syncrip* Δ/Δ (n=3) mice described in Figure 4.2A. **(B)** Volcano plots showing genes

differentially expressed between *Syncrip* f/f vs. *Syncrip* Δ/Δ LSCs. The most differentially expressed genes are highlighted. **(C-F)** GSEA analysis between *Syncrip* f/f vs. *Syncrip* Δ/Δ LSCs and gene signatures pertaining to cell development/maturation (C), stem cell maintenance (D), HOXA9 and MEIS1 program (E), and HSF1 activation/protein refolding (F). **(G)** Western blot showing efficient SYNCRIP hairpin mediated depletion in MOLM13 cells. **(H)** Epichaperome representative flow plot (left) and quantification of normalized epichaperome probe MFI signal (right). **(I-J)** PU-H71 dose response curves determined by CellTiter-Glo in MOLM13 (I) and THP1 (J) upon SYNCRIP depletion. Non-linear dose response inhibition (built into Prism) equation used to calculate IC50.
All data represent mean ± s.e.m. p values were calculated by two-tailed t test unless specified. * $p<0.05$, ** $p<0.01$, *** $p<0.001$ and ns: not significant.

enrichment for HSF1 activation and protein re-folding signatures (**Figure 4.3F**). This is very similar to the pathways we observed being activated in SYNCRIP KO HSCs and suggests SYNCRIP's regulation on proteostasis is not unique to only normal hematopoietic stem cells, but also observed in leukemia stem cells. Since we observe chaperone upregulation, and HSF1 pathway activation in SYNCRIP depleted LSCs, we next wanted to assess what reduction of *Syncrip* does to the epichaperome in a leukemia setting. As discussed in chapter II, the chaperone network referred to as the epichaperome plays a role in tumor cell survival and has been shown to facilitate cancer cell survival [196]. Using the same PU-FITC probe we described in Figure 2.7G-H, we investigated the epichaperome in *Syncrip* hairpin knockdown MOLM13 cells (human cell line) (**Figure 4.3G**). We observed a modest increase in epichaperome signal upon SYNCRIP reduction (**Figure 4.3H**). This mimics what we observed with SYNCRIP depletion in HSCs. The epichaperome inhibitor, PU-H71 has shown promise as a novel therapeutic for use in AML [197], and is under clinical trial investigation (NCT01393509, NCT01581541). Additionally, previous work has found a positive correlation between epichaperome abundance and response to PU-H71 [212]. Since we observe an increase in epichaperome signal upon SYNCRIP reduction, we asked whether this could sensitize human cell lines to PU-H71 inhibition. We treated two human cell lines, MOLM13 and THP1, which are previously characterized to be sensitive and not sensitive to PU-H71

respectively [213]. We observe that SYNCRIP shRNA mediated depletion in MOLM13 didn't cause cells to be more sensitive to PU-H71 treatment (**Figure 4.3I**). Similarly, we also didn't observe a change in sensitivity with THP1 cells (**Figure 4.3J**). This suggests that although SYNCRIP enhances the epichaperome abundance, it's not sufficient to cause an increase in PU-H71 sensitivity. The reasons for this are unclear, but it may be a result of SYNCRIP only causing a modest change in the epichaperome, and perhaps a more dramatic change is required to sensitize cells.

Compensation mechanism upregulates *Hoxa9* expression upon SYNCRIP Depletion in Transplants

Given that we observe a decreasing delay in leukemia, and a transcriptional program wherein HOXA9 is not being downregulated we wanted to investigate what was occurring with SYNCRIP and HOXA9 at the protein level. To do this we sorted cKit high (top 10-15% expressing cKit cells) and cKit low (lowest 30% expressing cKit cells) from all our transplants described in Figure 4.1 and 4.2. We evaluated the levels of SYNCRIP and HOXA9 by western blot. In the primary initiation transplant we found that SYNCRIP is highly expressed in cKit high cells compared to cKit low cells (**Figure 4.4A**), suggesting SYNCRIP expression is higher in LSCs than in leukemia blasts. Additionally, we observe that most the KO mice in this transplant select for SYNCRIP (**Table 3**). The HOXA9 expression in this primary transplant doesn't appear to have any significant trend (**Figure 4.4A**). However, when we sorted cells from the secondary leukemia initiation transplant, we found increased HOXA9 abundance in the SYNCRIP deficient leukemias compared to the controls (**Figure 4.4B**). This increase could be identified in both cKit high (LSCs) and cKit low (leukemia blast) populations. This upregulation of

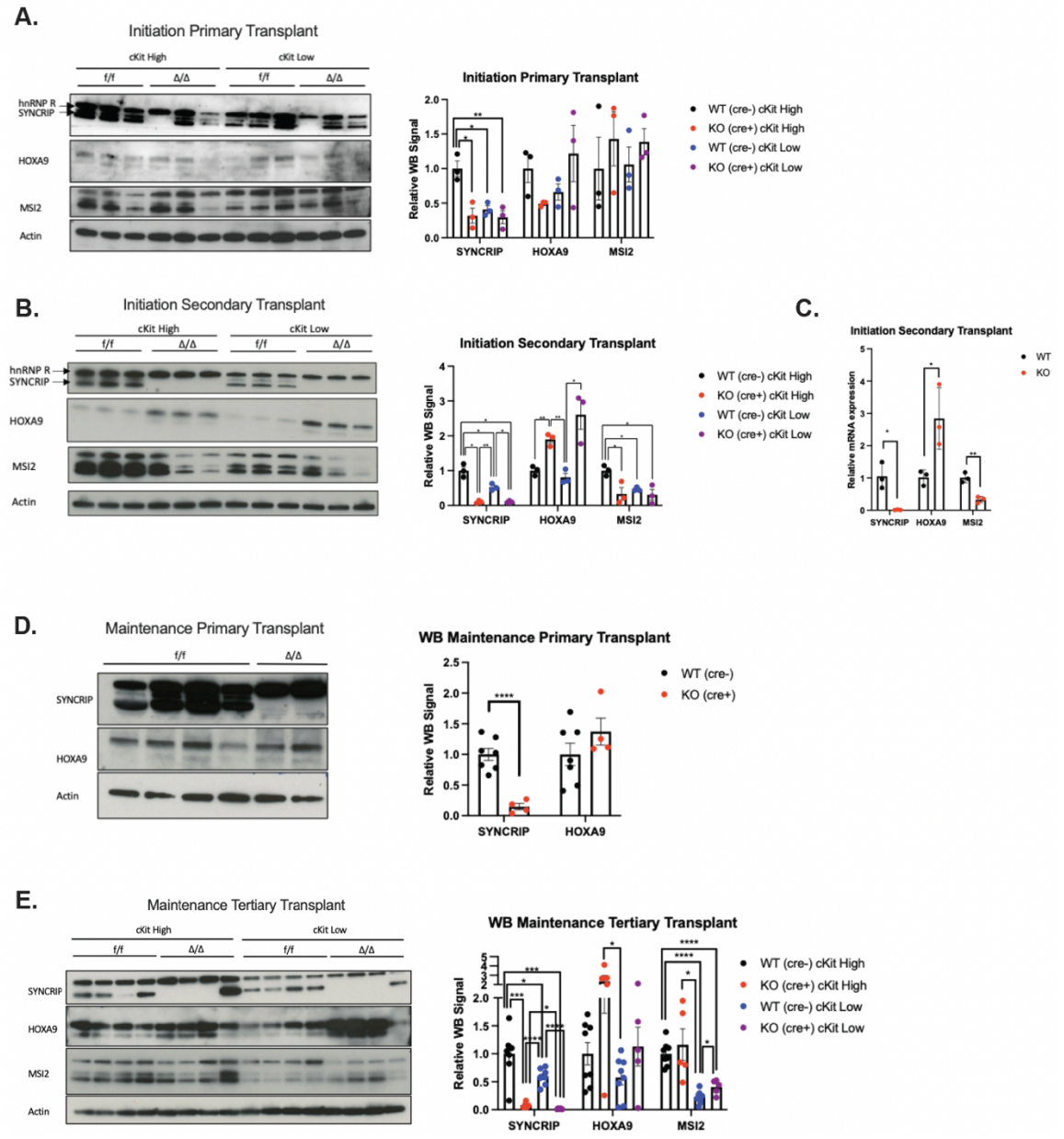

Figure 4.4: Transplanted LSCs show HOXA9 upregulation upon SYNCRIP depletion

(A) Western blot from leukemia initiation primary transplant (left) with sorted GFP+ cKit high (top 10-15% expressing) and cKit low (lowest 30% expressing) cells. ACTIN used as loading control. Quantification of western blot signal (right), normalized to ACTIN expression, f/f n=3, Δ/Δ n=3 **(B)** Western blot from leukemia initiation secondary transplant (left) with sorted GFP+ cKit high (top 10-15% expressing) and cKit low (lowest 30% expressing) cells. ACTIN used as loading control. Quantification of western blot signal (right), normalized to ACTIN expression, f/f n=3, Δ/Δ n=3 **(C)** RT-qPCR from leukemia initiation secondary transplant, cells sorted for GFP+ cKit high (top 10-15% expressing). **(D)** Western blot from leukemia maintenance primary transplant (left) with GFP+ cells (left). Quantification of western blot signal (right), normalized to ACTIN expression, f/f n=7, Δ/Δ n=4 **(E)** Western blot from leukemia maintenance secondary transplant (left) with

sorted GFP+ cKit high (top 10-15% expressing) and cKit low (lowest 30% expressing) cells. ACTIN used as loading control. Quantification of western blot signal (right), normalized to ACTIN expression, f/f n=5, Δ/Δ n=4. All data represent mean ± s.e.m. p values were calculated by two-tailed t test unless specified. * p<0.05, **p<0.01, ***p<0.001 and ns: not significant.

HOXA9 protein abundance doesn't appear to be driven by compensation from MSI2, since MSI2 protein levels decrease upon SYNCRIP depletion in this transplant (**Figure 4.4B**). Interestingly, RT-qPCR shows that *Syncrip* loss leads to upregulation of *Hoxa9* transcripts and downregulation of *Msi2* (**Figure 4.4C**). This suggests that a resistance mechanism has developed in these transplanted cells and is influencing *Hoxa9* transcriptionally, independently of *Msi2* expression. These observations are not unique to the leukemia initiation transplant as we also observe similar effects in the maintenance leukemia transplants described in Figure 4.2. In the primary leukemia maintenance transplant, we don't observe a significant change in HOXA9 upon SYNCRIP depletion (**Figure 4.4D**). However, in the tertiary leukemia maintenance transplant we observe the same increase in HOXA9 protein upregulation upon SYNCRIP depletion (**Figure 4.4E**). In this transplant it's unclear if MSI2 is involved in the upregulation of HOXA9, since we see MSI2 increase but only in the ckit low population and not the LSCs (ckit high) (**Figure 4.4E**).

This trend of upregulated HOXA9 continued in all secondary, tertiary, and quaternary transplants for both leukemia initiation and maintenance transplants (data not shown). Altogether this data suggests that *Hoxa9* is being transcriptionally regulated through a compensation mechanism in the SYNCRIP depleted leukemia cells, which becomes evident by protein levels in the secondary and tertiary transplants. This could have occurred through clonal selection or rewiring of the transcriptional and translational

program, however exactly what is driving this *Hoxa9* upregulation remains unknown and will require further investigation.

Acute SYNCRIP depletion shows HOXA9 is translationally downregulated

Given that we observe a resistance pathway with *Hoxa9* transcriptional upregulation in SYNCRIP depleted LSCs that have undergone transplantation, we wanted to better assess the acute impact SYNCRIP has after being reduced. Therefore, we developed an additional system to study SYNCRIP. Using the f/f mouse cells from MLL-AF9 leukemia transplants, we transduced them with concentrated Puro-CreER retrovirus and used puromycin to select the cells. Tamoxifen (4-OHT) treatment can be used to induce *Syncrip* excision in this system (**Figure 4.5A**). We observe efficient SYNCRIP depletion starting at 25nM 4-OHT treatment at 24hrs (**Figure 4.5B**). Within the first 72hrs post 4-OHT treatment, HOXA9 levels do appear to be mildly reduced as well (**Figure 4.5B**).

Next, we continued assessment of this system, to see if it could produce a phenotype like the one previously described by our group [167]. We observed that *in vitro* 4-OHT treatments of 25nM and 100nM reduced cell growth capacities (**Figure 4.5C**), caused an increase in apoptosis (**Figure 4.5D**), increase in differentiation (**Figure 4.5E**), and a reduction of colony formation capacities (**Figure 4.5F**). We also conducted *in vivo* assessment, by transplanting cells into recipient mice, and treating the mice with tamoxifen. With this system we also observed a delay in leukemia progression (**Figure 4.5G**), and the SYNCRIP depleted mice that got sick all had selected for SYNCRIP (**Figure 4.5H**). This all recapitulates our previous work [167] and suggests that this system is useful for further investigation of *Syncrip's* mechanistic role in AML. To begin addressing this, we conducted transcriptomic profiling with this Puro CreER system

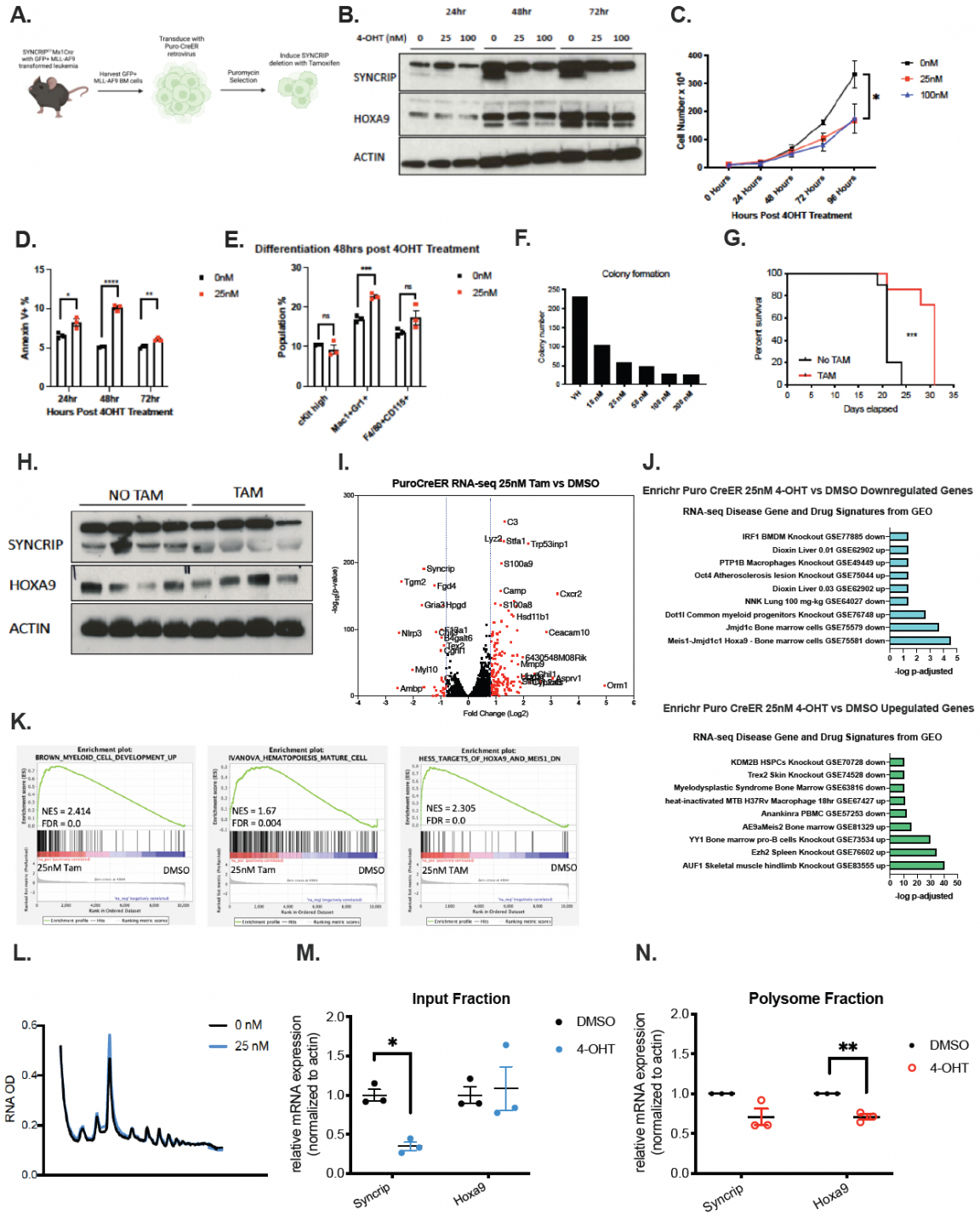

Figure 4.5: Puro-CreER system shows HOXA9 program reduction upon SYNCRIP depletion

(A) Schematic for generation of SYNCRIP Puro-CreER system. Briefly, MLL-AF9 cells from primary maintenance transplants were transduced with concentrated Puro-CreER

retrovirus twice and selected with 3ug/mL puromycin. **(B)** Western blot of SYNCRIP Puro-CreER cells treated with 0, 25, and 100nM 4-OHT with collections at 24hrs, 48hrs and 72 hrs post treatment. ACTIN used as loading control. **(C)** Proliferation assay where 10000 cells were initially seeded for each condition. 0nM 4-OHT n=3, 25nM 4-OHT n=3, 100nM 4-OHT n=3. **(D)** Quantitative summary of apoptotic (Annexin V+) cells as measured by flow cytometry 0nM 4-OHT n=3, 25nM 4-OHT n=3. **(E)** Quantitative summary of differentiation based on cKit, Mac1+Gr1+, and F4/80+CD115+ expression determined through flow cytometry, 0nM 4-OHT n=3, 25nM 4-OHT n=3. **(F)** Colony formation assay with Puro-CreER cells plated in methylcellulose media and counted 7 days post seeding. For each concentration n=1. **(G)** Kaplan-Meier analysis of secondary transplant set up from Puro-CreER cells described in (A). Mice were sub lethally irradiated and transplanted with Puro-CreER cells. Subsequently, mice were either treated with tamoxifen (TAM) or corn-oil (No TAM). TAM n=10, No TAM n= 7. **(H)** Western blot from mice described in (G) showing selection of SYNCRIP in No TAM condition. ACTIN used as loading control. **(I)** Volcano plot of RNA-seq from Puro-CreER 25nM 4-OHT vs. DMSO. **(J)** Enrichr analysis for RNA-seq Disease gene and drug signatures from GEO in Puro-CreER 25nM 4-OHT vs DMSO downregulated and upregulated genes. X-axis: $\log_{10}$(p value). **(K)** GSEA from Puro-CreER 25nM 4-OHT vs DMSO transcriptomic profile on myeloid cell development, hematopoiesis mature cell, and HOXA9/MEIS1 program signatures. **(L)** Representative polysome profile of cell extracts resolved on sucrose gradient. **(M-N)** Polysome profiling from RT-qPCR on input (M) and polysome (N) fractions, 25nM 4-OHT n=3, DMSO n=3. All data represent mean ± s.e.m. p values were calculated by two-tailed t test unless specified. * $p<0.05$, ** $p<0.01$, *** $p<0.001$ and ns: not significant.

using 25nM 4-OHT 24 hours post treatment to assess the acute effects of SYNCRIP depletion. RNA-seq results showed 174 upregulated and 30 downregulated genes upon 4-OHT induced SYNCRIP depletion after 24hrs (FDR < 0.05, Log2FC > 0.8). Volcano plot shows the most upregulated and downregulated hits (**Figure 4.5I**) and Enrichr pathway analysis shows the HOXA9 pathway being downregulated in our SYNCRIP depleted condition (**Figure 4.5J**). Additionally, GSEA analysis shows enrichment of myeloid cell development upon SYNCRIP depletion, as well as a downregulation of the HOXA9 program signature (**Figure 4.5K**). This indicates that SYNCRIP's acute effects are influencing the HOXA9 program, where loss of *Syncrip* leads to a loss of the HOXA9 signature.

To determine more specifically how SYNCRIP is regulating global translation, we conducted polysome profiling using these Puro CreER cells, treating the cells with 25nM

4-OHT and harvesting 24hrs post treatment. We observed that Syncrip loss led to no major changes in global translation (**Figure 4.5L**). Additionally, we found by RT-qPCR that *Hoxa9* is not altered in the input (cytosolic) fraction (**Figure 4.5M**), but it's decreased in the polysome fraction (**Figure 4.5N**). Suggesting that less *Hoxa9* is being translated upon SYNCRIP depletion. Altogether these data highlight the importance of SYNCRIP's impact on the *Hoxa9* program and HOXA9 translation.

Characterizing SYNCRIPs binding activity in leukemia and LSCs

Given that we see a continued delay in our leukemia initiation and maintenance transplants even in the presence of upregulated *Hoxa9*, this suggests that SYNCRIP is binding to and influencing other targets that have a functional effect in creating this leukemia delay. We next sought out to map out SYNCRIP's binding activity within leukemia cells and LSCs. To do this we utilized the same HyperTRIBE technology described in Figure 3.1, and we used two cell types, the RN2 MLL-AF9 mouse cell line and LSCs (top 10-12% cKit expressing cells) from dsRed MLL-AF9 mouse cells. Both cell types were transduced with SYNCRIP HyperTRIBE retrovirus and assessed for expression of the fusion protein. We confirmed the presence of this fusion (**Figure 4.6A**). Next, we evaluated the characteristics of the binding and saw that in RN2 cells there are >40000 edit sites (**Figure 4.6B**), while LSCs had <2300 edit sites (**Figure 4.6C**). It is not clear why we detected more targets in RN2s over the LSCs. We believe that it might be merely due to technical issues with the efficiency of viral transductions as they were done independently. However, in both cell types, ~80% of the binding activity is occurring on the 3'UTR, which is very similar to what we saw in HSCs and MPPs and suggests that SYNCRIP predominantly binds the 3'UTR in blood stem and progenitor cells. Additionally, we observed a total of 4957 target genes in RN2 cells, while LSCs

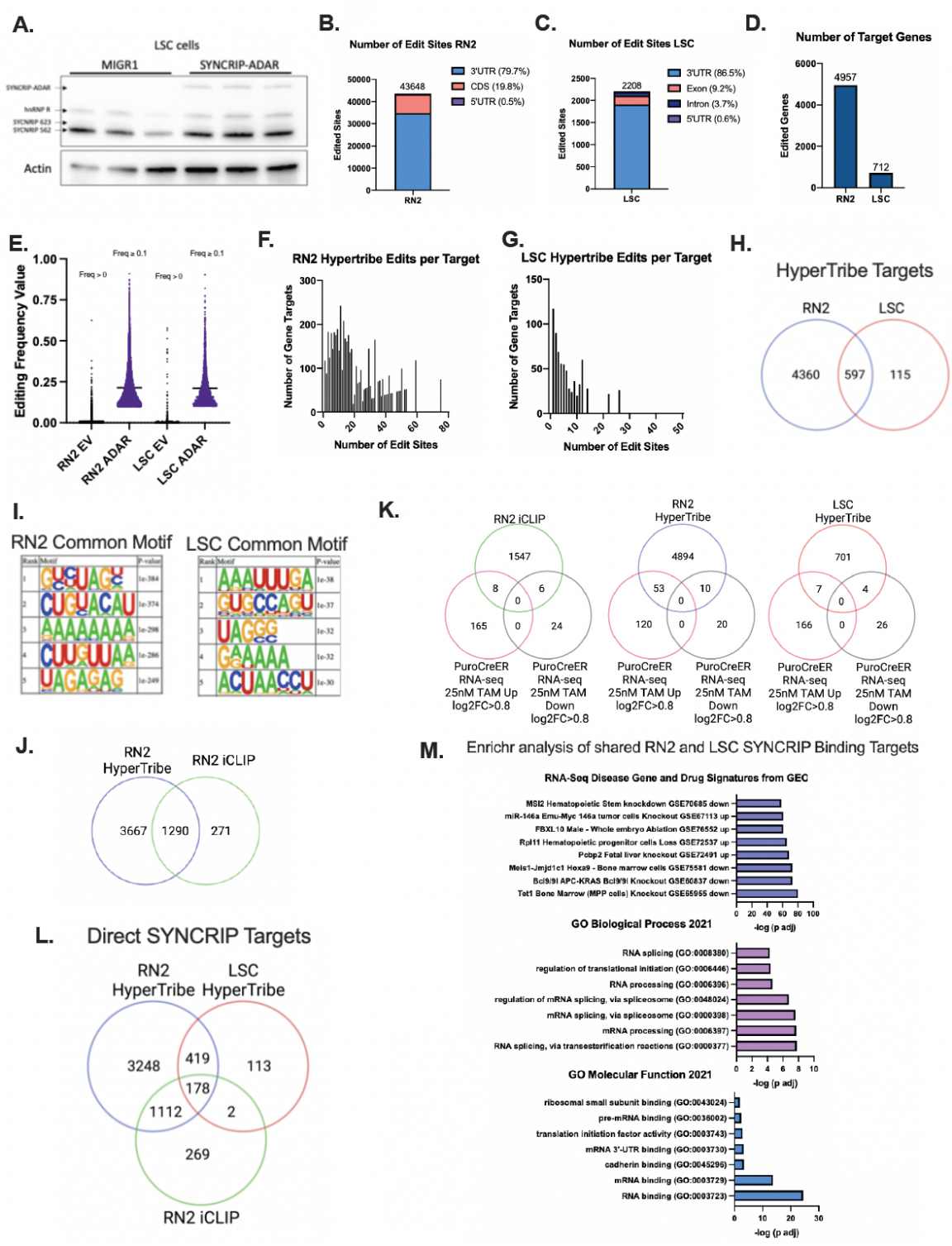

Figure 4.6: Characterizing SYNCRIP's direct binding targets in leukemia
(A) Representative western blot of empty vector (EV, MIGR1) and SYNCRIP-ADAR fusion in LSC cells. Cells were GFP+ sorted 48hrs post transduction. EV n=3, SYNCRIP-ADAR

n=3. **(B-C)** Number of edit sites in RN2 cells (B) and LSCs (FDR < 0.05, differential editing frequency ≥ 0.1) and their genetic locations. **(D)** Number of target genes with edit sites described in (B-C). **(E)** Number of total ADAR-mediated edit sites with no cutoff (frequency > 0) and with cutoff (frequency > 0.1) in RN2 and LSCs with control empty vector (EV, MIGR1) or SYNCRIP-ADAR (RN2-ADAR, LSC-ADAR). **(F-G)** Distribution of the number of genes with corresponding number of edit sites in RN2 (F) and LSCs (G). **(H)** Venn diagram showing overlapping SYNCRIP RN2 and LSC gene targets, (FDR < 0.05, differential editing frequency ≥ 0.1). **(I)** De novo HOMER motif search identifies SYNCRIP specific binding motifs enriched in mRNA targets. **(J)** Venn diagram showing overlapping SYNCRIP RN2 targets as determined by HyperTRIBE, (FDR < 0.05, differential editing frequency ≥ 0.1) and iCLIP. **(K)** Venn diagram showing overlap between SYNCRIP HyperTRIBE (FDR < 0.05, differential editing frequency ≥ 0.1) and iCLIP data sets, with transcriptomic profiling in SYNCRIP Puro-CreER system (FDR < 0.05, differential editing frequency ≥ 0.1). **(L)** Venn diagram showing overlap between SYNCRIP HyperTRIBE (FDR < 0.05, differential editing frequency ≥ 0.1) LSC and RN2 cells with and iCLIP RN2 data set. **(M)** Enrichr analysis for GO biological processes, GO molecular function and RNA-seq Disease Gene and Drug Signatures from GEO using 178 SYNCRIP direct binding target signature described in (L).

only showed 712 target genes (**Figure 4.6D**). In both cell types we note a significant increase in editing frequency compared to empty vector indicating these editing events are a result of the fusion protein (**Figure 4.6E**). We also notice that most gene targets have less than 20 edit sites in both RN2 cells (**Figure 4.6F**) and LSCs (**Figure 4.6G**). Upon overlap of the gene targets from both cell types we see that most the LSC target genes are also RN2 target genes, indicating that only a small subset (~16%) is unique to LSCs (**Figure 4.6H**). Using the same methods described in Figure 3.1, we ran HOMER motif analysis in both cell types and found the top common motifs for RN2 cells include GUCUAGU and CUGUACAU, while for LSCs the top common motifs are AAAUUUGA and GUGCCAGU (**Figure 4.6I**). Very interestingly, just like in our HSPC HOMER motif analysis we observe the UAG motif appear frequently, which also happens to be MSI2's binding motif. This provides further support that SYNCRIP and MSI2 share binding motif similarities in their targets (i.e HOXA9 etc).

In addition to HyperTRIBE, we also conducted iCLIP in RN2 cells. As mentioned before, CLIP is a gold standard method for capturing protein-RNA interacting activity, therefore

we can use iCLIP and HyperTRIBE datasets to see how comparable they are with SYNCRIP binding. We see that most the iCLIP gene targets,~83%, overlap with HyperTRIBE gene targets (**Figure 4.6J**), suggesting that our HyperTRIBE technique is efficient in capturing similar results like the previously more established method. We next wanted to compare our *Syncrip* Puro-CreER system transcriptomic profiling to our various SYNCRIP RNA binding datasets. We noticed there is little overlap with transcriptional changes upon SYNCRIP depletion in all our SYNCRIP RNA-binding datasets (4-30% for upregulated genes, 13-33% for downregulated genes) (**Figure 4.6K**). This indicates that SYNCRIP induced transcriptional changes are largely not a result of direct SYNCRIP binding to those transcripts. This suggests that SYNCRIP's influence on it's direct targets may be more translational, however we don't have a leukemia proteomic dataset to compare with our binding activity datasets.

Lastly, we also wanted to compare the overlap between the three SYNCRIP RNA binding activity datasets and observe 178 target genes that appear in each dataset (**Figure 4.6L**). Enrichr pathway analysis shows that this 178 SYNCRIP direct binding target signature is involved in the MSI2 and HOXA9 program (**Figure 4.6M**). Providing further evidence that SYNCRIP directly regulates the HOXA9 program through direct binding activity, and that it is also involved in the MSI2 program, perhaps through shared binding targets. Additionally, we also see biological processes involved in RNA splicing and translation, as well as molecular functions in ribosomal binding and RNA binding (**Figure 4.6M**). This is very similar to the pathway analysis we saw with HSPCs and suggests that SYNCRIP's binding activity on other RNA binding proteins is not unique to one cell type. This may also suggest that SYNCRIP's impact on the RBP network (especially the translational and splicing machinery) may be through direct binding of RBP transcripts, however this is something that will need further exploration.

Mapping SYNCRIP's direct binding activity on *Hoxa9*

Our characterization of SYNCRIP's direct binding targets with HyperTRIBE and iCLIP showed somewhat conflicting results when it came to *Hoxa9* binding. HyperTRIBE shows SYNCRIP binds to the 3'UTR of *Hoxa9*, while the iCLIP results shows SYNCRIP binding at both the 3'UTR and the CDS region of *Hoxa9*. Given that we know SYNCRIP regulates HOXA9 translation, we wanted to investigate which SYNCRIP binding region was most essential for regulating translation. To test this, we utilized a luciferase reporter assay expressing mouse *Hoxa9* CDS or *Hoxa9* 3'UTR regions (**Figure 4.7A**). Transfecting these reporter constructs into HEK293T cells along with SYNCRIP shRNA or overexpression SYNCRIP (562 amino acid isoform), we found that in the *Hoxa9* 3'UTR region there is no change in the luciferase activity. However, in the *Hoxa9* CDS region we see a loss of signal upon SYNCRIP depletion and an increase in luciferase activity upon SYNCRIP overexpression (**Figure 4.7B**). This suggests that although both regions have SYNCRIP binding activity, only the CDS region is essential for HOXA9 translation regulation. Next, we wanted to investigate deeper into what region of the CDS is most essential for HOXA9 translation. Using the same luciferase reporter plasmids, we truncated the first 86bp of the CDS region (Delta1), as this contained a binding site according to iCLIP data. Upon SYNCRIP depletion we see the same reduction in luciferase activity in the full length CDS condition, however in the Delta1 truncation we observe a dramatic loss of signal even in the scramble condition. This is further reduced upon SYNCRIP depletion (**Figure 4.7B**). Overall, these results indicate that regardless of SYNCRIP expression this initial 86bp region of *Hoxa9* CDS is essential for translation, and that SYNCRIP binding to this portion of the CDS play a large role in translation efficiency.

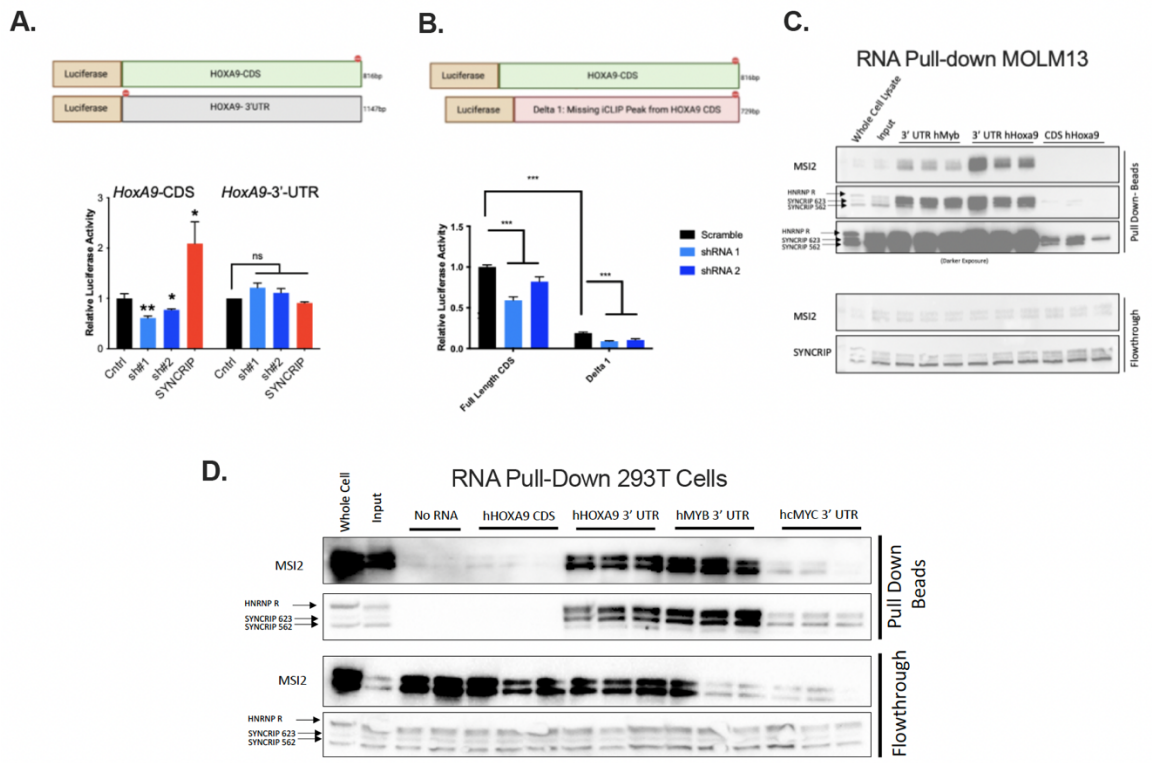

Figure 4.7: Mapping SYNCRIP's binding activity on Hoxa9
(A) Luciferase reporter assay. Top shows schematic of firefly luciferase reporter with *Hoxa9* CDS and *Hoxa9* 3'UTR regions. Bottom shows relative luciferase activity in 293T cells with SYNCRIP shRNA conditions and SYNCRIP 562 overexpression. **(B)** Luciferase reporter assay. Top shows schematic of firefly luciferase reporter with *Hoxa9* full length CDS and *Hoxa9* Delta1 CDS region. Bottom shows relative luciferase activity in 293T cells with SYNCRIP shRNA conditions. **(C)** RNA pull down assay using MOLM13 cell lysate and human in vitro transcribed biotinylated transcripts: 3'UTR *Myb*, 3'UTR *Hoxa9* and CDS *Hoxa9*. **(D)** RNA pull down assay using 293T cell lysate and human in vitro transcribed biotinylated transcripts 3'UTR *Myb*, 3'UTR *Hoxa9*, CDS *Hoxa9* and 3'UTR *cMyc*.

Given that we see binding in both 3'UTR and CDS regions of the *Hoxa9* transcript, we next sought to investigate if this also occurred in human *Hoxa9* transcripts. We also wanted to explore SYNCRIP's binding to other oncogenic related transcripts like *Myb* and *Myc*. We performed an RNA-pull down assay using MOLM13 cells. We observe that SYNCRIP does bind to the 3'UTR of *Myb* (as described in HyperTRIBE) and it also binds to both 3'UTR and CDS regions of *Hoxa9* (**Figure 4.7C**). However, it appears that

the binding to the 3'UTR is more abundant and could explain why we don't see it in our HyperTRIBE results.

We also noted some differential binding activity between SYNCRIP's isoforms. We saw that the larger SYNCRIP 623 isoform binds more frequently to all transcripts despite being less abundant than the SYNCRIP 562 isoform (**Figure 4.7C**). This is not unique to MOLM13 cell lysate, as we also observed SYNCRIP 623 binding more frequently in HEK293T cell lysate (**Figure 4.7D**). This suggests that there may be some differential activity or requirement between the two isoforms in regulating these transcripts. However, further investigation will be necessary to uncover exactly how SYNCRIP is binding to these transcripts and why the larger isoform binds more frequently.

Discussion

SYNCRIP's role in AML was first established by our group through investigation of MSI2's interactome [167]. It was shown that SYNCRIP reduction led to increased differentiation and apoptosis, reduced cell growth, and a pronged survival in mice [167]. This study by our group also identified a transcriptomic connection between SYNCRIP and LSCs [167], however until now we had not functionally assessed if SYNCRIP played a role in regulating LSCs. Using our conditional knockout mouse model for transplantation, we see that SYNCRIP depletion leads to a delay in leukemia, and we found that SYNCRIP is important for maintaining LSC self-renewal capacities under leukemia initiation and maintenance conditions. However, this delay in leukemia progression is shortened after each sequential transplant. We also saw a transcriptomic profile in these primary transplanted LSCs that indicated the HOXA9 program was not being downregulated, suggesting these cells were experiencing secondary

transformation or clonal selection where these *Hoxa9* expressing cells were outcompeting other clones. Interestingly, western blot and qPCR analysis found upregulation of HOXA9 protein and transcript levels, indicating transcriptional regulating of *Hoxa9* led to this compensation mechanism that was reducing the delay in leukemia. How this is occurring is not clear and will require additional investigation. Perhaps through barcoding strategies, we can begin to understand the clonal evolution upon SYNCRIP depletion in LSCs.

HOXA9 (Homeobox A9) is a transcription factor that is known as being overexpressed in more than half of AML cases, and higher expression is connected with poorer prognosis [214, 215]. Therefore, understanding how *Hoxa9* is regulated could lead to the development of novel therapeutic strategies. Our group has found that SYNCRIP is directly involved in regulating HOXA9 translation and we've now uncovered that the most essential region for translation is within the first 86bp region of the CDS. This is unexpected as we noticed most SYNCRIP binding occurs at the 3'UTR region. In addition to HOXA9 we've also characterized SYNCRIP's binding activity in leukemia and LSCs. Although HOXA9 plays a vital role in promoting leukemia progression, SYNCIRIP is targeting additional pathways that lead to functional effects as seen in the secondary transplants with upregulated HOXA9 but continued delay in leukemia progressing. Deeper exploration into these other pathways will be necessary to uncover how SYNCRIP depletion leads to prolonged survival. One interesting pathway we found, that is not unique to leukemia as we also see it in HSPCs, are other RBPs. It appears that SYNCRIP is involved in direct binding to translation and splicing machinery, which may have consequences on those transcripts' translation. However, we require proteomic or additional ribosomal profiling data to determine what targets SYNCRIP is influencing translationally.

Overall, with this work we've uncovered SYNCRIP's functional effects in LSCs and have found additional connections between SYNCRIP and the HOXA9 program. This work also suggests that SYNCRIP is a potential novel therapeutic target for myeloid leukemias.

Contributions

Figure 4.1: All transplants and analysis were performed by Florisela.

Figure 4.2: Primary and Secondary transplants were performed by Ly Vu. Florisela performed tertiary, quaternary, heterozygous and AMLETO9a transplants. All analysis was done by Florisela.

Figure 4.3: LSC RNA-seq cells were sorted by Ly Vu and prepared by Florisela. MSKCC IGO core performed sequencing and analysis was conducted by Basepair. Florisela generated GSEA analysis. All MOLM13 experiments were performed by Florisela.

Figure 4.4: All western blots, qPCR and analysis were conducted by Florisela.

Figure 4.5: Syncrip Puro CreER system was generated by Ly Vu. Ly also conducted colony formation assay and *in vivo* experiments with assistance from Alexandra Schurer. All other characterization was performed by Florisela. Ly Vu performed Puro-CreER RNA-seq, polysome profiling and RT-qPCR. Florisela generated the Enrichr and GSEA plots.

Figure 4.6: HyperTRIBE constructs were designed by Diu Nguyen. Ly Vu performed RN2 HyperTRIBE experiment and Florisela performed LSC HyperTRIBE experiment. Karen Chu conducted the analysis for RN2 HyperTRIBE and Ilyes Baali conducted analysis for LSC HyperTRIBE. Diu Nguyen performed RN2 iCLIP, with analysis conducted by members of Christina Leslie's group.

Figure 4.7: Ly Vu conducted luciferase assay in panel A, and Florisela conducted luciferase assay in panel B. RNA pull down assay protocol was conducted by Florisela with essential advice from Christine Myer's lab and assistance from Chiara Evans. Panel C western blot was developed with help from rotation student, Andrew Rappa.

Chapter V: Thesis Summary and Future Directions

SYNCRIP is required to maintain long term HSPC self-renewal capacities and proteostasis in hematopoietic stem cells

Previous work by our group had uncovered that SYNCRIP plays an important role in AML [167]. This initial study claimed SYNCRIP was dispensable for normal hematopoiesis, however the mouse model used at the time didn't address adult hematopoiesis. Thus, to fully understand SYNCIRP's role in normal hematopoiesis, our lab developed an alternative mouse model. Using a conditional knockout mouse model, we've uncovered that SYNCRIP plays a modest role in normal hematopoiesis. More interestingly, we've uncovered that SYNCRIP is essential in maintaining long-term self-renewal capacities in HSCs, where loss of SYNCRIP leads to a loss of engraftment most dramatically seen during secondary transplantation. Mechanistically, we observed that SYNCRIP doesn't influence HSC cell cycling, but does play a role in regulating MPP exit from quiescence. Through scRNA-seq profiling, we observed HSCs have a unique dysregulated stress response that is not observed in MPPs. We went on to validate this activated stress state, by confirming that *Syncrip* loss led to increased unfolded protein, an altered epichaperome, and increased ER stress in HSCs. Altogether our work indicates that SYNCRIP plays a vital role in promoting protein homeostasis under conditions of regenerative stress (**Figure 5.1**).

SYNCRIP regulates cell polarity through direct regulation of CDC42 and maintains proper inheritance of cell fate determinants in HSCs

Recent advancements in RBP techniques have led to the development of HyperTRIBE as a method of detecting novel RBP-transcript interactions. One of the advantages of

HyperTRIBE is that it has proven to be suitable for use in rare stem cell populations, unlike the gold-standard CLIP methods. Using HyperTRIBE, we've been able to map out SYNCRIP's binding profile, and in conjunction with proteomics and RNA-seq datasets, we've uncovered translationally regulated SYNCRIP hits which consists of multiple other RBPs and several GTPase associated targets. Deeper exploration into SYNCRIP's role on the Rho GTPase CDC42, we found that SYNCRIP regulates CDC42 protein expression. As a result, SYNCRIP also regulates cytoskeleton organization and cell polarity. Since these processes are required for asymmetric cell division of cell fate determinates, we hypothesized that SYNCRIP may also be influencing HSC cell fate decisions. We found multiple cell fate determinants (NUMB and LAMP1) that are impacted by SYNCRIP depletion and found there is a reduction in HSC asymmetric division upon *Syncrip* loss. Very interestingly, we also found that SYNCRIP impacts the asymmetric division patterns of unfolded protein. Upon SYNCRIP depletion, HSCs lose their ability to dilute unfolded protein into daughter cells. Additionally, we found SYNCRIP's influence on CDC42 has a functional effect in regulating HSC self-renewal *in vitro*, however *in vivo* SYNCRIP's influence seems more complex and not entirely attributed to CDC42 regulation. Collectively, we see that SYNCRIP impacts HSC self-renewal capacities through direct regulation of CDC42 expression and cell polarity, which ultimately disrupts cell division and clearance of unfolded protein (**Figure 5.1**).

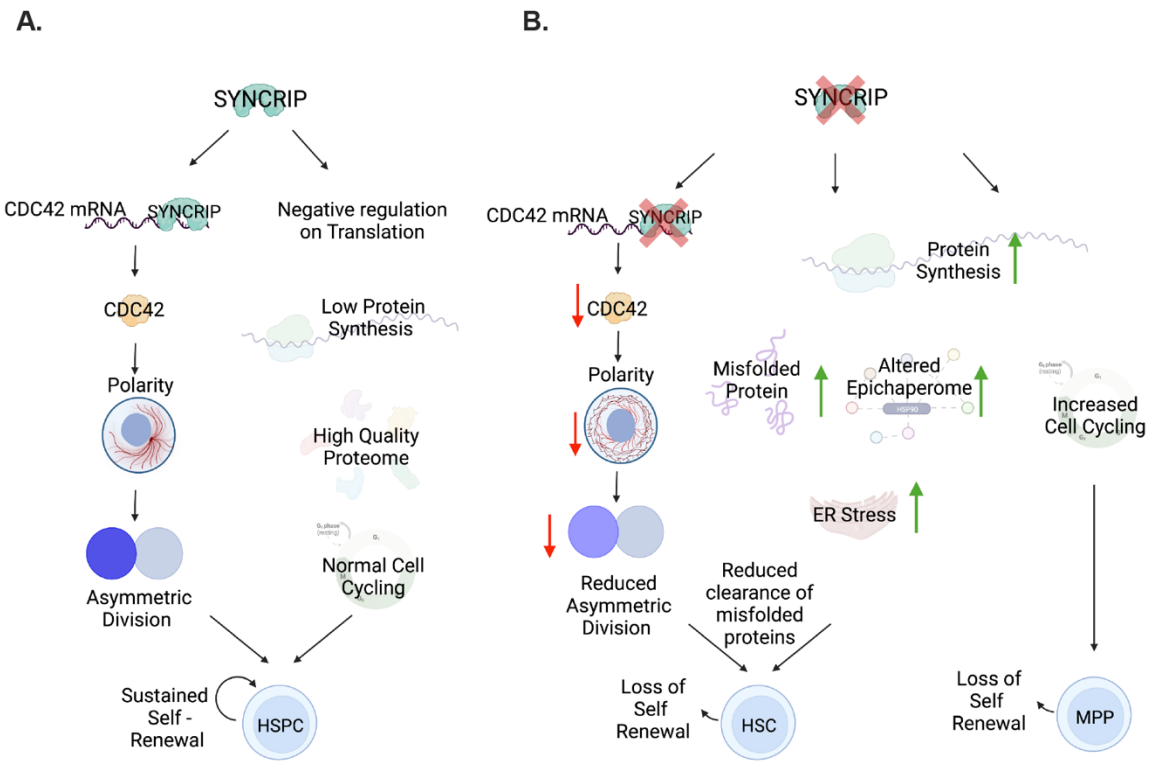

Figure 5.1: Graphical abstract illustrating SYNCRIP controls proteome quality and CDC42-mediated cell polarity and division to maintain self-renewal of HSCs

SYNCRIP is Required for Leukemia Stem Cell Self-Renewal

As mentioned above, SYNCRIP was found as a novel regulator of leukemia through our groups previous work investigating MSI2's interactome. However, SYNCRIP's requirement for LSC functional activity has not been explored until now. Using our conditional knockout mouse model, we've been able to establish that SYNCRIP is required for leukemia initiation and maintenance and prolongs survival when depleted. Additionally, we found that SYNCRIP is required for maintaining LSC self-renewal. Unexpectedly, we also uncovered a resistance mechanism that upregulates *Hoxa9* transcription in SYNCRIP depleted cells. This leads to a shortening in leukemia delay caused by SYNCRIP depletion. Additional exploration into SYNCRIP's relationship with *Hoxa9*, we've verified that it's translationally regulated by SYNCRIP and have mapped out the most essential binding region. Interestingly, we also observed differential binding

activity between two SYNCRIP isoforms on *Hoxa9* transcripts. Lastly, we also mapped out SYNCRIP binding in leukemia and LSCs using HyperTRIBE and iCLIP techniques. Overlap between our datasets revealed a signature of binding targets that resemble the SYNCRIP targets we observe in HSPCs, including various RBPs involved in the spliceosome and translation machinery. Collectively, our data supports the hypothesis that SYNCRIP represents a novel therapeutic target in AML.

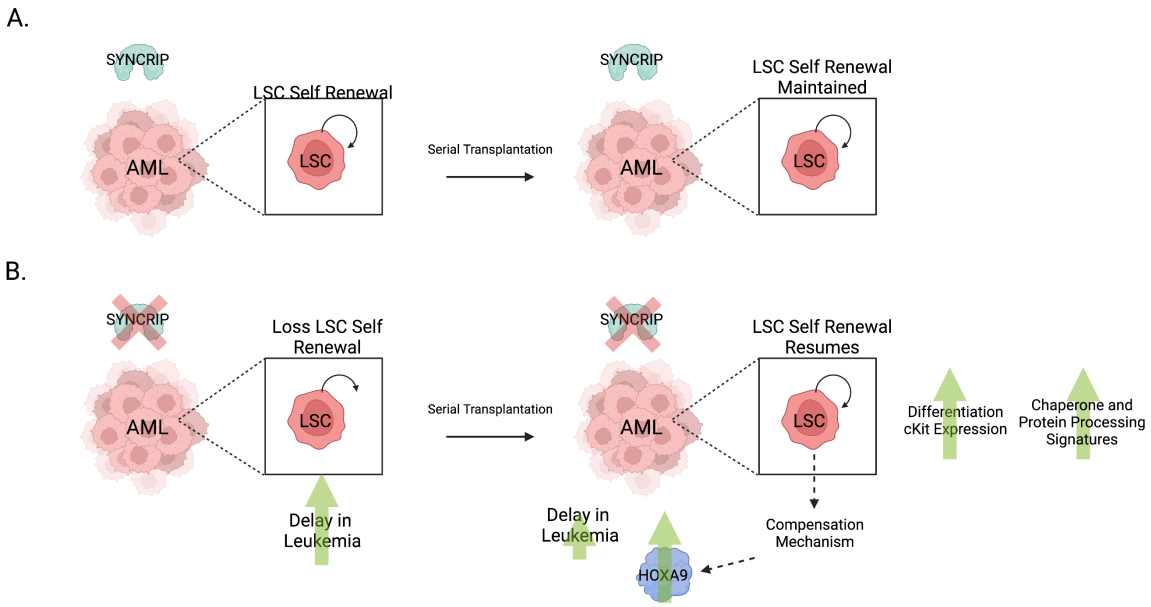

Figure 5.2: Graphical abstract illustrating SYNCRIP regulating LSC self-renewal and the emergence of a HOXA9 compensation mechanism

Future Directions

Although the work in this thesis supports SYNCRIP's role as a regulator of normal and malignant hematopoietic stem cells, there are several remaining questions regarding how SYNCRIP mechanistically influences normal and malignant hematopoiesis.

Regarding SYNCRIP's role in human HSCs, our work only investigated SYNCRIP's impact on human HSPC function *in vitro*. Since we observe a decrease in human CB-CD34+ HSPC replating capacity, we predict that SYNCRIP would also be important in

regulating human HSPC function *in vivo* however this remains to be explored. Transplantation experiments with SYNCRIP depleted human CB-CD34+ HSPCs would help answer this question. Our *in vitro* methods also only utilized hairpins to reduce SYNCRIP expression, further methods like CRISPR mediated knockout could be used to verify our results. Additionally, we only explored the effects of SYNCRP reduction in human HSPCs, we didn't evaluate SYNCRIP overexpression. SYNCRIP overexpression may lead to enhancement of HSPC self-renewal but may also have oncogenic properties as we know it positively regulates HOXA9 expression in human cell lines.

Our scRNA-seq analysis uncovered SYNCRIP's role in protecting HSCs from experiencing protein related stress. However, how SYNCRIP impacts HSC C1 and HSC C2 remains to be further explored. Our results suggest that HSC C1 resembles the previously characterized low output HSC [191], which has been shown to be the driver of secondary transplantation. Barcoding experiments could help us isolate the exact impact SYNCRIP has on the ability of HSC C1 to repopulate during transplantation. Additionally, further isolation of HSC C1 with a reporter system could help functional assessment of SYNCRIP's impact on the reserve HSCs. A reporter *Tcf15-Venus* mouse has been developed to isolate the low output HSC [191], crossing this reporter line to our *Syncrip* conditional knockout mouse model could help in the isolation of this reserve HSC population under SYNCRIP depleted conditions.

Although our normal hematopoiesis studies predominantly focused on SYNCRIP's regulation of the Rho GTPase CDC42, we did identify various other RBPs such as MSI2 and members of the splicing machinery (like Srsf1 and Srsf3) that are influenced by SYNCRIP. Additional work will be necessary to explore the functional role these RBPs play in mediating the SYNCRIP KO HSC self-renewal defect we observe *in vitro* and *in*

vivo. Additionally, we saw that *in vivo*, CDC42 was not sufficient to rescue the SYNCRIP KO HSC repopulation defect, indicating that other SYNCRIP targets are involved. Even in the colony formation assay, CDC42 overexpression was only partially capable of rescuing serial replating defects. Thus, a miniaturized colony formation assay screen with the other SYNCRIP target hits would be helpful in identifying additional targets that have functional activity in causing the loss of self-renewal we see upon SYNCRIP depletion. We could overexpress other SYNCRIP targets and observe which ones cause full or partial rescue in SYNCRIP KO HSPCs colony formation abilities.

With regards to SYNCRIP's role with LSCs and leukemia, we observed a very prominent compensation mechanism emerge after primary transplantation. Our investigation into these transplants led to observation that *Hoxa9* is being transcriptionally upregulated. However, exactly how this is occurring is not something we have further explored, but we predict there may be some secondary mutation event, or clonal selection that occurs which leads to the outgrowth of these cells. To see the clonal evolution that occurs, a barcoding experiment could be conducted between the primary and secondary transplantation as this is when we see the outgrowth of the *Hoxa9* overexpression clone. Additionally, it is unclear if this is unique to MLL-AF9 or if this resistance mechanism may also occur in leukemia's of other oncogenic backgrounds. To test this, we would need to do secondary transplants with other types of leukemia, and we could start with AML-ETO9a as we already see a delay in leukemia at the primary transplant setting.

We developed a SYNCRIP Puro-CreER system to help us answer mechanistic questions on how SYNCRIP regulates AML and LSCs after a short time of being depleted. Our qPCR results showed *Hoxa9* being translationally influenced by SYNCRIP, however we could also use this system to identify additional targets that are

translationally impacted. To address this, we could conduct RiboSTAMP, as described in chapter I, to profile the ribosomal activity on each transcript after SYNCRIP depletion.

Additionally, we could conduct deeper investigation into SYNCRIP's two isoforms found in the blood. There may also be functional requirements for each SYNCRIP isoform that remain to be investigated. We know from previous studies that SYNCRIP 623 contains an extra nuclear localization signal (NLS) domain and localizes more in the nucleus, whereas the SYNCRIP 562 isoform is found in the cytoplasm[170]. This suggests there may be some differences in mRNA processing between the two isoforms. Deeper exploration on how each isoform binds to and regulates HOXA9 translation will be necessary. To address this, we could overexpress each isoform in the absence of the endogenous SYNCRIP to observe how cell growth, differentiation, apoptosis and various known SYNCRIP targets (such as *Hoxa9, Myb*, and *Myc*) are influenced. Alternatively, we could selectively degrade each isoform and assess the effects that has on transcripts and translation; however, this would require the development of knock-in dTag systems for each isoform.

Like the SYNCRIP binding profile we characterized in HSPCs, we also identified various RBPs that are direct SYNCRIP targets in leukemia and LSCs. A deeper investigation into these relationships will be required to see if any of them play a functional role in causing the loss of LSC self-renewal. However, we'd require a proteomic, or translational dataset to help us narrow down which targets are changing in expression upon SYNCRIP depletion. This could be achieved with the RiboSTAMP experiment, alternatively we could conduct mass spectrometry on LSCs sorted from the Puro-CreER system. In addition to new targets, we also need to further explore SYNCRIP's translation regulation mechanism on *Hoxa9*. Although we've uncovered where SYNCRIP

binds, we still need to understand how SYNCRIP binding regulates translation. This could be occurring through a complex that SYNCRIP forms, in which case mass spectrometry of co-immunoprecipitation or an RNA-pull down assay may lead to identification of SYNCRIP-protein interactions.

In addition to understanding SYNCRIP's mechanism it will also be necessary to uncover novel therapeutics that can inhibit SYNCRIP activity, in particular translational regulation on oncogenic transcripts (like *Hoxa9*). To test this, we'll require a better understanding of what regions or domains SYNCRIP uses to regulate HOXA9 translation. We could screen for novel compounds that are specific to this interaction, and block SYNCRIP's ability to enhance HOXA9 translation.

The data presented in this thesis supports our rationale that SYNCRIP is important in HSPC and LSC function, and that it represents a potential therapeutic target for leukemia treatment. Additional exploration of the remaining questions will continue to elucidate SYNCRIP's mechanistic influence in normal and malignant hematopoiesis.

Methods

Normal Hematopoiesis Mouse Transplants

In the noncompetitive primary transplant $2x10^6$ whole bone marrow cells from *Syncrip f/f*, Mx1-Cre+ or Mx1-Cre- mice were transplanted into lethally irradiated B6SJL congenic CD45.1 recipients. In the competitive primary transplants 10^6 whole bone marrow cells from *Syncrip* cKO mice and 10^6 cells from congenic CD45.1 mice were injected into CD45.1 recipients. In the cell-autonomous transplants we transplant $2x10^6$ whole bone marrow cells from *Syncrip f/f*, Mx1-Cre+ or Mx1-Cre- into congenic CD45.1 recipient mice. Mice are bled at 5 weeks post-transplant to ensure engraftment, and after 6 weeks of engraftment mice deletion is induced via pIpC (InVivogen, Vac-Pic) intraperitoneal injections at a dose of 10 mg/kg on 2 consecutive days as showed previously [188].

Western Blot

Syncrip f/f and *Syncrip* Δ/Δ bone marrow cells were harvested; 250,000 cells were then lysed in 40uL 1x Laemmli protein loading buffer and boiled for 5 minutes. Whole cell lysates were run on 4% -15% gradient SDS-PAGE and transferred to nitrocellulose membrane. Membranes were probed with the SYNCRP and ACTIN antibody. For leukemia western blots, GFP+ cells were sorted and lysed as described above.

Flow cytometry and cell sorting

Flow cytometry and FACS were performed as previously described [36, 188]. Bone marrow cells were isolated and subjected to red blood cell (RBC) lysis. To measure the HSPC compartments, cells were stained with the following cocktail of flow cytometry antibodies: Lineage markers (CD3, CD4, CD8, Gr1, B220, CD19 and Ter119) – PE Cy5, cKit-APC Cy7, Sca-1-Pacific Blue, CD150-APC, CD48-PE. To monitor linage cells

differentiation, cells were stained with cocktail including Gr1-APC, Mac1-Pacific Blue, Ter119-PE Cy5, CD71-FITC, CD41-PE, or a cocktail containing CD3-Pacific Blue, CD4-PE, B220-PE Cy7, CD19-PE Cy5, IgM-APC, CD43-FITC. For transplanted mice, we added CD45.1-PE Texas Red and CD45.2-A700 to distinguish donor and recipient cells. For HSPC (LSK) or HSC (LSK, CD150+CD48-) cell sorting, bone marrow cells were harvested and incubated with 50uL CD117 MACS beads for 30 minutes, then run on AutoMACS according to manufacturer's instructions. Cells were then stained with antibody cocktail: Lineage marker (CD3, CD4, CD8, Gr1, B220, CD19, Ter119)-PE Cy5, cKit-APC Cy7, Sca-1-Pacific Blue, CD150-APC, CD48-PE, and included CD45.1-PE Texas Red, CD45.2-A700 for transplanted mice. Specific cell populations were sorted on BD Aria instrument. For leukemia transplants, bone marrow cells were harvested from mice, and underwent RBC lysis. Cells expressed MLL-AF9-GFP, and were stained with cKit APC-Cy7, Mac1 Pacific Blue, and Gr1 PE-Cy5 antibodies for flow cytometry.

Colony Formation Assay

10,000 whole *Syncrip* f/f or *Syncrip* Δ/Δbone marrow cells were plated in M3434 methylcellulose media, colonies were scored at 7 days post plating. For PU-H71 treatments and CDC42 Rescue, 750 LSK (Lin-Sca1+cKit+) cells were plated in methylcellulose media for the first plating, and colonies were scored at 7 days post plating. Subsequent replatings were done with 5000 cells and colonies were scored 7 days post plating.

Immunofluorescence

HSCs were sorted from *Syncrip* f/f and *Syncrip* Δ/Δ mice following protocol shown above. We performed NUMB daughter cell assay as previously described [36, 188]. Sorted HSCs were cultured with SFEM media containing 10ng/mL SCF and 20ng/mL TPO in 96 round-

bottom wells for 16-18 hr and then treated cells with 10nM Nocodazole for 24 hr. After incubation cells were fixed with 1.6% paraformaldehyde 15 minutes at room temperature and permeabilized with ice cold methanol. Fixed HSCs were then cytospun onto poly-L-lysine coated glass slides and blocked for 1hr with PBS + 0.5%BSA. Slides were then stained with anti-Numb, anti-*Syncrip*, and secondary Ab, followed by DAPI counterstaining. We evaluate symmetric and asymmetric percentages based on the fluorescence signal intensity of each cell acquired by Axio Imager M2 microscope (Carl Zeiss) and quantified by FIJI. Thresholds to determine NUMB high/low/asymmetric were set for experimental replicates. Briefly, both daughter cells with high NUMB staining or average staining intensity is above NUMB high threshold and there is less than 2-fold difference in the daughter pairs, this condition was counted as symmetric commitment. Daughter pair cells were scored as a symmetric renewal division when both of them were low or no staining or average staining intensity is below NUMB high threshold and there is less than 2-fold difference in the daughter pairs. If else, the division was considered an asymmetric division [36, 188]. HSC cells were also stained for SYNCRIP, CDC42, and TUBULIN using secondary Ab donkey anti-mouse Alexa Fluor 647, donkey anti-rabbit Alexa Fluor 568, and goat anti-rat Alexa Fluor 488 respectively. Separately, we also stained HSC for tubulin and Lamp1 using secondary Ab goat anti-rat Alexa Fluor 488 and donkey anti-rabbit Alexa Fluor 568 respectively. For LAMP1 daughter assay, cell pairs were scored as asymmetric if their intensities had a Log2FC $\geq \pm 0.6$, while pairs with Log2FC $< \pm 0.6$ intensities were scored as symmetric. A separate batch of cells was stained for ATF4 and CHOP using secondary Ab donkey anti-rabbit Alexa Fluor 568 and donkey anti-mouse Alexa Fluor 647 respectively. For unfolded protein IF daughter assay, HSCs were sorted and treated with nocodazole as previously described. Cells were then live stained with Tetraphenylethene maleimide (TMI) at a final concentration of 50uM in

PBS for 45 minutes at 37°C and subsequently fixed with 1.6% paraformaldehyde and permeabilized with ice cold methanol same as described above. TMI asymmetry was scored in a similar manner as LAMP1, if pair intensities had Log2FC $\geq \pm 0.6$ cells were scored as asymmetric and if pair intensities had Log2FC $< \pm 0.6$ then they were scored as symmetric. For CDC42 Rescue, LSK cells were sorted and transduced. 48hrs post transduction cells were fixed in 1.6% paraformaldehyde for 15 minutes at room temperature then permeabilized with ice cold methanol. Cells were imaged on confocal microscope (Leica TCS SP5 II in an upright configuration) utilizing a 63x objective and images were quantified by FIJI. To score polarity, integrated intensity was determined across all z-stacks and cells were split in half. If the Log2FC > 0.6 between the two halves, then that cell was scored as polar.

Retroviral Production

Virus was produced in HeK 293T cells using pCL-Eco (Addgene #12371) and pMD2.G (Addgene #12259). SYNCRIP-ADAR and CDC42 were separately cloned into MSCV-IRES-GFP (MIGR1, Addgene #27490) and used to generate retrovirus. HeK 293T cells were transfected with 0.25M $CaCl_2$, and BES buffered saline solution. Media was changed 12-16 hrs post transfection and the first virus suspension was collected 24hrs post media change. A second collection was harvested 48hrs post media change. Concentrated stocks of virus were prepared by precipitating virus using 50% PEG 6000 (poly (ethylene glycol)) and 4M NaCl for 2 hours, with inversion every 20 minutes. Precipitates were pelleted down at 2000xg for 30 minutes at 4℃. Virus pellets were vigorously resuspended in HBSS (without Ca, Mg, and phenol red), suspension was pelleted down again. Supernatant was collected and used for retroviral transductions.

HSPC Retroviral Transduction

HSPCs were sorted as described above and cultured with SFEM media supplemented with murine cytokines (50 ng/ml SCF, 10 ng/ml IL-3, and 10 ng/ml IL-6, 10ng/ml TPO and 20 ng/ml FLT3L). Cells were transduced with retroviral suspensions in the presence of 10ug/mL polybrene and followed with spin infection for 1 hr. After 24hrs, cells were transduced again as previously described. 48hrs later, cells were FACS sorted for GFP expression using BD Aria instrument.

O-Propargyl-puromycin (OP-Puro) Flow Analysis

Protein synthesis was assessed by O-Propargyl-puromycin (OP-Puro) using the Click-iT® Plus OPP Alexa Fluor 594 Protein Synthesis Assay Kit, following the manufacturer's instructions. Control cells were treated with 150ug/mL cycloheximide for 15 min. *Syncrip* f/f and *Syncrip* Δ/Δ HSC cells were sorted and then treated with 30uM Click-iT OPP Reagent (component A) for 1hr. Cells were then washed and fixed in 1.6% paraformaldehyde for 15 minutes room temperature, and permeabilized in ice cold methanol. Labeled cells were analyzed using a BD Fortessa instrument.

Measurement of unfolded proteins

Unfolded protein was measured as previously described [89]. *Syncrip* f/f and *Syncrip* Δ/Δ bone marrow cells were isolated, lysed with RBC lysis buffer twice and washed twice with Ca2+- and Mg2+-free PBS. $6x10^6$ *Syncrip* f/f and *Syncrip* Δ/Δ cells were treated with Tetraphenylethene maleimide (TMI; stock 2mM in DMSO). TMI was diluted in PBS (50uM final concentration) and added to each sample, the samples were then incubated at 37°C for 45 minutes. Samples were washed twice in PBS and then stained with flow cytometry cell surface markers as described above. Cells were analyzed using a BD Fortessa instrument.

Transmission Electron Microscopy (TEM)

Mouse bone marrow was isolated and ~9x10^4 HSCs were sorted as described above. Samples were washed with PBS then fixed with a modified Karmovsky's fix of 2.5% glutaraldehyde, 4% parafomaldehye and 0.02% picric acid in 0.1M sodium caocdylate buffer at pH 7.2 [216]. Following a secondary fixation in 1% osmium tetroxide, 1.5% potassium ferricyanide [217] J Ultrastruct. Res 42:29, samples were dehydrated through a graded ethanol series, and embedded in an epon analog resin. Ultrathin sections were cut using a Diatome diamond knife (Diatome, USA, Hatfield, PA) on a Leica Ultractu S ultramicrotome (Leica, Vienna, Austria). Sections were collected on copper grids and further contrasted with lead citrate [218] and viewed on a JEM 1400 electron microscope (JEOL, USA, Inc., Peabody, MA) operated at 100 kV. Images were recorded with a Veleta 2K x2K digital camera (Olympus-SIS, Germany). Images were quantified in Fiji.

Epichaperome Detection Flow Cytometry Assay

The epichaperome probes, PU FITC and FITC9, were synthesized as described in [219]. And the assay was performed as previously described [196, 219]. Mouse whole bone marrow was isolated, lysed twice with RBC lysis buffer and washed with FACS buffer (PBS + 2% FBS + 5mM EDTA). 6x10^6 bone marrow cells per condition were incubated with 1uM PU FITC at 37°C for 4 hr. Cells were then washed three times with FACS buffer and stained with flow cytometry cell surface markers as described above. Cells were analyzed using a BD Fortessa instrument. The FITC derivative FITC9 was used as a negative control, and the fold PU FITC binding was calculated relative to FITC9 control.

Single-Cell RNA-seq Analysis

Single-cell RNA-seq data was processed and aligned to mouse reference mm10 using CellRanger with default parameters. Normalization, dimensionality reduction and Louvain clustering were performed using Scanpy (v1.4.4[220]. Cells with < 200 detected genes or percentage of mitochondrial reads > 15% were filtered. Data were log normalized using a scale factor of 10,000. Louvain clusters were assigned the cell type with the best match by scoring expression of marker genes of clusters from [188]. Diffusion maps of early hematopoiesis were calculated by limiting to cells in clusters assigned to cell types: HSC-C1, HSC-C2, MPP1, MPP2 [221].

In-gel digestion and Mass Spectrometry

All reagent used where mass spectrometry grade._Proteomes were resolved by SDS-PAGE 10% polyacrylamide Bis-Tris gels (Invitrogen) at 100 V (~30 minutes).To visualize proteins, gel was stained using Silver Stain for Mass Spectrometry kit (Pierce) according to manufacturer's instructions. Relevant gel portions were excised and destained using 50 μl of 30 mM $K_3[Fe(CN)_6]$ in 100 mM $Na_2S_2O_3$ by incubation at room temperature for 30 mins, under constant agitation at 700 rpm. Following destaining, 500 μl 25 mM NH_4HCO_3 (ABC) was added to each tube and incubated for 5 min at room temperature under constant agitation. Solution was removed and gel pieces were washed trice for 10 minutes with 500 μl 50% acetonitrile in 25 mM aqueous ABC. All solution was removed and 100μl acetonitrile was added to each tube and incubated for 5 min at room temperature under constant agitation, followed by lyophilization using a vacuum centrifuge. Gel slabs were re-hydrated with 25 μl of 10 mM dithiothreitol (DTT) in 100 mM ABC (1h at 56^{o}C), followed by alkylation with 25 μl of 55 mM iodoacetamide in 100 mM ABC (30 min, room temperature in the dark), and quenching with 5 microliters of 100 mM DTT in 100 mM ABC (5 min at room temperature). Gel fragments were washed trice by adding 50 μl of

acetonitrile and incubating for 5 min at room temperature, followed by addition of 500 µl 100 mM ABC and incubation for 10 min at room temperature. After a final wash with 100 µl acetonitrile for 10 min at room temperature, gel fragments were lyophilized. Gel slabs were reconstituted in 50 µl of 12.5 ng/µl Sequencing Grade Modified trypsin (Promega) in 50 mM ABC, and proteolysis was performed for 16 hours at 37°C. Peptides were eluted twice by incubating the gel slabs for 30 minutes with 50 µl 1% acqueus formic acid in 70% acetonitrile under constant agitation at 1400 rpm. Eluates were pooled, lyophilized, and stored at -80°C until analysis. Samples were resuspended in 20 µl 0.1% acqueus formic acid, and 3 µl were analyzed by LC-MS. The LC system consisted of a vented trap-elute configuration (Ekspert NanoLC 425 chromatograph, Eksigent) coupled to a Orbitrap Fusion mass spectrometer (Thermo Fisher Scientific) via a nano electro-spray DPV-565 PicoView ion source (New Objective), as previously described [222]. After being loaded on the trap column (5 cm × 150 µm ID, packed with Poros R2-C18 10 µm particles (Life Technologies)) peptides were resolved on a nanoscale reversed phase analytical column (60 cm × 75 µm ID, packed with ReproSil-Pur C18-AQ 30 µm particles (Dr. Maisch), and kept at constant 55°C), using a 180 min 3%–40% linear gradient of acetonitrile/ 0.1% formic acid (buffer B) in water/0.1% formic acid (buffer A) at 300 nL/minute. Eluted peptides were transferred in gas phase by electrospray ionization using a 3 µm ID silica emitter with potential decreasing from 1800 V to 1600 V in 50 V steps over the elution. Precursor ions in the 385–1600 m/z range were isolated using the quadrupole and recorded every 3 s using the Orbitrap detector (120,000 resolution), with an automatic gain control target set at 10^6 ions and a maximum injection time of 50 ms. The Targeted Mass trigger was applied to bias precursor selection towards the ions predicted to be generated from targeted proteins (Supplementary table 15), with a mass tolerance of 10 ppm. For each targeted protein, tryptic peptides and charge states were predicted using

the Skyline [223] software for up to 3 unique peptides per proteins, based on consensus sequences from mouse UniProt database as of October 2019 [224]. If no targeted trigger ions were detected, the mass spectrometer was set to perform data-dependent MS2 precursor selection, limiting fragmentation to monoisotopic ions with charge 2–4, and dynamically excluding already fragmented precursors for 30 s (10 ppm tolerance). Selected precursors were isolated (Q1 isolation window 1.2 Th) and HCD fragmentated (stepped normalized collision energy 26-32-38%) using the top speed algorithm. Product ion spectra were recorded in the orbitrap at 30,000 resolutions (AGC $5x10^4$ ions, maximum injection time 32 ms), in centroid mode. The mass spectrometry proteomics data have been deposited to the ProteomeXchange Consortium via the PRIDE [225] partner repository with the dataset identifier PXD019460. Mass spectra were analyzed using Peaks Studio version 10.5 (BSI) For identification, spectra were matched against the murine UniProt database (as of October 2019), supplemented with contaminant proteins from the cRAP database [226] with FDR <0.01. Mass tolerance was set at 10 ppm and 0.1 Da for precursor and fragment ions, respectively. Cysteine carbamidomethylation was set as fixed chemical modification, while methionine oxidation, NQ deamidation and protein N-terminus acetylation were set as variable. Protease specificity was set to trypsin, with up to 3 missed cleavages allowed (max 3 PTM per peptide. The match between runs feature was enabled (0.7 min tolerance, 20 min alignment). Quantification was performed using the LFQ algorithm.

CFSE staining for homing and *in vivo* proliferation

To test homing capacities, LSK cells were sorted as previously described. Cells were stained with 3uM CFSE in PBS for 7 minutes at 37°C in the dark. $1.8x10^4$ CFSE stained LSK cells were transplanted into lethally irradiated congenic CD45.1 recipients. Mice were sacrificed 16hrs after transplantation and the BM from femora, tibiae and pelvis was

collected and evaluated using flow cytometry as previously described. For *in vivo* proliferation, LSK cells were sorted as described above and stained with 3uM CFSE in PBS for 7 minutes at 37°C in the dark. $3.2x10^4$ CFSE stained cells were transplanted into lethally irradiated congenic CD45.1 recipients. Mice were sacrificed 1 week post-transplant. BM from femora, tibiae and pelvis were collected and evaluated using flow cytometry as previously described.

***In vitro* Live Cell Imaging**

HSC cells were sorted as previously described. All live imaging was conducted on the CellRaft AIR System (Cell Microsystems) according to the manufacturer's instructions. Briefly, the raft array was prepared by rinsing the reservoir with warm PBS and incubating for 3 minutes at room temperature. This process was repeated 3 times, without letting the wells dry. The reservoir was then coated with Poly-D-Lysine and left to incubate overnight. The following day the reservoir was washed 3 times with DI water, and subsequently filled with media. Media conditions were the same as described above for HSPCs. The cell suspension was added dropwise into the reservoir. Cells were incubated at 37°C for 3 hours before taking any images. For image acquisition, the raft array was scanned on the CellRaft AIR system following system instructions and returned to a 37°C incubator after every scan. Full array scans were conducted at various timepoints for brightfield images.

***In vivo* BrdU proliferation Assay**

Primary transplanted mice were intraperitoneal (IP) injected with 100mg/kg BrdU solution, 16hrs post injection mice were euthanized and bone marrow cells were collected. 6×10^6 bone marrow cells were stained with stem cell flow panel as described above. Cells were then fixed and probed with a FITC BrdU antibody using BD Pharmingen BrdU Flow Kit, following manufactures protocol. Briefly, cells were fixed and permeabilized in BD

cytofix/cytoperm buffer for 20 minutes at room temperature in the dark, followed by a wash with BD perm/wash buffer. Next, cells were incubated for 10 minutes on ice with BD cytoperm permeabilization buffer plus, followed by a wash with BD perm/wash buffer. The cells were then re-fixed for 5 minutes at room temperature for 5 minutes in BD cytofix/cytoperm buffer, followed by a wash with BD perm/wash buffer. Next, the cells were DNase treated to expose the incorporated BrdU. Cells were treated with 30ug DNase/6x10^6 cells for 1hr at 37℃ in the dark, followed by a wash with BD perm/wash buffer. Finally, the cells were stained with FITC anti-BrdU antibody and incubated for 30 minutes at room temperature in the dark. Cells were run on flow cytometry BD Fortessa instrument.

Purification, culture and shRNA mediated depletion of SYNCRIP in human cord blood-derived CD34+ HSPCs

For each purification of CD34+ HSPCs, three cord blood units from the national cord blood program were used. Units of blood were diluted in RPMI+10% FBS and spun down 400xg for 20minutes. RBC lysis (5mL) was added and cells were incubated for 10minutes on ice, afterwards 10mL PBS was added and cells were spun down at 400xg for 10 minutes. CD34+ cells were enriched using the Miltenyi Biotec CD34 microbead kit following manufactures instructions, using the LS columns during magnetic separation. Cells were cultured in basic media for 48hrs, basic media was composed of Iscove's modified dulbecco's medium (IMDM), 20% BIT 9500 serum, 100ng/mL SCF, 10ng/mL FLT-3 ligand, 20ng/mL IL6, 100ng/mL TPO and 1% pen-strep. After 48hrs recovery, CD34+ cells were transduced by spinfection with lentivirus expressing scramble control or SYNCRIP targeting shRNA and 10ug/mL polybrene. Cells were transduced again 24hrs post initiation transduction. 24hrs post second transduction, cells were treated with 2ug/mL puromycin for selection, and the cells were selected for 48hrs. After selection, cells were

counted and used for appropriate experiment. For CFA and proliferation assay, cells were maintained in culture conditions with 0.5ug/mL puromycin.

Generation of MLL-AF9, BCR-ABL and AML-ETO9a leukemia cells

For generation of MLL-AF9 leukemia cells, bone marrow was extracted from 6-8week old *Syncrip* f/f and *Syncrip* Δ/Δ mice (same procedure used for heterozygous mice). Bone marrow cells underwent RBC lysis. For LSK cell isolation, bone marrow cells were enriched for cKit+ cells by incubation with Miltenyi Biotec CD117 microbeads and processed through the autoMACS Pro Seperator (Miltenyi Biotec) following manufactures instructions. cKit enriched cells were stained with lineage cocktail (CD3, CD4, CD8, B220, Ter119, and Gr1 all conjugated to PE-Cy5), Sca1-Pacific Blue, cKit APC-Cy7. Stained cells were sorted for Lin^{low}Sca1+cKit+ expression (LSK cells) using BD FACS Aria II instrument. Sorted cells were incubated in Stemspan SFEM medium (supplemented with 10ng/mL IL3, 10ng/mL IL6, 50ng/mL SCF, 10ng/mL TPO, 20ng/mL FLT-3 ligand and 1% pen-strep) overnight in 96well round bottom non-TC treated plate, at a ratio of 10000 cells per well. Next day, cells were transduced with MLL-AF9 retrovirus and 4ug/mL polybrene (expressing GFP, a gift from Scott Armstrong, Dana Farber Cancer Institute) on retronectin coated plates and spun for an hour. Cells were transduced again 24hrs post initial transduction, ~4 hours post second transduction cells were plated onto methylcellulose media and expanded for a week. Afterwards, cells were harvested and sorted for GFP+ expression. 150,000-200,000 cells were injected (along with 250,000 support BM cells) into recipient B6 mice.

For BCR-ABL and AML-ETO9a, LSK cells were harvested in the same manner as described above. For BCR-ABL cells were transduced with BCR-ABL (GFP expressing) retrovirus + 10ug/mL polybrene twice (24hours apart for each transduction). After 2nd

transduction 45,000-100,000 cells were injected into B6 mice. For AML-ETO9a cells were transduced with AML-ETO9a retrovirus + 10ug/mL polybrene (24hours apart for each transduction). After 2nd transduction 35,000-45,000 GFP+ cells were injected into B6 recipient mice.

Leukemia Transplants

For primary transplants (initiation or maintenance), 200,000-250,000 GFP+ leukemia cells were retro-orbitally injected (along with 250,000 support BM) into 7-8week old C57BL/6 mice, that had undergone 900 rads of lethal irradiation. For secondary, tertiary and quaternary transplants 100,000 GFP+ cells (from the previous transplant) were retro-orbitally injected into 7-8week old C57BL/6 mice that had undergone 450 rads of sub-lethal irradiation. *In vivo* leukemia maintenance experiments with *Syncrip*$^{f/f}$ Puro-CreER were performed by injecting 100,000 cells per mouse, into sublethally irradiated mice, and treating mice with 160mg/kg Tamoxifen or corn oil for 3 days post-transplant.

shRNA mediated depletion of SYNCRIP in human cell lines and PU-H71 drug treatments

Leukemia cells were cultured in RPMI media supplemented with 10% FBS, glutamine, and pen-strep. Cells were grown at 37℃ with 5% CO_2. MOLM13 and THP1 were transduced by spinfection with lentivirus expressing either control scramble or shRNA targeting SYNCRIP and 10ug/mL polybrene. Cells were transduced twice and during second transduction cells were also selected with 3ug/mL puromycin for 24hrs. 24hrs after second transduction, cells were plated on 96 well flat bottom non-TC treated plates. 5000 cells were seeded in each well, with 3ug/mL puromycin and the appropriate concentration of PU-H71. The drug treatments ranged from 2000nM-0.48nM. Cell viability was determined 3 days post treatment using Cell Titer Glo (promega).

Generation of *Syncrip*$^{f/f}$ Puro-CreER cells and Tamoxifen-mediated deletion

Mouse leukemia bone marrow cells from primary transplanted *Syncrip*$^{f/f}$ MLL-AF9 mice were expanded in RPMI medium (supplemented with 10% FBS, 10ng/mL IL3, 10ng/mL SCF, 10ng/mL IL6, 10 ng/mL GM-SCF and 1% pen-strep. Cells were transduced with concentrated MSCV-Cre-ER-puromycin retrovirus twice (24hrs apart from each transduction). 24hrs post the second transduction cells were selected with 3ug/mL puromycin. For deletion of *Syncrip*, *Syncrip*$^{f/f}$ Puro-CreER cells were treated with 25nM or 100nM 4-OHT tamoxifen or DMSO. Cells were collected at various timepoints for different assessments.

Polysome Profiling with *Syncrip*$^{f/f}$ Puro-CreER cells and Tamoxifen-mediated deletion

Syncrip$^{f/f}$ Puro-CreER cells were expanded and treated with 4-OHT for 24hrs. This was conducted in triplicate, to have 3 replicates. Cells were treated with cycloheximide (CHX) at 100ug/mL for 10 minutes at 37℃. Cell were then lysed on ice for 10 minutes in 400uL lysis buffer (20mM Tris HCl pH 7.4, 100mM KCl, 5mM $MgCl_2$, 1% TritonX-100, 100ug/mL CHX, 10mM DTT, EDTA-free protease inhibitors, and 500U/mL RNasin RNase inhibitor. Lysates were cleared by centrifugation at 15000g, for 15 minutes at 4℃. Some cleared lysate was saved for use as input and remaining was loaded onto linear 20-50% sucrose gradient in 40mM Tris HCl pH 7.5, 300mM KCl, 20mM $MgCl_2$, and 100ug/mL CHX. Samples were centrifuged at 42000rpm for 3hrs at 4℃ using a TH641 rotor in a Sorvall wX+Ultra series centrifuge (Thermo Scientific). After centrifugation, fractions were collected using a BioComp Gradient Station ip. RNA content was measured at A260 concurrent with fraction collection using Triax Flow Cell v1.50A software. AUCs and analysis thereof were calculated using Prism 8 software.

After collection, fractions were prepared for RNA precipitation by adding 0.1 volume of 3M NaOAc and 1 volume isopropanol alcohol to each fraction. Mixtures are incubated at -80℃ overnight. Precipitated RNAs were extracted by spinning at 16000g for 20 minutes, pellet was then washed with 70% ethanol, and spun again for 5 minutes at 16000g. Pellets were resuspended in RNase free water and Trizol. RNA was extracted using Direct-zol RNA Miniprep Kit following manufactures instructions. RNA was reverse transcribed into cDNA with iScript (BioRad) and used for RT-qPCR.

Luciferase Reporter Assay with *Hoxa9* Regions

Murine *Hoxa9* fragments (3'UTR, CDC, Delta1) were cloned downstream of firefly luciferase reporter gene in pGL3 (promega). The various *Hoxa9* fragments were co-transfected, using lipofectamine, along with renilla luciferase control (pRL-CMV). Simultaneously, cells were transfected with control, SYNCRIP shRNA or SYNCRIP 562 overexpression plasmids. After 48hrs of transfection, expression of renilla and firefly luciferase was determined by dual luciferase assay kit (Promega) following manufactures instructions.

RNA-Pull down with *In Vitro* Transcribed Biotinylated *Hoxa9*, *Myb* and *Myc* regions

PCR products of each transcript of interest was generated using protocol described in [227]. Briefly, PCR products were generated from MOLM13 derived cDNA. *In vitro* RNA transcription was performed using MEGAscript T7 kit (Invitrogen) following manufactures instructions. In the mixture 150-200ng of independent transcripts PCR product was added to ribonucleotides. Biotin-UTP was added to biotin label the RNAs and the ratio of ribonucleotide solution was ATP:CTP:GTP:UTP:Biotin-UTP = 1: 0.9: 0.9: 0.945: 0.055. After labeling RNAs were recovered using Phenol:Chloroform extraction methods and

precipitated with isopropanol (3hr incubation in -20℃). The quality and concentration of RNA was determined on Agilent bioanalyzer (Agilent technologies).

Either MOLM13 or HEK293T cells were used to run pull-down. Seven million cells were harvested per condition and cells were lysed for 20 minutes on ice (inverting every 5 minutes), using lysis buffer composed of 20mM Tris-HCl pH 7.5, 250mM NaCl, 50mM $MgCl_2$, 0.25% NP-40, 0.5% Triton X-100, 1mM EDTA ph8, and 2X protease inhibitor (Halt cocktail, Thermo Fisher). Cell lysates were clarified by centrifugation at max speed for 10 minutes at 4℃. Some of this lysate was saved as input. Pull-down mixture was prepared as follows: 450uL cell lysate, 1.5ug appropriate transcript biotinylated RNA, and 2.5uL RNaseOUT (with nuclease free water added to final volume 500uL). The reaction mixture was incubated at 4℃ for 1.5hrs with rotation. Pierce streptavidin magnetic beads (Thermo Fisher) were washed in the following wash butter: 10mM Tris-HCL, 250mM NaCl, 0.5% Triton X-100, 1mM EDTA ph8, and 2X protease inhibitor. After beads were washed 3 times and resuspended in original volume, 50uL of beads were added to each pull-down reaction and the mixtures were incubated for another 40 minutes at 4℃ with rotation. Afterwards, the pull down beads were washed 5 times with the same wash buffer described above. After the last wash the beads were resuspended in 1X Laemmli protein loading buffer and boiled for 5 minutes. The samples were loaded into western blot gels, along with their input and no RNA control conditions. Western blots were run and transferred onto nitrocellulose film.

References

1. Chao, M.P., J. Seita, and I.L. Weissman, *Establishment of a Normal Hematopoietic and Luekemia Stem Cell Hierarchy.* Cold Spring Harbor Laboratory Press 2008.
2. Doulatov, S., et al., *Hematopoiesis: A Human Perspective.* Cell Stem Cell, 2012. **10**(2): p. 120-136.
3. Zhang, Y., et al., *Hematopoietic Hierarchy – An Updated Roadmap.* Trends Cell Biol, 2018. **28**(12): p. 976-986.
4. Huang, X., S. Cho, and G.J. Spangrude, *Hematopoietic stem cells: generation and self-renewal.* Cell Death and Differentiation, 2007. **14**: p. 1851-1859.
5. Moran-Crusio, K., et al., *Tet2 Loss Leads to Increased Hematopoietic Stem Cell Self-Renewal and Myeloid Transformation.* Cancer Cell, 2011. **20**(1): p. 11-24.
6. Wilson, A., et al., *c-Myc controls the balance between hematopoietic stem cell self-renewal and differentiation.* Cold Spring Harbor Laboratory Press, 2004.
7. Wendorff, A.A., et al., *Phf6 Loss Enhances HSC Self-Renewal Driving Tumor Initiation and Leukemia Stem Cell Activity in T-ALL.* Cancer Discovery, 2019. **9**(3): p. 436-451.
8. Ceccaldi, R., et al., *Bone Marrow Failure in Fanconi Anemia Is Triggered by an Exacerbated p53/p21 DNA Damage Response that Impairs Hematopoietic Stem and Progenitor Cells.* Cell Stem Cell, 2012. **11**(1): p. 36-49.
9. Giudice, V., et al., *Bone Marrow Failure Syndromes, Overlapping Diseases with a Common Cytokine Signature.* International Journal of Molecular Sciences, 2021. **22**(2).
10. Passegue, E., et al., *Normal and leukemic hematopoiesis: Are leukemias a stem cell disorder or a reacquisition of stem cell characteristics?* PNAS, 2003.
11. Stevens, B.M., et al., *Characterization and targeting of malignant stem cells in patients with advanced myelodysplastic syndromes.* Nature Communications, 2018.
12. Long, N.A., et al., *Acute Myeloid Leukemia Stem Cells: Origin, Characteristics, and Clinical Implications.* Stem Cell Rev and Rep, 2022. **18**: p. 1211-1226.
13. Chen, Z., et al., *Molecular regulation of hematopoietic stem cell quiescence.* Cellular and Molecular Life Sciences, 2022. **79**.
14. Laurenti, E., et al., *CDK6 Levels Regulate Quiescence Exit in Human Hematopoietic Stem Cells.* Cell Stem Cell, 2015. **16**(3): p. 302-313.
15. Matsumoto, A., et al., *p57 Is Required for Quiescence and Maintenance of Adult Hematopoietic Stem Cells.* Cell Stem Cell, 2011. **9**(3): p. 262-271.
16. Cheng, T., et al., *Hematopoietic Stem Cell Quiescence Maintained by p21cip1/waf1.* Science, 2000. **287**(5459): p. 1804 - 1808.
17. Liu, Y., et al., *p53 Regulates Hematopoietic Stem Cell Quiescence.* Cell Stem Cell, 2009. **4**(1): p. 37-48.
18. Laurenti, E., et al., *Hematopoietic Stem Cell Function and Survival Depend on c-Myc and N-Myc Activity.* Cell Stem Cell, 2008. **3**(6): p. 611-624.
19. Wilson, A., et al., *c-Myc controls the balance between hematopoietic stem cell self-renewal and differentiation.* Genes & Development, 2004.

20. Liang, R., et al., *Restraining Lysosomal Activity Preserves Hematopoietic Stem Cell Quiescence and Potency.* Cell Stem Cell, 2020. **26**(3): p. 359-376.
21. Jung, H.E., et al., *The autophagy Protein Atg5 Plays a Crucial Role in the Maintenance and Reconstitution Ability of Hematopoietic Stem Cells.* Immune Network, 2019. **19**(2).
22. Mortensen, M., et al., *The autophagy protein Atg7 is essential for hematopoietic stem cell maintenance.* Journal of Experimental Medicine, 2011: p. 455-467.
23. Choi, J.S. and B.A.C. Harley, *Marrow-inspired matrix cues rapidly affect early fate decisions of hematopoietic stem and progenitor cells.* Science Advances, 2017. **3**(1).
24. Dao, M.A., et al., *Adhesion to Fibronectin Maintains Regenerative Capacity During Ex Vivo Culture and Transduction of Human Hematopoietic Stem and Progenitor Cells.* Blood, 1998.
25. Khurana, S., et al., *Outside-in integrin signalling regulates haematopoietic stem cell function via Periostin-Itgav axis.* Nature Communications, 2016. **7**.
26. Arai, F., et al., *Role of N-cadherin in the regulation of hematopoietic stem cells in the bone marrow niche.* Annals of the New York Academy of Sciences, 2012.
27. Zhao, M., et al., *N-Cadherin-Expressing Bone and Marrow Stromal Progenitor Cells Maintain Reserve Hematopoietic Stem Cells.* Cell Reports, 2019. **26**(3): p. 652-669.
28. Sinclair, A., et al., *CXCR2 and CXCL4 regulate survival and self-renewal of hematopoietic stem/progenitor cells.* Blood, 2016.
29. Bruns, I., et al., *Megakaryocytes regulate hematopoietic stem cell quiescence through CXCL4 secretion.* Nature Medicine, 2014. **20**: p. 1315-1320.
30. Yamazaki, S., et al., *Nonmyelinating Schwann Cells Maintain Hematopoietic Stem Cell Hibernation in the Bone Marrow Niche.* Cell, 2011.
31. Qian, H., et al., *Critical Role of Thrombopoietin in Maintaining Adult Quiescent Hematopoietic Stem Cells.* Cell Stem Cell, 2007. **1**(6): p. 671-684.
32. Wattrus, S.J., et al., *Quality assurance of hematopoietic stem cells by macrophages determines stem cell clonality.* Science, 2022. **377**(6613): p. 1413-1419.
33. Wilson, A., et al., *Hematopoietic Stem Cells Reversibly Switch from Dormancy to Self-Renewal during Homeostasis and Repair.* Cell, 2008. **135**(6): p. 1118-1129.
34. Ito, K. and K. Ito, *Hematopoietic stem cell fate through metabolic control.* Experimental Hematology, 2018. **63**: p. 1-11.
35. Loeffler, D., et al., *Asymmetric lysosome inheritance predicts activation of haematopoietic stem cells.* Nature, 2019. **573**(7774): p. 426-429.
36. Park, S.M., et al., *Musashi-2 controls cell fate, lineage bias, and TGF-beta signaling in HSCs.* J Exp Med, 2014. **211**(1): p. 71-87.
37. Knoblich, J.A., Jan, and Y.N. Jan, *Asymmetric segregation of Numb and Prospero during cell division.* Nature, 1995. **377**: p. 624-627.
38. Beckmann, J., et al., *Asymmetric cell division within the human hematopoietic stem and progenitor cell compartment: identification of asymmetrically segregating proteins.* Blood, 2007: p. 5494-5501.

39. Florian, C.M., et al., *Aging alters the epigenetic asymmetry of HSC division.* PLoS Biol, 2018.
40. Mizukawa, B., et al., *The cell polarity determinant CDC42 controls division symmetry to block leukemia cell differentiation.* Blood, 2017. **130**(11): p. 1336-1346.
41. Katajisto, P., et al., *Asymmetric apportioning of aged mitochondria between daughter cells is required for stemness.* Science, 2015. **348**(6232): p. 340-343.
42. Hinge, A., et al., *Asymmetrically Segregated Mitochondria Provide Cellular Memory of Hematopoietic Stem Cell Replicative History and Drive HSC Attrition.* Cell Stem Cell, 2020. **26**(3): p. 420-430.
43. Florian, C.M. and H. Geiger, *Concise Review: Polarity in Stem Cells, Disease, and Aging.* Stem Cells, 2010. **28**(9): p. 1623–1629.
44. Kandi, R., et al., *Cdc42-Borg4-Septin7 axis regulates HSC polarity and function.* EMBO Rep, 2021. **22**(e52931).
45. Florian, C.M. and H. Geiger, *CDC42 is a key regulator of cell polarity and cytoskeletal organization in HSCs.* Stem Cells, 2010. **10.1002/stem.481**.
46. de Rooij, L., et al., *Post-transcriptional regulation in hematopoiesis: RNA binding proteins take control (1).* Biochem Cell Biol, 2019. **97**(1): p. 10-20.
47. Aguilar-Garrido, P., et al., *The Role of RNA-Binding Proteins in Hematological Malignancies.* International Journal of Molecular Sciences, 2022. **23**.
48. Liao, J.Y., et al., *EuRBPDB: a comprehensive resource for annotation, functional and oncological investigation of eukaryotic RNA binding proteins (RBPs).* Nucleic Acids Research, 2020. **48**(D1): p. D307-D313.
49. Helm, M. and Y. Motorin, *Detecting RNA modifications in the epitranscriptome: predict and validate.* Nature Reviews Genetics, 2017. **18**: p. 275-291.
50. Jiang, X., et al., *The role of m6A modification in the biological functions and diseases.* Sig Transduct Target Ther, 2021. **6**.
51. Shen, C., et al., *RNA Demethylase ALKBH5 Selectively Promotes Tumorigenesis and Cancer Stem Cell Self-Renewal in Acute Myeloid Leukemia.* Cell Stem Cell, 2020. **27**(1): p. 64-80.
52. Zhang, C., et al., *m6A modulates haematopoietic stem and progenitor cell specification.* Nature 2017: p. 273-276.
53. Zhang, P., et al., *G protein-coupled receptor 183 facilitates endothelial-to-hematopoietic transition via Notch1 inhibition.* Cell Reserach, 2015. **25**: p. 1093-1107.
54. Lv, J., et al., *Endothelial-specific m6A modulates mouse hematopoietic stem and progenitor cell development via Notch signaling.* Cell Reserach, 2017. **28**: p. 249-252.
55. Lee, H., et al., *Stage-specific requirement for Mettl3-dependent m6A mRNA methylation during haematopoietic stem cell differentiation.* Nature Cell Biology, 2019. **21**: p. 700-709.
56. Cheng, Y., et al., *m6A RNA Methylation Maintains Hematopoietic Stem Cell Identity and Symmetric Commitment.* Cell Reports, 2019. **28**(7): p. 1703-1716.

57. Scholler, E., et al., *Interactions, localization, and phosphorylation of the m6A generating METTL3–METTL14–WTAP complex.* RNA Journal, 2018.
58. Yao, Q.J., et al., *Mettl3–Mettl14 methyltransferase complex regulates the quiescence of adult hematopoietic stem cells.* Cell Research, 2018. **28**(9): p. 952-954.
59. Weng, H., et al., *METTL14 Inhibits Hematopoietic Stem/Progenitor Differentiation and Promotes Leukemogenesis via mRNA m6A Modification.* Cell Stem Cell, 2018. **22**(2): p. 191-205.
60. Patil, D.P., et al., *m6A RNA methylation promotes XIST-mediated transcriptional repression.* Nature, 2016. **537**: p. 369-373.
61. Raffel, G.D., et al., *Ott1(Rbm15) has pleiotropic roles in hematopoietic development.* PNAS, 2007. **104**(14).
62. Niu, C., et al., *c-Myc is a target of RNA-binding motif protein 15 in the regulation of adult hematopoietic stem cell and megakaryocyte development.* Blood, 2009. **114**(10): p. 2087-2096.
63. Wang, X., et al., *N6-methyladenosine-dependent regulation of messenger RNA stability.* Nature, 2013. **505**: p. 117-120.
64. Roundtree, I.A., et al., *YTHDC1 mediates nuclear export of N6-methyladenosine methylated mRNAs.* eLife, 2017. **6**.
65. Wang, X., et al., *N6-methyladenosine Modulates Messenger RNA Translation Efficiency.* Cell, 2015. **161**(6).
66. Li, Z., et al., *Suppression of m6A reader Ythdf2 promotes hematopoietic stem cell expansion.* Cell Research, 2018. **28**: p. 904–917.
67. Mapperley, C., et al., *The mRNA m6A reader YTHDF2 suppresses proinflammatory pathways and sustains hematopoietic stem cell function.* Journal of Experimental Medicine, 2020. **218**.
68. Zhang, X., et al., *YTHDF3 modulates hematopoietic stem cells by recognizing RNA m6A modification on Ccnd1.* Hematologica, 2022. **107**(10).
69. Gehring, N.H. and J.-Y. Roignant, *Anything but Ordinary – Emerging Splicing Mechanisms in Eukaryotic Gene Regulation.* Trends in Genetics, 2020. **37**(4): p. 355-372.
70. Chen, S. and O. Abdel-Wahab, *Splicing regulation in hematopoiesis.* Current Oppinion in Hematology, 2021. **DOI:10.1097/MOH.0000000000000661**.
71. Isono, K., et al., *Mammalian Polycomb-mediated repression of Hox genes requires the essential spliceosomal protein Sf3b1.* Genes & Development, 2005. **19**: p. 536-541.
72. Wang, C., et al., *Depletion of Sf3b1 impairs proliferative capacity of hematopoietic stem cells but is not sufficient to induce myelodysplasia.* Blood, 2014.
73. Matsunawa, M., et al., *Haploinsufficiency of Sf3b1 leads to compromised stem cell function but not to myelodysplasia.* Leukemia, 2014. **28**: p. 1844-1850.
74. Dutta, A., et al., *U2af1 is required for survival and function of hematopoietic stem/progenitor cells.* Leukemia, 2021. **35**: p. 2382-2398.

75. Shirai, C.L., et al., *Mutant U2AF1 Expression Alters Hematopoiesis and Pre-mRNA Splicing In Vivo.* Cancer Cell, 2015. **27**(5).
76. Liang Fei, D., et al., *Impaired hematopoiesis and leukemia development in mice with a conditional knock-in allele of a mutant splicing factor gene U2af1.* PNAS, 2018. **115**: p. E10437-E10446.
77. Liang Fei, D., et al., *Impaired hematopoiesis and leukemia development in mice with a conditional knock-in allele of a mutant splicing factor gene U2af1.* PNAS, 2018. **115**(44): p. 10437-10446.
78. Masaki, S., et al., *Myelodysplastic Syndrome-Associated SRSF2 Mutations Cause Splicing Changes by Altering Binding Motif Sequences.* Frontiers in Genetics, 2019.
79. Komeno, Y., et al., *SRSF2 Is Essential for Hematopoiesis, and Its Myelodysplastic Syndrome-Related Mutations Dysregulate Alternative Pre-mRNA Splicing.* Molecular and Cellular Biology, 2015. **35**.
80. Kim, E., et al., *SRSF2 Mutations Contribute to Myelodysplasia by Mutant-Specific Effects on Exon Recognition.* Cancer Cell, 2015. **27**(5): p. 617-630.
81. Madan, V., et al., *Aberrant splicing of U12-type introns is the hallmark of ZRSR2 mutant myelodysplastic syndrome.* Nature Communications, 2015. **6**.
82. Inoue, D., et al., *Minor intron retention drives clonal hematopoietic disorders and diverse cancer predisposition.* Nature Genetics, 2021. **53**: p. 707-718.
83. Savva, Y.A., L.E. Rieder, and R.A. Reenan, *The ADAR protein family.* Genome Biol, 2012. **13**.
84. Wang, Q., et al., *Stress-induced Apoptosis Associated with Null Mutation of ADAR1 RNA Editing Deaminase Gene.* Journal of Biolocical Chemistry, 2004. **279**(6): p. 4952-4961.
85. Wang, Q., et al., *Requirement of the RNA Editing Deaminase ADAR1 Gene for Embryonic Erythropoiesis.* Science, 2000. **290**(5497).
86. Hartner, J.C., et al., *ADAR1 is essential for the maintenance of hematopoiesis and suppression of interferon signaling.* Nature Immunnology, 2009. **10**: p. 109-115.
87. XuFeng, R., et al., *ADAR1 is required for hematopoietic progenitor cell survival via RNA editing.* PNAS, 2009. **106**(42).
88. Signer, R.A., et al., *Haematopoietic stem cells require a highly regulated protein synthesis rate.* Nature, 2014. **509**(7498): p. 49-54.
89. Hidalgo San Jose, L., et al., *Modest Declines in Proteome Quality Impair Hematopoietic Stem Cell Self-Renewal.* Cell Rep, 2020. **30**(1): p. 69-80 e6.
90. Ambrosini, C., F. Garilli, and A. Quattrone, *Reprogramming translation for gene therapy.* Progress in Molecular Biology and Translational Science, 2021. **182**: p. 439-476.
91. Signer, R.A., et al., *The rate of protein synthesis in hematopoietic stem cells is limited partly by 4E-BPs.* Genes & Development, 2016. **30**(15): p. 1698-1703.
92. Kharas, M.G. and C.J. Lengner, *Stem Cells, Cancer, and MUSASHI in Blood and Guts.* Trends in Cancer, 2017. **3**(5): p. 347-356.

93. Imai, T., et al., *The Neural RNA-Binding Protein Musashi1 Translationally Regulates Mammalian numb Gene Expression by Interacting with Its mRNA.* Molecular and Cellular Biology, 2001. **21**(12): p. 3888-3900.
94. Kawahara, H., et al., *Neural RNA-binding protein Musashi1 inhibits translation initiation by competing with eIF4G for PABP.* Journal of Cell Biology, 2008. **181**(4): p. 639-653.
95. Kharas, M.G., et al., *Musashi-2 regulates normal hematopoiesis and promotes aggressive myeloid leukemia.* Nat Med, 2010. **16**(8): p. 903-8.
96. Hope, K.J., et al., *An RNAi Screen Identifies Msi2 and Prox1 as Having Opposite Roles in the Regulation of Hematopoietic Stem Cell Activity.* Cell Stem Cell 2010. **7**: p. 101–113.
97. De Andres-Aguayo, L., et al., *Musashi 2 is a regulator of the HSC compartment identified by a retroviral insertion screen and knockout mice.* Blood, 2011. **118**(3): p. 554-564.
98. Nguyen, D.T.T., et al., *HyperTRIBE uncovers increased MUSASHI-2 RNA binding activity and differential regulation in leukemic stem cells.* Nat Commun, 2020. **11**(1): p. 2026.
99. Pelcovits, A. and R. Niroula, *Acute Myeloid Leukemia: A Review* Updates in Hematology/Oncology, 2020. **103**(3): p. 38-40.
100. Kantarjian, H., et al., *Acute myeloid leukemia: current progress and future directions.* Blood Cancer Journal, 2021. **11**(41).
101. Olivia, E.N., et al., *A systematic literature review of disease burden and clinical efficacy for patients with relapsed or refractory acute myeloid leukemia.* American Journal of Blood Research, 2021. **11**(4): p. 325-360.
102. Lapidot, T., et al., *A cell initiating human acute myeloid leukaemia after transplantation into SCID mice.* Nature, 1994. **367**: p. 645-648.
103. Bonnet, D. and J.E. Dick, *Human acute myeloid leukemia is organized as a hierarchy that originates from a primitive hematopoietic cell.* Nature Medicine, 1997. **3**: p. 730-737.
104. Jan, M., et al., *Clonal Evolution of Preleukemic Hematopoietic Stem Cells Precedes Human Acute Myeloid Leukemia.* Science Translational Medicine, 2012. **4**(149).
105. Stauber, J., J.M. Greally, and U. Steidl, *Preleukemic and leukemic evolution at the stem cell level.* Blood Spotlight, 2021. **137**(8): p. 1013-1018.
106. Ishikawa, F., et al., *Chemotherapy-resistant human AML stem cells home to and engraft within the bone-marrow endosteal region.* Nature Biotechnology, 2007. **25**: p. 1215-1321.
107. Barbieri, I., et al., *Promoter-bound METTL3 maintains myeloid leukaemia by m6A-dependent translation control.* Nature, 2017. **552**: p. 126-131.
108. Vu, L.P., et al., *The N6-methyladenosine (m6A)-forming enzyme METTL3 controls myeloid differentiation of normal hematopoietic and leukemia cells.* Nature Medicine, 2017. **23**: p. 1369-1376.
109. Li, Z., et al., *FTO Plays an Oncogenic Role in Acute Myeloid Leukemia as a N6-Methyladenosine RNA Demethylase.* Cancer Cell, 2017. **31**(1): p. 127-141.

110. Cully, M., *Chemical inhibitors make their RNA epigenetic mark.* Nat Rev Drug Disco., 2019. **18**: p. 892-894.
111. Yankova, E., et al., *Small-molecule inhibition of METTL3 as a strategy against myeloid leukaemia.* Nature 2021. **593**: p. 597-601.
112. Huang, Y., et al., *Small-Molecule Targeting of Oncogenic FTO Demethylase in Acute Myeloid Leukemia.* Cancer Cell, 2019. **35**(4): p. 677-691.
113. Su, R., et al., *Targeting FTO Suppresses Cancer Stem Cell Maintenance and Immune Evasion.* Cancer Cell, 2020. **38**(1): p. 79-96.
114. Taylor, J. and S.C. Lee, *Mutations in spliceosome genes and therapeutic opportunities*
in myeloid malignancies. Genes, Chromosomes, and Cancer, 2019. **58**(12): p. 889-902.
115. Bamopoulos, S.A., et al., *Clinical presentation and differential splicing of SRSF2, U2AF1 and SF3B1 mutations in patients with acute myeloid leukemia.* Leukemia, 2020. **34**: p. 2621-2634.
116. Mian, S.A., et al., *SF3B1 mutant MDS-initiating cells may arise from the haematopoietic stem cell compartment.* Nature Communications, 2015. **6**.
117. Mai, S., et al., *Global regulation of alternative RNA splicing by the SR-rich protein RBM39.* Gene Regulatory Mechanisms, 2016. **1859**(8): p. 1014-1024.
118. Xu, C., et al., *RNA-binding protein 39: a promising therapeutic target for cancer.* Cell Death and Discovery, 2021. **7**.
119. Wang, E., et al., *Targeting an RNA-Binding Protein Network in Acute Myeloid Leukemia.* Cancer Cell, 2019. **35**(3): p. 369-384.
120. Salton, M. and T. Misteli, *Small Molecule Modulators of Pre-mRNA Splicing in Cancer Therapy.* Trends in Molecular Medicine, 2016. **22**(1): p. 28-37.
121. Seiler, M., et al., *H3B-8800, an orally available small-molecule splicing modulator, induces lethality in spliceosome-mutant cancers.* Nature Medicine, 2018. **24**: p. 497-504.
122. Gollner, S. and C. Nuller-Tidow, *AKTing on XPO1 inhibition in AML.* Nature Cancer, 2022. **3**: p. 787-789.
123. Tan, D.S.P., et al., *Promising SINEs for Embargoing Nuclear–Cytoplasmic Export as an Anticancer Strategy.* Cancer Discovery, 2014. **4**(5): p. 527-537.
124. Wang, A.Y. and H. Liu, *The past, present, and future of CRM1/XPO1 inhibitors.* Stem Cell Investigation, 2019.
125. Newlands, E.S., G.J.S. Rustin, and M.H. Brampton, *Phase I trial of elactocin.* British Journal of Cancer, 1996. **74**: p. 648-649.
126. Garzon, R., et al., *A phase 1 clinical trial of single-agent selinexor in acute myeloid leukemia.* Blood, 2017. **129**(24): p. 3165-3174.
127. Bhatnagar, B., et al., *Selinexor in combination with decitabine in patients with acute myeloid leukemia: results from a phase 1 study.* Leukemia and Lymphoma, 2020. **61**(2): p. 387-396.
128. Wang, A.Y., et al., *A phase I study of selinexor in combination with high-dose cytarabine and mitoxantrone for remission induction in patients with acute myeloid leukemia.* Journal of Hematology and Oncology, 2018. **11**(1).

129. Xiao, H., et al., *ADAR1 may be involved in the proliferation of acute myeloid leukemia cells via regulation of the Wnt pathway.* Cancer Manag Res, 2019. **11**: p. 8547-8555.
130. Rossetti, C., et al., *RNA editing signature during myeloid leukemia cell differentiation.* Leukemia, 2017. **31**: p. 2824-2832.
131. Zipeto, M.A., et al., *ADAR1 Activation Drives Leukemia Stem Cell Self-Renewal by Impairing Let-7 Biogenesis.* Cell Stem Cell, 2016. **19**(2): p. 177-191.
132. Wang, X., et al., *Targeting ADAR1 with a Novel Small-Molecule for the Treatment of Prostate Cancer.* ResearchSquare, 2021.
133. Kentsis, A., et al., *Ribavirin suppresses eIF4E-mediated oncogenic transformation by physical mimicry of the 7-methyl guanosine mRNA cap.* PNAS, 2004. **101**: p. 18105-18110.
134. Topisirovic, I., et al., *Aberrant Eukaryotic Translation Initiation Factor 4E-Dependent mRNA Transport Impedes Hematopoietic Differentiation and Contributes to Leukemogenesis.* Molecular and Cellular Biology, 2003. **23**: p. 8992-9002.
135. Assouline, S., et al., *Molecular targeting of the oncogene eIF4E in acute myeloid leukemia (AML): a proof-of-principle clinical trial with ribavirin.* Blood, 2009. **114**(2): p. 257-260.
136. Zahreddine, H.A., et al., *The sonic hedgehog factor GLI1 imparts drug resistance through inducible glucuronidation.* Nature, 2014. **511**: p. 90-93.
137. Yang, X., W. Zhong, and R. Cao, *Phosphorylation of the mRNA cap-binding protein eIF4E and cancer.* Cellular Signalling, 2020. **73**.
138. Kim, H.-J., *Cell Fate Control by Translation: mRNA Translation Initiation as a Therapeutic Target for Cancer Development and Stem Cell Fate Control.* Biomolecules, 2019. **9**(11): p. 665.
139. Suarez, M., et al., *Inhibitory effects of Tomivosertib in acute myeloid leukemia.* Oncotarget, 2021. **12**: p. 955-966.
140. Nishida, Y., et al., *Inhibition of translation initiation factor eIF4a inactivates heat shock factor 1 (HSF1) and exerts anti-leukemia activity in AML.* Leukemia, 2021. **35**: p. 2469-2481.
141. Lee, J., et al., *Musashi-2 is a novel regulator of paclitaxel sensitivity in ovarian cancer cells.* International Journal of Oncology, 2016. **49**(5): p. 1945-1952.
142. Topchu, I., et al., *Musashi 2 (MSI2) expression as an independent prognostic biomarker in non-small cell lung cancer (NSCLC).* Journal of Thoracic Disease, 2021. **13**(3): p. 1370-1379.
143. Wang, S., et al., *Transformation of the intestinal epithelium by the MSI2 RNA-binding protein.* Nature Communications, 2015. **6**.
144. Dong, P., et al., *Musashi-2, a novel oncoprotein promoting cervical cancer cell growth and invasion, is negatively regulated by p53-induced miR-143 and miR-107 activation.* Journal of Experimental and Clinical Cancer Research, 2017. **36**.
145. Jiang, L., et al., *Prognostic value of Musashi 2 (MSI2) in cancer patients: A systematic review and meta-analysis.* Front. Oncol., 2022. **12**.

146. Barbouti, A., et al., *A Novel Gene, MSI2, Encoding a Putative RNA-binding Protein Is Recurrently Rearranged at Disease Progression of Chronic Myeloid Leukemia and Forms a Fusion Gene with HOXA9 as a Result of the Cryptic t(7;17)(p15;q23).* Cancer Res, 2003. **63**(6): p. 1202-1206.
147. De Weer, A., et al., *EVI1 overexpression in t(3;17) positive myeloid malignancies results from juxtaposition of EVI1 to the MSI2 locus at 17q22.* Hematologica, 2008. **93**(12).
148. Saleki, R., et al., *A novel TTC40–MSI2 fusion in de novo acute myeloid leukemia with an unbalanced 10;17 translocation.* Leukemia and Lymphoma, 2015. **56**(4): p. 1137-1139.
149. Wang, K., et al., *Patient-derived xenotransplants can recapitulate the genetic driver landscape of acute leukemias.* Leukemia, 2016. **31**: p. 151-158.
150. Ito, T., et al., *Regulation of myeloid leukaemia by the cell-fate determinant Musashi.* Nature, 2010. **466**: p. 765-768.
151. Thol, F., et al., *Prognostic significance of expression levels of stem cell regulators MSI2 and NUMB in acute myeloid leukemia.* Annals of Hematology, 2013. **92**: p. 315-323.
152. Park, S.M., et al., *Musashi2 sustains the mixed-lineage leukemia–driven stem cell regulatory program.* J Clin Invest., 2015. **125**(3): p. 1286-1298.
153. Clingman, C.C., et al., *Allosteric inhibition of a stem cell RNA-binding protein by an intermediary metabolite.* eLife, 2014. **3**.
154. L., L., et al., *Natural product (−)-gossypol inhibits colon cancer cell growth by targeting RNA-binding protein Musashi-1.* Molecular Oncology, 2015. **9**(7): p. 1406-1420.
155. Minuesa, G., et al., *A 1536-well Fluorescence Polarization Assay to Screen for Modulators of the MUSASHI Family of RNA-Binding Proteins.* Combinatorial Chemistry and High Throughput Screening, 2014. **17**(7): p. 596-609.
156. Minuesa, G., et al., *Small-molecule targeting of MUSASHI RNA-binding activity in acute myeloid leukemia.* Nature Communications, 2019. **10**.
157. Nakano, Y., et al., *Acute Myeloid Leukemia With RBM15-MKL1 Presenting as Severe Hepatic Failure.* Glob Pediatr Health, 2017. **4**.
158. Hsiao, H.-H., et al., *RBM15-MKL1 (OTT-MAL) Fusion Transcript in an Adult Acute Myeloid Leukemia Patient.* American Journal of Hematology, 2005. **79**: p. 43-45.
159. Yang, Y., et al., *Biological effects of decreasing RBM15 on chronic myelogenous leukemia cells.* Leukemia & Lymphoma, 2012. **53**(11).
160. Paris, J., et al., *Targeting the RNA m6A Reader YTHDF2 Selectively Compromises Cancer Stem Cells in Acute Myeloid Leukemia.* Cell Stem Cell, 2019. **25**(1): p. 137-148.
161. Micaelli, M., et al., *Small-Molecule Ebselen Binds to YTHDF Proteins Interfering with the Recognition of N6-Methyladenosine-Modified RNAs.* ASC Pharmacol. Transl. Sci., 2022. **5**(10): p. 872-891.
162. Wang, X., et al., *Transient regulation of RNA methylation in human hematopoietic stem cells promotes their homing and engraftment.* Leukemia, 2022.

163. Shirai, C.L., et al., *Mutant U2AF1-expressing cells are sensitive to pharmacological modulation of the spliceosome.* Nature Communications, 2017. **8**.
164. Visconte, V., M.O. Nakashima, and H.J. Rogers, *Mutations in Splicing Factor Genes in Myeloid Malignancies: Significance and Impact on Clinical Features.* Cancers, 2019. **11**: p. 1844.
165. McMahon, A.C., et al., *TRIBE: Hijacking an RNA-Editing Enzyme to Identify Cell-Specific Targets of RNA-Binding Proteins.* Cell, 2016. **165**(3): p. 742-53.
166. Brannan, K.W., et al., *Robust single-cell discovery of RNA targets of RNA-binding proteins and ribosomes.* Nature Methods, 2021. **18**: p. 507-519.
167. Vu, L.P., et al., *Functional screen of MSI2 interactors identifies an essential role for SYNCRIP in myeloid leukemia stem cells.* Nat Genet, 2017. **49**(6): p. 866-875.
168. Prieto, C., et al., *Transcriptional control of CBX5 by the RNA-binding proteins RBMX and RBMXL1 maintains chromatin state in myeloid leukemia.* Nature Cancer, 2021. **2**: p. 741-757.
169. Mourelatos, Z., et al., *SMN interacts with a novel family of hnRNP and spliceosomal proteins.* The Embo Journal, 2001. **20**(19): p. 5443-5452.
170. Chen, H.-H., et al., *The RNA Binding Protein hnRNP Q Modulates the Utilization of Exon 7 in the Survival Motor Neuron 2 (SMN2) Gene.* Molecular and Cellular Biology, 2008. **28**(22): p. 6929-6938.
171. Kabat, J.L., S. Barberan-Soler, and A.M. Zahler, *HRP-2, the Caenorhabditis elegans homolog of mammalian heterogeneous nuclear ribonucleoproteins Q and R, is an alternative splicing factor that binds to UCUAUC splicing regulatory elements.* J Biol Chem, 2009. **284**(42): p. 28490-7.
172. Chen, S., et al., *SYNCRIP facilitates porcine parvovirus viral DNA replication through the alternative splicing of NS1 mRNA to promote NS2 mRNA formation.* Veterinary Research 2021. **52**.
173. McDermott, S.M., et al., *Drosophila Syncrip modulates the expression of mRNAs encoding key synaptic proteins required for morphology at the neuromuscular junction.* RNA, 2014. **20**: p. 1593-1606.
174. Svitkin, Y.V., et al., *Control of translation and miRNA-dependent repression by a novel poly(A) binding protein, hnRNP-Q.* PLoS Biol, 2013. **11**(5): p. e1001564.
175. Santangelo, L., et al., *The RNA-Binding Protein SYNCRIP Is a Component of the Hepatocyte Exosomal Machinery Controlling MicroRNA Sorting.* Cell Rep, 2016. **17**(3): p. 799-808.
176. Duning, K., et al., *SYNCRIP, a component of dendritically localized mRNPs, binds to the translation regulator BC200 RNA.* Journal of Neurochemistry, 2007. **105**(2): p. 351-359.
177. Grosset, C., et al., *A Mechanism for Translationally Coupled mRNA Turnover.* Cell, 2000. **103**(1): p. 29-40.
178. Samuels, T.J., et al., *Neuronal upregulation of Prospero protein is driven by alternative mRNA polyadenylation and Syncrip-mediated mRNA stabilisation.* Biology Open, 2020. **9**(5).

179. Mukhopadhyay, R., et al., *The GAIT system: a gatekeeper of inflammatory gene expression.* Trends in Biochemical Sciences, 2009. **34**(7): p. 324-331.
180. Khudayberdiev, S., et al., *The cytoplasmic SYNCRIP mRNA interactome of mammalian neurons.* RNA Biology, 2020. **18**(9).
181. Halstead, J.M., et al., *Syncrip/hnRNP Q influences synaptic transmission and regulates BMP signaling at the Drosophila neuromuscular synapse.* Biology Open, 2014. **3**(9).
182. McDermott, S.M., et al., *Drosophila Syncrip binds the gurken mRNA localisation signal and regulates localised transcripts during axis specification.* Biology Open, 2012. **1**(5).
183. Gachet, S., et al., *Deletion 6q Drives T-cell Leukemia Progression by Ribosome Modulation.* Cancer Discovery, 2018. **8**(12): p. 1614-1631.
184. Bagger, F.O., S. Kinalis, and N. Rapin, *BloodSpot: a database of healthy and malignant haematopoiesis updated with purified and single cell mRNA sequencing profiles* Nucleic Acids Research, 2018. **47**(D1): p. D881-885.
185. Liu, Y., et al., *ATF3 Prevents Stress-Induced Hematopoietic Stem Cell Exhaustion.* Frontiers in Cell and Developmental Biology, 2020.
186. Ma, Z., et al., *Hes1 deficiency causes hematopoietic stem cell exhaustion.* Stem Cells, 2020. **38**(6): p. 756-768.
187. Singh, S.K., et al., *Id1 Ablation Protects Hematopoietic Stem Cells from Stress-Induced Exhaustion and Aging.* Cell Stem Cell, 2018. **23**(2): p. 252-265.
188. Cheng, Y., et al., *m(6)A RNA Methylation Maintains Hematopoietic Stem Cell Identity and Symmetric Commitment.* Cell Rep, 2019. **28**(7): p. 1703-1716 e6.
189. Giladi, A., et al., *Single-cell characterization of haematopoietic progenitors and their trajectories in homeostasis and perturbed haematopoiesis.* Nat Cell Biol, 2018. **20**(7): p. 836-846.
190. Paul, F., et al., *Transcriptional Heterogeneity and Lineage Commitment in Myeloid Progenitors.* Cell, 2015. **163**(7): p. 1663-77.
191. Rodriguez-Fraticelli, A.E., et al., *Single-cell lineage tracing unveils a role for TCF15 in haematopoiesis.* Nature, 2020. **583**(7817): p. 585-589.
192. Pietras, E.M., et al., *Functionally Distinct Subsets of Lineage-Biased Multipotent Progenitors Control Blood Production in Normal and Regenerative Conditions.* Cell Stem Cell, 2015. **17**(1): p. 35-46.
193. Cabezas-Wallscheid, N., et al., *Vitamin A-Retinoic Acid Signaling Regulates Hematopoietic Stem Cell Dormancy.* Cell, 2017. **169**(5): p. 807-823 e19.
194. Chen, E.Y., et al., *Enrichr: interactive and collaborative HTML5 gene list enrichment analysis tool.* BMC Bioinformatics, 2013. **14**: p. 128.
195. Chen, M.Z., et al., *A thiol probe for measuring unfolded protein load and proteostasis in cells.* Nat Commun, 2017. **8**(1): p. 474.
196. Rodina, A., et al., *The epichaperome is an integrated chaperome network that facilitates tumour survival.* Nature, 2016. **538**(7625): p. 397-401.
197. Sugita, M., et al., *Targeting the epichaperome as an effective precision medicine approach in a novel PML-SYK fusion acute myeloid leukemia.* npj Precicion Oncology, 2021. **5**(44).

198. Moran-Crusio, K., L.B. Reavie, and I. Aifantis, *Regulation of hematopoietic stem cell fate by the ubiquitin proteasome system.* Trends in immunology, 2012. **33**(7): p. 357-363.
199. Chapple, R.H., et al., *ERα promotes murine hematopoietic regeneration through the Ire1α-mediated unfolded protein response.* eLife, 2018. **7:e31159**.
200. van Galen, P., et al., *The unfolded protein response governs integrity of the haematopoietic stem-cell pool during stress.* Nature, 2014. **510**(7504): p. 268-72.
201. Chua, B.A. and R.A. Signer, *Hematopoietic stem cell regulation by the proteostasis network.* Current Oppinion in Hematology, 2020. **27**(4): p. 254-263.
202. Kruta, M., et al., *Hsf1 promotes hematopoietic stem cell fitness and proteostasis in response to ex vivo culture stress and aging.* Cell Stem Cell, 2021. **28**(11): p. 1950-1965.
203. Xu, W., R. Rahman, and M. Rosbash, *Mechanistic implications of enhanced editing by a HyperTRIBE RNA-binding protein.* RNA, 2017. **24**(2): p. 173-182.
204. Zhang, Z., M. Liu, and Y. Zheng, *Role of Rho GTPases in stem cell regulation.* Biochemical Society Transactions, 2021. **49**(6): p. 2941-2955.
205. Florian, M.C., et al., *Cdc42 activity regulates hematopoietic stem cell aging and rejuvenation.* Cell Stem Cell, 2012. **10**(5): p. 520-30.
206. Yang, L., et al., *Rho GTPase Cdc42 coordinates hematopoietic stem cell quiescence and niche interaction in the bone marrow.* Proc Natl Acad Sci U S A, 2007. **104**(12): p. 5091-6.
207. Will, B., et al., *Satb1 regulates the self-renewal of hematopoietic stem cells by promoting quiescence and repressing differentiation commitment.* Nature Immunnology, 2013. **14**: p. 437-445.
208. Wu, M., et al., *Imaging Hematopoietic Precursor Division in Real Time.* Cell Stem Cell, 2007. **1**(5).
209. Jackson, M.P. and E.W. Hewitt, *Cellular proteostasis: degradation of misfolded proteins by lysosomes.* 60, 2016(2): p. 173-180.
210. Yang, F.C., et al., *Rac and Cdc42 GTPases control hematopoietic stem cell shape, adhesion, migration, and mobilization.* Proceedings of the National Academy of Sciences, 2001. **98**(10): p. 5614-5618.
211. Kumar, S., et al., *Repolarization of HSC attenuates HSCs failure in Shwachman-Diamond syndrome.* Leukemia, 2021. **35**: p. 1751–1762.
212. Tavakkoli, M., et al., *Epichaperome Abundance Predicts Response to the Epichaperome Inhibitor, Puh-71, in Acute Myeloid Leukemia.* Blood, 2019. **134**: p. 5145.
213. Zong, H., et al., *A Hyperactive Signalosome in Acute Myeloid Leukemia Drives Addiction to a Tumor-Specific Hsp90 Species.* Cell Reports, 2015. **13**(10): p. 2159-2173.
214. Lambert, M., et al., *Direct and Indirect Targeting of HOXA9 Transcription Factor in Acute Myeloid Leukemia.* Cancers, 2019. **11**(6): p. 839.
215. Collins, C.T. and J.L. Hess, *Role of HOXA9 in leukemia: dysregulation, cofactors and essential targets.* Oncogene, 2016. **35**: p. 1090-1098.

216. Ito, S. and M.J. Karnovsky, *Formaldehyde-Glutaraldehyde Fixatives Containing Trinitrocompounds.* The Journal of Cell Biology, 1968. **39**: p. 168A-169A.
217. De Brujin, W.C. and P.D. Beejen, *Glycogen, its chemistry and morphological appearance in the electron microscope.11. The complex formed in the selective contrast staining of glycogen.* The Histochemical Journal, 1975. **7**: p. 205–229.
218. Venable, J.H. and R. Coggeshall, *A SIMPLIFIED LEAD CITRATE STAIN FOR USE IN ELECTRON MICROSCOPY.* j Cell Biol., 1965. **25**(2): p. 407–408.
219. Merugu, S., et al., *Chemical probes and methods for single-cell detection and quantification of epichaperomes in hematologic malignancies.* Methods in Enzymology, 2020. **639**: p. 289-311.
220. Wolf, F.A., P. Angerer, and F.J. Theis, *SCANPY: large-scale single-cell gene expression data analysis.* Genome Biol, 2018. **19**(1): p. 15.
221. Haghverdi, L., et al., *Diffusion pseudotime robustly reconstructs lineage branching.* Nat Methods, 2016. **13**(10): p. 845-8.
222. Cifani, P. and A. Kentsis, *High Sensitivity Quantitative Proteomics Using Automated Multidimensional Nano-flow Chromatography and Accumulated Ion Monitoring on Quadrupole-Orbitrap-Linear Ion Trap Mass Spectrometer.* Molecular and Cellular Proteomics, 2017. **16**(11): p. 2006-2016.
223. MacLean, B., et al., *Skyline: an open source document editor for creating and analyzing targeted proteomics experiments.* Bioinformatics, 2010. **26**(7): p. 966-968.
224. Apweiler, R., et al., *UniProt: the Universal Protein knowledgebase.* Nucleic Acids Research, 2004. **32**: p. D115-D119.
225. Perez-Riverol, Y., et al., *The PRIDE database and related tools and resources in 2019: improving support for quantification data.* Nucleic Acids Research, 2019. **47**(D1): p. D442-D350.
226. Mellacheruvu, D., et al., *The CRAPome: a contaminant repository for affinity purification–mass spectrometry data.* Nature Methods, 2013. **10**: p. 730-736.
227. Lee, S.-H. and C. Mayr, *Gain of Additional BIRC3 Protein Functions through 3'-UTR-Mediated Protein Complex Formation.* Molecular Cell, 2019. **74**(4): p. 701-712.